SCREENING APPLICATIONS OF NEMATODE MICROFLUIDIC ELECTROTAXIS

CHEMICAL AND GENETIC SCREENING APPLICATIONS OF A MICROFLUIDIC ELECTROTAXIS ASSAY USING NEMATODE CAENORHABDITIS ELEGANS

By

JUSTIN TONG, B.A.Sc.

A Thesis

Submitted to the School of Graduate Studies

in Partial Fulfillment of the Requirements

for the Degree

Doctor of Philosophy

DOCTOR OF PHILOSOPHY (2014) McMaster University

MiNDS Neuroscience Hamilton, Ontario, Canada

TITLE: Chemical and Genetic Screening Applications of a Microfluidic Electrotaxis Assay Using Nematode *Caenorhabditis elegans*

AUTHOR: Justin Tong, B.A.Sc. (McMaster University)

SUPERVISOR: Professor Bhagwati P. Gupta

NUMBER OF PAGES: xvi, 166

Abstract

Combining the nematode *Caenorhabditis elegans* with novel microfluidic technology has produced a phenotypic movement assay that is at once rapid, sensitive, and low-cost. The method is based on the neurophysiologic phenomenon of worms exhibiting robust, continuous, directed locomotion in response to mild electric fields inside a microchannel. As we demonstrate with the studies reported herein, our microfluidic electrotaxis platform is a unique tool for studying the effects of environmental and genetic manipulations on *C. elegans*' movement behaviour, which in turn indicates the state of the organism's neuronal and muscular systems.

In one initiative to develop an inexpensive biosensor, we use the setup to measure the response of worms to common environmental pollutants. Results indicate that worms' electrotactic swimming behaviour is particularly susceptible to metal salts. A comparison with traditional assays measuring fecundity, growth, and lifespan reveals that electrotactic speed shows a comparable level of sensitivity as a toxicity endpoint.

Another study demonstrates that worms expressing a mutant form of α-synuclein, a familial Parkinson's disease-related protein, show deficits in electrotactic swimming speed that coincide with dopaminergic neuron damage. We further show that both the electrotaxis and neuronal phenotypes can be ameliorated by treatment with curcumin, a putative neuroprotective agent.

We have also used the platform to investigate the effects of other environmental and genetic stresses on electrotactic behaviour. Our findings indicate that the response can withstand many different insults but is affected by stresses that induce the mitochondrial and ER unfolded protein responses, which themselves play roles in preserving electrotactic swimming behaviour alongside the heat shock response.

These data expand our knowledge of how the motor output component of *C. elegans*' electrotactic response is perturbed by environmental and genetic manipulations, and also support the utility of microfluidic electrotaxis as a functional output of nematode locomotory circuits in a multitude of contexts.

Acknowledgements

Having begun this research as a complete ignoramus, I am indebted to my colleagues and mentors in McMaster Biology and MiNDS for allowing me to stand on their shoulders to reach my goals in the lofty heavens. This thesis is a true testament to the fact that anyone can achieve anything given the proper supports.

Foremost among the scientists deserving my undying gratitude is my supervisor, Dr. Bhagwati P. Gupta. He made a remarkable leap of faith in accepting me as a student despite knowing that I had no prior wet lab experience; if it were not for him and the trust he placed in me, I would probably have taken my undergraduate degree to the fast food industry or something. I have learned so much from Bhagwati, not only about biology and academia, but also about balancing work with life's other aspects. Thank you for your stoic patience and guidance over the years, for your unfailing support of my life choices, and for driving me to be the best that I could be.

I would also like to thank my committee members Dr. P. Ravi Selvaganapathy and Dr. Ram K. Mishra. My project's existence was a by-product of Ravi's collaboration with the Gupta lab; for that, and for the helpful comments born from his extensive knowledge on such a wide range of topics, I am grateful. Ram, too, was a valuable source of guidance whose insights played an important role in guiding the direction of my work. He was also prone to heaping disproportionate amounts of praise upon my head, which definitely helped to raise my spirits in dark times.

My fellow Gupta lab grad students deserve shout-outs as well, of course: Sangeena Salam, my partner in electrotactic crime; Siavash "Scott" Amon, drama queen and font of frivolity; Devika Sharanya Premkumar, mistress of Muv and complainer incessant; Ayush Ranawade, the fabled Phantom of the Lab; and Jessica Knox, The One Who Chose Freedom. Thank you to all of you for your company, support, advice, and humour. Every day shone the brighter for my interactions with you.

It would be unseemly of me to forget my other contemporaries in the Gupta lab and beyond: Bavithra Thillainathan, our lab technician; Mike Chong, Veena Deekonda, Isvarya Venu, Baekjun "Ron" Sung, Prabhjot Kaur, Cory Richman, Iqra Effendi, Beth Culp, Anne Xia, Komal Prajapati, and Shreya Prashar, undergrad thesis students; Parth Patel, Sally Hong, Adrienne Lee, Ria Oommen, and Anum Rahman, undergrad volunteers; Pouya Rezai, Reza Ghaemi, and Dingsheng Liu, engineers from Ravi's lab; Alex Scigajlo, computer engineer

from Dr. Shahram Shirani's lab; and all my classmates in the MiNDS program. It was my pleasure to work with and alongside you, and I wish you all the best in your future endeavours.

In the end, this stack of paper is dedicated to all my loved ones, without whom my life would have no meaning. Hear me, members of the Grapeview Fantastic Four! Daniel "Big Chief" Samosh, Andrew Malmloff, Nigel "Nig Dogg" Parkes, Brandon Armstrong, and Will "Johji" Joh – your names are in a PhD thesis! (Dan will have his own in a few years, but it's still awesome for now, right?) Also included are my dear friends from undergrad: Angel Lai, Airey Lau, Rebecca Ang, Eduard Dwinugrahanto and the other Rifle Range boys. I became a hermit after we parted ways because I didn't want to fill the holes you left in my heart, but at least I managed to put that isolation to good use. And finally, of course, my kin. Mumsy and Bubsy, now that you know what I've been doing with my life over the past few years, I hope you're still convinced that grad school was a good idea. Jon, Josh, and Jas – have I brought honour to the family? Lily, Anna, Athan, Andrew, and Martin – when you're older, I'm going to use this wad of tree pulp to prove that Uncle Justin used to be kind of smart.

Table of Contents

List of Figures and Tables

Chapter 1

Chapter 2

Chapter 3

Chapter 4

Chapter 5

List of Abbreviations

6-OHDA - 6-hydroxydopamine
αSyn - α-synuclein
AC - Alternating current
AD - Alzheimer's disease
ACMF - Alternating current magnetic field
ALS - Amyotrophic lateral sclerosis
APAF1 - Apoptotic protease activating factor 1
ASK1 - Apoptosis signal-regulating kinase 1
ASTM - American Society for Testing and Materials
ATF4 - Activating transcription factor 4
ATF6 - Activating transcription factor 6
BAK - BCL-2 antagonist/killer
BAX - BCL-2-associated X protein
BiP - Binding immunoglobulin protein
BSR - Basal slowing response
CHOP - C/EBP homologous protein
DA - Dopamine
DC - Direct current
DMSO - Dimethylsulfoxide
EGFR - Epidermal growth factor receptor
eIF2 - Eukaryotic initiation factor
EOD - Electric organ discharge
EPA - Environmental Protection Agency
ER - Endoplasmic reticulum
ERAD - ER-associated protein degradation
ETC - Electron transport chain
GADD34 - Growth arrest and DNA damage-inducible protein 34
GFP - Green fluorescent protein
GRP78 - Glucose-regulated protein 78
HD - Huntington's disease
HS - Heat shock
HSF - Heat-shock factor
HSE - Heat-shock element
HSP - Heat-shock protein
HTS - High-throughput screening
ICP-MS - Inductively coupled plasma-mass spectrometry
IRE1 - inositol-requiring enzyme 1
JAR - Jamming avoidance response
JNK - c-Jun N-terminal kinase

L1 to L4 - Larval stages
LB - Lewy body
LC_{50} - Lethal concentration 50
MeHg - Methylmercury
MPTP - 1-methyl-1,2,3,6-tetrahydropyridine
PCR - Polymerase chain reaction
PD - Parkinson's disease
PDMS - Polydimethylsiloxane
PERK - PKR-like ER kinase
PI3K - Phosphoinositide 3-kinase
PKR - Protein kinase R
RNAi - RNA interference
ROS - Reactive oxygen species
SMF - Static magnetic field
SNpc - Substantia nigra pars compacta
SOD - Superoxide dismutase
SWIP - Swimming-induced paralysis
TH - Tyrosine hydroxylase
TNF - Tumour necrosis factor
TRAF2 - TNF receptor-associated factor 2
uORF - Upstream open reading frame
UPR - Unfolded protein response
UPR^{ER} - Endoplasmic reticulum unfolded protein response
UPR^{mt} - Mitochondrial unfolded protein response
XBP1 - X-box-binding protein 1
YFP - Yellow fluorescent protein

Declaration of Academic Achievement

This thesis comprises a total of six chapters. Chapter 1 provides a general introduction and background for research. Chapters 2 through 5 are reproductions of scholarly works that have either been published in, submitted to, or prepared for submission to peer-reviewed journals. Chapter 6 discusses the importance of this research, and future directions.

Chapter 1 is an original work but makes mention of an in-preparation scholarly article to which I contributed. For this study, I was responsible for preparing biological materials and providing worm-related expertise to the primary author Reza Ghaemi. Chapter 2 has been published in the *Journal of Visualized Experiments*. For this work, I was involved in optimization of the methodology alongside colleagues Pouya Rezai and Sangeena Salam, and was also responsible for all data collection, analysis (including incorporation of novel software designed in-house), and preparation of the manuscript. Chapters 3 through 5 are also written in the style of scholarly articles, with Chapter 3 submitted to the *Journal of Applied Toxicology*. For these studies, I oversaw all aspects of research, designing experiments with guidance from my supervisor Dr. Bhagwati Gupta, executing experimental procedures for data collection (with contributions from undergraduate student Baekjun Sung in the case of Chapter 5), analyzed all data, and prepared manuscripts with editing assistance from my supervisory committee members Dr. Bhagwati Gupta, Dr. P. Ravi Selvaganapathy, and Dr. Ram Mishra. Chapter 6 is an original work but makes mention of an additional scholarly article to which I contributed, though the manuscript is still in preparation. For this study, I was responsible for biological experiments and data collection alongside Sangeena Salam, providing worm-related expertise to the primary author Alexander Scigajlo, and preparation of the manuscript alongside Sangeena Salam and Alexander Scigajlo.

This work was funded by the Ontario Ministry of Research and Innovation and the Collaborative Health Research Projects award, co-funded by the Natural Sciences and Engineering Research Council of Canada and the Canadian Institutes of Health Research. I received support from the Ontario Graduate Scholarship for year 2 of this research.

Chapter 1-Introduction

1.1 Response to environmental stimuli

All species depend on their ability to adapt to changing environments to survive and proliferate. For individual organisms, adaptability includes real-time responsiveness to a variety of environmental cues. The resultant behaviours, such as the pheromone trail of an ant scout that has found food or the phalanx formation of threatened muskoxen, are often crucial for locating resources or avoiding predation. While differing in complexity from simple reflexes to fixed action patterns to learned behaviours, all contribute to fitness and are therefore important to study. Moreover, the cellular and molecular characterization of the processes involved have increased our understanding of neuronal signaling and neurobiology in general. Such studies commonly employ model organisms, both vertebrate and invertebrate.

1.1.1 Vertebrate models

Vertebrates are the models of choice for addressing questions with direct implications for human health. They have also been useful for studying the general phenomenon of behavioural responses to stimuli.

Perhaps the best known and most widely used vertebrate model is the laboratory mouse, *Mus musculus*. Being one of the definitive classical model organisms, the mouse has been used to study a wide variety of behavioural responses and their relation to neurological phenomena as fundamental as learning and memory (**1**). For instance, one common assay for novel object recognition, which relies on the hippocampus and cortex, has been used to evaluate the role of histamine signaling in the mouse's ability to distinguish novel from familiar objects. The study found that mice treated with histamine receptor H_3R antagonists did not display novel object recognition, indicating a role for histamine in learning and memory (**2**). Another well-known assay, called the forced-swim test, measures behavioural despair in studies using mice to model depression (**1**). The test involves placing the mouse into a cylinder filled with water to a level that allows the animal to neither rest on its tail nor climb out of the cylinder, leaving it with only the options of futile struggle and immobile floating, with immobility duration being scored as a measure of depression. In one study, compounds were evaluated for antidepressant activity by measuring their

effects on forced-swim test results. The study found that administration of melatonin, among other agents, could significantly attenuate the duration of the immobility period, supporting further exploration of this hormone as a potential treatment for depression (**3**). Together with the plethora of research not mentioned here, these findings have improved our understanding of fundamental processes in metazoan behaviour.

1.1.2 Invertebrate models

Although vertebrate models best reflect the biological processes in humans, their relatively slow development and long lifespans hinder the speed of experiments. Moreover, the use of model organisms from a wide assortment of lineages on the tree of life is desirable for the purposes of comparative molecular biology. Hence, invertebrates such as fruit flies also enjoy a high degree of popularity. *Drosophila melanogaster* is especially famous, having been the subject of Thomas Hunt Morgan's classic studies of mutation in the early 20th century, and has been used to study behavioural phenomena such as phototaxis, olfactory and gustatory chemotaxis, hygrotaxis, thermotaxis, and geotaxis (**4**). Screens utilizing these and other behavioural responses have helped to isolate genes involved in vision, olfaction, audition, learning and memory, courtship, pain, and other processes (**5**).

The nematode *Caenorhabditis elegans* has also been instrumental in expanding our knowledge of behavioural responses to environmental stimuli, with many of its taxis behaviours already widely studied. The strengths and distinguishing features of this model are discussed in the following subsection.

1.1.3 *C. elegans* model

C. elegans is a popular model system due in large part to its ease of culture and maintenance (**6**). First introduced to developmental biologists by Sydney Brenner (**7**), this free-living hermaphroditic species has since become a staple in a variety of fields. *C. elegans* thrives in laboratory conditions, feeds on bacteria, and is able to produce over 300 progeny across its lifetime, which generally spans no more than 2-3 weeks. Eggs hatch to produce L1 larvae, which then proceed via a series of molts through the L2, L3, and L4 stages before finally entering adulthood a mere 2-3 days after hatching (**Figure 1**). The majority of *C. elegans* are self-fertilizing hermaphrodites, though males are also present and reproduce by mating with hermaphrodites; combined with its short generation time, this reproductive strategy renders *C. elegans* highly amenable to genetic manipulation. Under stressful conditions such as food shortage or overcrowding, larval *C.*

elegans adopt an alternative developmental stage called dauer instead of L3. Dauers can survive for months without food and re-enter the normal life cycle as L4s upon encountering better conditions, making strains easy to maintain over long periods. Furthermore, *C. elegans* can be stored in liquid nitrogen and thawed years later to re-establish growing cultures when needed.

Of course, the strengths of *C. elegans* extend beyond its culture convenience. With only 959 somatic cells in the adult hermaphrodite, this animal provides a relatively simple metazoan system in which to explore intercellular networks, behaviour, and other biological phenomena. At the same time, *C. elegans* shares many conserved disease mechanisms and roughly half of its genes with humans, allowing disease-related findings to be successfully translated to human health (**8**). In addition, its transparent body allows *in vivo* visualization of cellular and molecular events in real time using green fluorescent protein (GFP)-based molecular markers without the need for sacrifice.

Because *C. elegans* is used so widely, an impressive array of online, freely available resources has been established (**9**). Its entire genome, which was the first among all multicellular organisms to be sequenced, is available on WormBase (*www.wormbase.org*), while its complete cell lineage has been mapped and is accessible on WormAtlas (*www.wormatlas.org*). Furthermore, a collection of reviews detailing techniques and other topics related to *C. elegans* biology, known as WormBook (*www.wormbook.org*), has been compiled through the contributions of nematode researchers across the globe. Indeed, this animal is commonly considered one of the most thoroughly studied multicellular organisms in terms of genetics, development, behaviour, and physiology.

Many key discoveries with direct implications for human health were first made in *C. elegans*. Nematode researchers Sydney Brenner, Robert Horvitz, and John Sulston were awarded the 2002 Nobel Prize in Physiology or Medicine for their discoveries regarding the genetic regulation of organ development and apoptosis. Not long afterwards, Andrew Fire and Craig Mello won the 2006 Nobel Prize in Physiology or Medicine for their discovery of double-stranded RNA-mediated gene silencing, or RNA interference (RNAi), in *C. elegans* (**10**). RNAi is now commonly employed in gene loss-of-function experiments, which are especially straightforward in *C. elegans* due to its uncommon ability to uptake RNA from its environment by virtue of its expression of the intestinal luminal transmembrane protein SID-2 (**11**). *C. elegans* has also been employed in the modeling of various disorders including obesity (**12**), hypertension (**13**), muscular and neuronal degeneration (**14**,**15**,**16**). Additionally, the ease of *C. elegans* maintenance allows performance of high-throughput genetic and chemical screens, which has accelerated drug discovery and identification of therapeutic targets (**17**,**18**).

1.2 Responses of *C. elegans* to external stimuli

Being highly mobile creatures that occupy diverse habitats, nematodes have evolved a number of behaviours allowing them to respond appropriately to different stimuli. Many of these behaviours amount to alterations in the animal's locomotory trajectory to guide movement either towards or away from the stimulus' origin. Such responses, known as taxes, have developed in *C. elegans* for a wide range of environmental cues including odours, tastes, temperature, touch, light, oxygen, magnetic field, and electric potential. These stimuli are largely detected by neurons in the amphids, and to a lesser extent, the phasmids, paired sensory organs in the head and tail regions respectively (**Figure 2**). Most sensory neurons are identical to their contralateral twins but otherwise unique regarding not only their synaptic connections, but also their sensitivities to particular cues. Some, known as polymodal neurons, even detect multiple classes of stimulus: AWC, for example, plays roles in both odorsensation and thermosensation (**19**). Upon activation, taxis-mediating sensory neurons stimulate subsets of an intricate interneuron network, with sensory inputs integrated at the cells known as command interneurons. These cells, in turn, synapse onto motor neurons to influence locomotion.

Perhaps the best characterized of *C. elegans* taxes is chemotaxis, which is employed to find food, avoid hazards, and mate (**20**). The *C. elegans* chemosensory system is highly developed and serves both olfactory and gustatory functions, being sensitive to volatile as well as water-soluble factors. 32 of *C. elegans*' 302 neurons are equipped with chemoreceptors that are either directly or indirectly exposed to the environment through openings generated by specialized glia called the socket and sheath cells (**20**). Of these chemosensory neurons, 11 are found in each of the two amphids, 2 are located in each of the two phasmids, and one resides in each of the six inner labial organs in the mouth area. Each neuron expresses a specific suite of receptor genes and detects a particular set of attractants and repellents.

When pursuing an attractive chemical stimulus, *C. elegans* employs a strategy called the "pirouette model," in which animals exhibit stretches of forward motion punctuated with random direction changes called pirouettes (**21**). The frequency of pirouettes is adjusted based on animals' perception of changes in attractant concentration: when travelling up a gradient of attractant, pirouettes are rare, but when travelling down a gradient of attractant, pirouettes are more frequent. In this way, worms make long movements toward the source of the stimulus and only short movements away from it. This approach, which is highly

similar to the "biased random walk" method of chemotaxis used by bacteria (**22**,**23**), is well suited to the inconstancy of natural conditions but sub-optimal for chemotaxis in more linear laboratory conditions.

Another well-studied *C. elegans* taxis behaviour is exhibited in response to thermosensation (**24**). A wild-type *C. elegans* can grow well at temperatures ranging from 15°C to 25°C but develops a preference in adulthood for the temperature at which it was cultivated, which can be observed by placing the animal into a thermal gradient. In the presence of a radial thermal gradient, *C. elegans* display "isoclines" of movement, circling the plate at precisely its preferred temperature (**25**). Similarly, in a linear thermal gradient, worms grown at a particular temperature tend to cluster around the region in the gradient where that temperature can be re-experienced (**25**). Thermosensation is mediated primarily by the AFD amphid neurons, with contributions from AWC and ASI as well (**26**,**19**,**27**). In a manner similar to the pirouette model of chemotaxis, these neurons act in concert to increase reversal and turning frequency upon detection of supra-optimal temperatures, resulting in thermotaxis back down the gradient to the worm's culture temperature.

Though not strictly considered a taxis, *C. elegans*' mechanosensory behaviour represents an additional system used by worms to respond to changes in their environment. The mechanosensory system, which comprises 30 mechanoreceptor neurons in the hermaphrodite, allows *C. elegans* to detect collisions and the forces generated by their own movement (**28**). The worm's response to mechanosensation is most easily observed in the lab by touching its body with a wire pick, which elicits avoidance behaviour: a prod along its anterior half causes it to move backward while a prod along its posterior half causes it to move forward or accelerate if it was already moving forward. Tapping the plate to cause vibrations in the substrate is believed to activate all touch receptor neurons at once, but stimulation of the anterior neurons appears to dominate and manifest as reversal of direction in wild-type adults (**28**). Repeated activation of mechanoreceptor neurons causes desensitization, however, and results in habituation to touch stimuli.

C. elegans possesses further movement-guiding senses, including an ability to detect light (**29**). Like its soil-dwelling relatives, *C. elegans* is partial to dark environs in the wild; keeping it in the shade is its negative phototactic behaviour. While the animal lacks eyes, a number of amphid sensory neurons including ASH, ASJ, ASK, and AWB have been identified as light-sensitive and responsible for *C. elegans*' aversion to light (**30**). A pulse of light focused on the head of a worm moving forward causes immediate cessation of forward locomotion and initiation of reversals, whereas directing a flash onto the tail of a worm moving backwards causes it to start moving forward. The penetrance of this response varies with both light intensity and wavelength: worms are more likely

to respond to stronger light stimuli and are more sensitive to shorter wavelengths, responding robustly to ultraviolet, violet, and blue light but only rarely responding to green or yellow light. It has been suggested that *C. elegans*' phototaxis is an important mechanism to protect it from the shorter-wavelength components of sunlight, given that prolonged exposure to ultraviolet, violet, and blue but not green or yellow light causes worms to paralyze and die (**30**). Because worms only exhibit strong phototaxis when the light is potentially harmful, light is not an ideal stimulus for studies requiring on-demand induction of *C. elegans* locomotion.

Oxygen level is another factor influencing worm movement. Like most multicellular eukaryotes, *C. elegans* requires oxygen to live and grow: under anoxic conditions, worms immobilize and eventually die (**31**). At the same time, hyperoxic conditions promote the production of reactive oxygen species (ROS) (**32**), which have a complex relationship with cellular stress but can certainly cause damage when present in excess (**33**). *C. elegans* therefore exhibits a strong preference for 5-12% oxygen, using aerotaxis to avoid lower and higher levels (**34**). Mediating this behaviour are the polymodal chemosensory neurons AQR, ASH, and ADF in the amphid and PQR in the phasmid, with additional contributions from the combination oxygen-sensor/interneuron URX (**35**). While an interesting phenomenon, the aerotactic response is variable and not fully penetrant, rendering oxygen an unsuitable stimulus to control movement of animals.

Magnetic field is yet another nonchemical agent whose guiding effect on *C. elegans* locomotion has been studied, though much of the relevant work is incomplete as of yet. Both static magnetic fields (SMFs) and alternating current magnetic fields (ACMFs) have deleterious effects on worm health: SMFs of 200 mT reduce lifespan and fertility (**36**,**37**), and ACMFs up to 1.7 T reduce fertility and growth (**38**). Changes in gene expression that accompany exposure to magnetic field have also been identified (**36**,**37**,**39**), and decreases in locomotory rate have been observed (**40**). However, while magnetotaxis has been reported (**41**), work demonstrating the use of magnetic fields to guide worms' direction of movement and studies identifying the neurons responsible have not yet been published.

Clearly, worms are able to detect and respond to a wide variety of environmental cues. However, among all the taxes of *C. elegans*, electrotaxis (formerly known as galvanotaxis, referring to directed movement initiated and maintained in response to detected electric field stimuli) stands out as the behaviour most easily exploited to robustly direct worm movement. Hence, the present study sought to better characterize aspects of this behaviour in particular. Electroreception and electrotaxis are described in greater detail in the following section.

1.2.1 Response to electric field stimulus

Electrotaxis is employed by many different taxa and for many different purposes. It is well-studied in motile cells: plant pathogenic microbes such as *Phytophthora* and *Pythium* oomycetes, for example, rely on electric fields to target plant roots (**42**), though the molecular mechanisms remain unknown at present. Some cells in metazoan systems are also known to exhibit electric field-dependent motility: for instance, during wound healing, epithelial cells use wound-generated electric fields to guide their migration to the site of injury (**43**,**44**,**45**). Mounting research indicates a role for electrotaxis in various other basic processes as well, including embryonic development (**46**,**47**) and nerve cell growth (**48**). During electrotaxis, different cell types under different conditions have different preferences for migration direction, but many will change their initial direction when the external electric field is first applied and again if the electric field is reversed in polarity, suggesting that electrical stimulus exerts stronger control than even chemical guidance on cell migration (**49**,**50**). Increasing evidence supports the hypothesis that electrical signals act on the same downstream motility pathways as chemical cues and general cell migration, inducing reorientation of cell surface and signalling molecules (**50**,**51**). Specific pathways thought to be involved include phosphoinositide 3-kinase (PI3K) signaling, polarization of epidermal growth factor receptor (EGFR), voltage-gated Na^+ channels, Ca^{2+} signaling, and Ca^{2+}-associated ROS generation (**52**). However, this field is still an emerging area of research, and the exact molecular mechanisms underlying the electrotactic behaviour of single cells have yet to be precisely characterized.

Whole-organism electric field-induced behaviour is well-studied in fish (**53**), many of which bear electroreceptors just beneath the body surface even if they lack electric organs. Electroreceptors are found in cartilaginous fish (sharks and rays), teleost and non-teleost ray-finned fish, lungfish, and coelacanths, and seem to have evolved in fish on four or more independent occasions (**53**). Different species employ electroreception for different purposes: for instance, non-electric fish such as sharks utilize passive electrolocation, wherein the shark senses the weak bioelectric fields generated by prey to locate them (**54**). Meanwhile, fish with electric organs (electrogenic, or more simply, electric fish) utilize active electrolocation, wherein the fish senses its surrounding environment by detecting distortions in self-generated electric fields, as well as electrocommunication, which involves modulating the waveform of self-generated electric fields for mate attraction and territorial displays (**55**). Passive electrolocation relies on ampullary receptors, which are sensitive to low frequencies (< 50 Hz) and consist of a jelly-filled canal leading from the sensory receptors to the skin surface, whereas active electrolocation and

electrocommunication use tuberous electroreceptors that are sensitive to higher frequencies (20-20,000 Hz) (**54**,**55**).

Due to the importance of electrosensation for navigation, weakly electric fish have evolved behavioural mechanisms for the maintenance of "private" frequency bands, or undisturbed frequency domains. The best studied of these behaviours is the jamming avoidance response (JAR), in which neighbouring fish actively adjust their electric organ discharge (EOD) frequencies to avoid overlap (**53**). The circuits involved in the JAR have been elucidated through lesion studies. Briefly, electrosensory information is collected by T-type and P-type electroreceptors, which encode amplitude and phase respectively. This information is relayed through separate pathways to the hindbrain, then converges in the midbrain. Encoding of the sign of the frequency difference between the fish's EOD and the interfering signal is performed by the nucleus electrosensorius in the diencephalon, which projects to different prepacemaker nuclei; these cells, in turn, project onto the pacemaker nucleus, which controls EOD frequency (**53**). Study of the JAR has shed light on how electrical signals are processed by the nervous system of weakly electric fish, and more broadly, how the circuitry underlying a specific behaviour can be unraveled.

Electroreception has also been reported in a number of other organisms, including monotremes such as the duck-billed platypus (**56**,**57**), dolphins (**58**), bees (**59**), and of course, a wide variety of nematodes, which respond to electrical signals with directed locomotion (**60**,**61**). The ecological significance of this behaviour is unclear in some cases, but in parasitic nematodes such as the steinernematids, increasing evidence suggests that electrotaxis may be important for host-finding (**62**,**63**). Host-finding strategies vary from species to species, ranging from ambush (sit & wait) to cruise (search & destroy), but all steinernematids exhibit electrotaxis, and the differences in their electrotactic responses correlate with their host-finding strategies. For instance, in the presence of electric field, cruisers such as *Steinernema glaseri* move towards the anode (higher electric potential) while ambushers such as *Steinernema carpocapsae* move towards the cathode (lower electric potential) (**62**). Being attracted to lower electric potential seems to draw animals towards plant roots, facilitating the finding of phytophagous hosts. Indeed, ambushers seem to be more successful in finding mobile hosts, while cruisers are better at finding sedentary hosts (**63**).

The electrotactic response of *C. elegans* in particular was first demonstrated by Sukul and Croll in 1978 (**64**), who showed that worms crawl toward the negative electrode in the presence of a direct current (DC) electric field in an agar environment. Electrotaxis studies were continued by Gabel and colleagues in 2007, who showed that worms approach the cathode at an angle proportional to field strength (**65**). Furthermore, cell ablation experiments conducted by the same group indicated that no single neuron is responsible for

sensing the electric field, though amphid sensory neurons ASH, ASJ, and to a lesser degree ASK, AWB, and AWC were shown to contribute. Moreover, ablating all dendrites in both amphid nerve bundles was observed to severely disrupt electrosensation, further implicating the importance of amphid neurons in electrosensation (**65**). The neuronal circuits thought to mediate electrotactic behaviour are shown in **Figure 3**. However, more work is required to fully explore the neuronal signaling and underlying mechanisms that mediate electrotaxis. The biological relevance of this behaviour also remains unclear, though the fact that electroreception facilitates food-finding in non-electric fish, electroreceptive mammals, and bees, as well as the evidence supporting electric field as a host-finding cue in parasitic nematodes (**66**,**62**), supports speculation that electrotaxis may help *C. elegans* to find food in the form of decaying plant matter and dying animals, which are likely to harbour bacteria.

Although electrotactic mechanisms overlap significantly with those of other taxes, there remains much that we do not understand about electrotaxis at the molecular level. Our lab is interested in exploring how this phenomenon is mediated. To address this question, one must appreciate that the behaviour is divisible into sensation, regulatory, and motor output components. Therefore, one aspect of our research approach involves identifying the neural circuits and genetic pathways responsible for electrosensation. This work is being led by my colleague, Sangeena Salam. A second aspect of our research approach is to study how the motor output of the response is affected by environmental and genetic manipulations; herein lies the focus of my work. I was specifically interested in investigating how *C. elegans*' response to stress manifests during electrotaxis, which I sought to address by studying the effects of environmental pollutants, genetic stress in the form of Parkinson's disease (PD) mutant α-synuclein (αSyn), and activation of cellular stress responses such as the unfolded protein response (UPR) on worms' electrotactic movement. The findings from this work reveal that the worm's motor response to electric field is regulated by specific mechanisms, and provides clues to the nature of those mechanisms, which may be relevant to electroreception phenomena in other taxa as well.

1.2.2 Investigations of *C. elegans* electrotaxis using a microfluidic setup

In addition to studies of how electric cues are detected, processed, and answered with directional locomotion, our group also explores engineering approaches to adapt electrotaxis for practical purposes such as drug discovery and high-throughput screens. In this process, our collaborators in the Selvaganapathy lab have developed a microfluidic system that increases uniformity of the electric field and eliminates the factor of the angle at which worms approach the cathode

(**67**). The platform, detailed in Chapter 2, projects a DC electric field through the axis of a buffer-filled microchannel made from polydimethylsiloxane (PDMS) (**Figure 4**). The DC field was seen to be a highly effective stimulus for inducing movement, with worms continuing to swim even during long exposures of over ten minutes. Importantly, animals responded to the stimulus immediately and with full penetrance, while reversing the field polarity caused them to quickly turn back and resume motion in the opposite direction; together, these characteristics afford investigators very tight control of *C. elegans* movement. It was further observed that exposure to the electric field has no adverse effect on worms' long-term health in terms of lifespan and fertility (**67**).

Worms appear to begin exhibiting electrotaxis in L3, increase in speed until young adulthood, and then become progressively more sluggish with age. Different stages are also sensitive to different ranges of field strength: L3s have been observed to respond to fields between 4 and 12 V/cm, L4s respond to fields between 4 and 10 V/cm, and adults respond to fields between 2 and 4 V/cm. For a given stage, speed is independent of electric field strength (**67**).

Although assays using constant DC signals are the focus of the present study, our colleagues have also explored the use of alternating current (AC) and pulse DC electric fields for control of nematode locomotion inside microchannels (**68**,**69**). Symmetric square-wave AC fields with frequencies of 1 Hz or greater were seen to inhibit *C. elegans* from traveling either forward or backward, allowing investigators to effectively localize animals at will (**68**); it has therefore been suggested that new microfluidic devices may be designed to incorporate both DC and AC fields to permit even more powerful manipulation of worms' movement. On the other hand, pulse DC signals generate responses in both *C. elegans* and its relative *C. briggsae* that are only subtly different from the responses resulting from constant DC signals, though robustness of electrotaxis decreases as the "on" proportion of the pulse signal is shortened. While these findings are interesting, AC and pulse DC signals were not utilized in the research conducted for this thesis.

In summary, by combining electrotaxis with microfluidic technology, we have created an environment where worms reliably choose to swim toward the negative electrode in the presence of a DC electric field. Since electrosensation and the decision to swim are mediated by neurons while the swimming itself is mediated by muscles, abnormalities in either neuronal signalling or muscular function can be detected by the assay using locomotion, specifically swimming speed, as a readout (**70**). Such control over worm locomotion makes the microfluidic electrotaxis assay a valuable technique with much utility.

1.3 Overall Goal & Specific Aims

Our group has previously designed a microfluidic chip for the study of nematode electrotaxis behaviour (**67**), and shown that it can be used to sort worms by age and phenotype (**71**) and localize worms with AC electric fields (**68**). Building on this work, **the overall goal of the present thesis was to further develop assays for the quantitative measurement of changes in the electrotactic swimming response of C. elegans, and to use these assays to dissect genetic and environmental factors that affect this behaviour**.

To achieve this goal, we sought to accomplish the following three aims.

Aim 1: Investigate the effect of environmental pollutants on electrotactic swimming behaviour. There are many anthropogenic chemicals regularly released into the environment that may affect animals' health in a variety of ways and hence stand to have an impact on the electrotactic swimming response. We were interested in exploring whether the behaviour is sensitive to such chemicals, both for the biological implications and to establish the microfluidic assay as a tool for future toxicological studies. We therefore addressed this aim by evaluating changes in electrotactic movement following the exposure of animals to a spectrum of pollutants including inorganic and organic metal salts, xenoestrogens, industrial solvent, herbicide, and a fish anesthetic. To allow comparison of the electrotaxis results with more traditional endpoints, we conducted other common nematode toxicological assays measuring reproduction, growth, and lifespan. We also used fluorescent marker strains, including ASEL marker *gcy-7*::GFP and GABAergic neuronal marker *unc-47*::GFP, to identify neuronal abnormalities that could at least partly account for the electrotactic defects observed in exposed worms. Additionally, we conducted inductively coupled plasma-mass spectrometry (ICP-MS) to measure toxicant levels inside worms as well as inside exposure media to ensure efficient uptake and evaluate bioaccumulation.

Aim 2: Investigate the effect of genetic stress, via ectopic expression of familial PD mutant αSyn, on electrotactic swimming behaviour. Genes contribute significantly to one's risk of developing neurodegenerative diseases such as PD. The *SNCA* gene in particular, which encodes αSyn, has been strongly associated with familial PD in humans, growth inhibition in yeast, and dopaminergic neurodegeneration in invertebrate models (**72**). Given its propensity for causing cellular stress, we deemed A53T mutant αSyn as an appropriate test condition for studying the impact of genetic stress factors on electrotactic swimming. We therefore addressed this aim by first obtaining and evaluating the

electrotactic behaviour of *unc-51*::αSyn(A53T) and *unc-54*::αSyn(A53T) transgenic animals. Next, we constructed *dat-1*::αSyn(A53T) transgenic lines to allow evaluation of dopaminergic neuron-specific effects. We validated these strains for dopamine neurodegeneration and defective dopamine-mediated behaviours, such as the food-sensing basal slowing response, and characterized their electrotaxis across a time course. To determine whether the αSyn-induced electrotactic swimming defects are specific to dopaminergic neurons, we also constructed and assessed the electrotaxis of *lin-11-int3*::αSyn(A53T) transgenic lines, in which αSyn is expressed in a subset of non-dopaminergic head sensory neurons. Together, these experiments showed that αSyn genetic stress in specific cell types impairs electrotactic motility, and support the association between dopamine signaling and electrotactic swimming first indicated by our colleague's work with neurotoxicants (**73**). To demonstrate the platform's potential for PD drug discovery, we proceeded to test the ability of curcumin, a putative neuroprotective agent, to ameliorate the neuronal and movement phenotypes of the *dat-1*::αSyn PD model worms.

Aim 3: Investigate the relationships between cellular stress response pathways, specifically the UPR^{mt}, UPR^{ER}, and heat shock response, and electrotactic swimming behaviour. After observing quantifiable impairments to electrotactic motility from metal exposure and ectopic αSyn expression but not various other stresses, we wished to know whether common themes could be found to link together the stress factors that do affect electrotactic swimming. Given the high energy demands of the muscles and neurons involved in electrotaxis, a particularly interesting avenue to explore was found in mitochondrial stress, which is known to activate the mitochondrial unfolded protein response (UPR^{mt}) (**74**). We expected that UPR^{mt}-inducing conditions and perturbations in the UPR^{mt} itself would manifest as deficits in electrotactic motility. Additionally, we wished to explore the UPR in other cellular compartments, as the endoplasmic reticulum (ER) UPR (UPR^{ER}) (**75**,**76**,**77**,**78**,**79**) and the cytosolic UPR (better known as the heat shock response) (**80**,**81**,**82**,**83**,**84**,**85**) have both been implicated in neuroprotection and neurodegeneration. We therefore addressed this aim by inducing a range of stresses, through both environmental and genetic means, and evaluating resultant changes in electrotactic movement. The test conditions included paraquat and tunicamycin treatments, heat stress, electron transport chain (ETC) mutations, UPR machinery mutations, and others. We used stress-responsive fluorescent marker strains to visualize activation of stress response pathways: *hsp-6*::GFP and *hsp-60*::GFP for the UPR^{mt}, *hsp-4*::GFP for the UPR^{ER}, and *hsp-16.2*::GFP for the heat shock response. To determine whether neuronal abnormalities might at least partially account for the observed behavioural defects, we examined the effects of the tested stress conditions on the morphology of dopaminergic neurons in *dat-1*::YFP transgenic worms.

Addressing these aims has revealed that the worm's motor response to electric field is regulated by specific mechanisms, and has provided clues to the nature of those mechanisms. Our findings are significant to the broader field of electric field-dependent behaviour because the effects of metal toxicity on electrosensory behaviour have not been reported in any organism to date, nor have any connections with the UPR been previously considered; therefore, our findings may indicate a novel set of mechanisms regulating organisms' response to electric stimuli. Moreover, we demonstrate the utility of the microfluidic electrotaxis system for myriad purposes, including the evaluation of potential neuroprotective compounds; hence, we posit that our assay will accelerate screening efforts and other research involving the phenomenon of nematode electrotaxis.

References

1. van Meer, P.; Raber, J. Mouse behavioural analysis in systems biology. *Biochem J* **2005,** *389* (Pt 3), 593-610.

2. Bongers, G.; Leurs, R.; Robertson, J.; Raber, J. Role of H3-receptor-mediated signaling in anxiety and cognition in wild-type and Apoe-/- mice. *Neuropsychopharmacology* **2004,** *29* (3), 441-449.

3. Raghavendra, V.; Kaur, G.; Kulkarni, S. K. Anti-depressant action of melatonin in chronic forced swimming-induced behavioral despair in mice, role of peripheral benzodiazepine receptor modulation. *Eur Neuropsychopharmacol* **2000,** *10* (6), 473-481.

4. Vang, L. L.; Medvedev, A. V.; Adler, J. Simple ways to measure behavioral responses of Drosophila to stimuli and use of these methods to characterize a novel mutant. *PLoS One* **2012,** *7* (5), e37495.

5. Ashburner, M.; Golic, K. G.; Hawley, R. S. *Drosophila: A Laboratory Handbook*, 2nd ed.; Cold Spring Harbor Laboratory Press: Cold Spring Harbor, NY, 2005; pp 162-164.

6. Stiernagle, T. Maintenance of C. elegans, 2006. WormBook. http://wormbook.org/chapters/www_strainmaintain/strainmaintain.html.

7. Brenner, S. The genetics of Caenorhabditis elegans. *Genetics* **1974,** *77* (1), 71-94.

8. Kaletta, T.; Hengartner, M. O. Finding function in novel targets: C. elegans as a model organism. *Nat Rev Drug Discov* **2006,** *5* (5), 387-398.

9. Antoshechkin, I.; Sternberg, P. W. The versatile worm: genetic and genomic resources for Caenorhabditis elegans research. *Nat Rev Genet* **2007,** *8* (7), 518-532.

10. Fire, A.; Xu, S.; Montgomery, M. K.; Kostas, S. A.; Driver, S. E.; Mello, C. C. Potent and specific genetic interference by double-stranded RNA in Caenorhabditis elegans. *Nature* **1998,** *391* (6669), 806-811.

11. Winston, W. M.; Sutherlin, M.; Wright, A. J.; Feinberg, E. H.; Hunter, C. P. Caenorhabditis elegans SID-2 is required for environmental RNA interference. *Proc Natl Acad Sci USA* **2007,** *104* (25), 10565-10570.

12. Ashrafi, K.; Chang, F. Y.; Watts, J. L.; Fraser, A. G.; Kamath, R. S.; Ahringer, J.; Ruvkun, G. Genome-wide RNAi analysis of Caenorhabditis elegans fat regulatory genes. *Nature* **2003,** *421* (6920), 268-272.

13. Kwok, T. C. Y.; Ricker, N.; Fraser, R.; Chan, A. W.; Burns, A.; Stanley, E. F.; McCourt, P.; Cutler, S. R.; Roy, P. J. A small-molecule screen in C. elegans yields a new calcium channel antagonist. *Nature* **2006,** *441,* 91-95.

14. Voisine, C.; Hart, A. C. Caenorhabditis elegans as a model system for triplet repeat diseases. *Methods Mol Biol* **2004,** *277,* 141-160.

15. Voisine, C.; Varma, H.; Walker, N.; Bates, E. A.; Stockwell, B. R.; Hart, A. C. Identification of Potential Therapeutic Drugs forHuntington's Disease using Caenorhabditis elegans. *PloS One* **2007,** *2* (6), e504.

16. Lakso, M.; Vartiainen, S.; Moilanen, A. M.; Sirviö, J.; Thomas, J. H.; Nass, R.; Blakely, R. D.; Wong, G. Dopaminergic neuronal loss and motor deficits in Caenorhabditis elegans overexpressing human alpha-synuclein. *J Neurochem* **2003,** *86* (1), 165-172.

17. Jones, A. K.; Buckingham, S. D.; Sattelle, D. B. Chemistry-to-gene screens in Caenorhabditis elegans. *Nat Rev Drug Discov* **2005,** *4* (4), 321-330.

18. van Ham, T. J.; Breitling, R.; Swertz, M. A.; Nollen, E. A. Neurodegenerative diseases: Lessons from genome-wide screens in small model organisms. *EMBO Mol Med* **2009,** *1* (8-9), 360-370.

19. Biron, D.; Wasserman, S.; Thomas, J. H.; Samuel, A. D.; Sengupta, P. An olfactory neuron responds stochastically to temperature and modulates Caenorhabditis elegans thermotactic behavior. *Proc Natl Acad Sci USA* **2008,** *105* (31), 11002-11007.

20. Bargmann, C. I. Chemosensation in C. elegans, 2006. WormBook. http://wormbook.org/chapters/www_chemosensation/chemosensation.html.

21. Pierce-Shimomura, J. T.; Morse, T. M.; Lockery, S. R. The fundamental role of pirouettes in Caenorhabditis elegans chemotaxis. *J Neurosci* **1999,** *19* (21), 9557-9569.

22. Berg, H. C. Chemotaxis in bacteria. *Annu Rev Biophys Bioeng* **1975,** *4* (00), 119-136.

23. Berg, H. C. *Random walks in biology;* Princeton University Press: Princeton, NJ,

1993.

24. Bargmann, C. I.; Mori, I. Chemotaxis and Thermotaxis. In *C. elegans II;* Riddle, D. L., Blumenthal, T., Meyer, B. J., Priess, J. R., Eds.; Cold Spring Harbor Laboratory Press: Cold Spring Harbor (NY), 1997; pp 717-737.

25. Hedgecock, E. M.; Russell, R. L. Normal and mutant thermotaxis in the nematode Caenorhabditis elegans. *Proc Natl Acad Sci USA* **1975,** *72* (10), 4061-4065.

26. Beverly, M.; Anbil, S.; Sengupta, P. Degeneracy and neuromodulation among thermosensory neurons contribute to robust thermosensory behaviors in Caenorhabditis elegans. *J Neurosci* **2011,** *31* (32), 11718-11727.

27. Kuhara, A.; Okumura, M.; Kimata, T.; Tanizawa, Y.; Takano, R.; Kimura, K. D.; Inada, H.; Matsumoto, K.; Mori, I. Temperature sensing by an olfactory neuron in a circuit controlling behavior of C. elegans. *Science* **2008,** *320* (5877), 803-807.

28. Goodman, M. B. Mechanosensation, 2006. WormBook. http://wormbook.org/chapters/www_mechanosensation/mechanosensation.html.

29. Burr, A. H. The photomovement of Caenorhabditis elegans, a nematode which lacks ocelli. Proof that the response is to light not radiant heating. *Photochem Photobiol* **1985,** *41* (5), 577-582.

30. Ward, A.; Liu, J.; Feng, Z.; Xu, X. Z. Light-sensitive neurons and channels mediate phototaxis in C. elegans. *Nat Neurosci* **2008,** *11* (8), 916-922.

31. Van Voorhies, W. A.; Ward, S. Broad oxygen tolerance in the nematode Caenorhabditis elegans. *J Exp Biol* **2000,** *203* (Pt 16), 2467-2478.

32. Yu, B. Cellular defenses against damage from reactive oxygen species. *Physiol Rev* **1994,** *74* (1), 139-162.

33. Back, P.; Braeckman, B. P.; Matthijssens, F. ROS in aging Caenorhabditis elegans: damage or signaling? *Oxid Med Cell Longev* **2012,** *2012*, 608478.

34. Gray, J. M.; Karow, D. S.; Lu, H.; Chang, A. J.; Chang, J. S.; Ellis, R. E.; Marletta, M. A.; Bargmann, C. I. Oxygen sensation and social feeding mediated by a C. elegans guanylate cyclase homologue. *Nature* **2004,** *430* (6997), 317-322.

35. Chang, A. J.; Chronis, N.; Karow, D. S.; Marletta, M. A.; Bargmann, C. I. A distributed chemosensory circuit for oxygen preference in C. elegans. *PLoS Biol.*

2006, *4* (9), e274.

36. Hung, Y. C.; Lee, J. H.; Chen, H. M.; Huang, G. S. Effects of static magnetic fields on the development and aging of Caenorhabditis elegans. *J Exp Biol* **2010,** *213* (Pt 12), 2079-2085.

37. Lee, C. H.; Hung, Y. C.; Huang, G. S. Static magnetic field accelerates aging and development in nematode. *Commun Integr Biol* **2010,** *3* (6), 528-529.

38. Bessho, K.; Yamada, S.; Kunitani, T.; Nakamura, T.; Hashiguchi, T.; Tanimoto, Y.; Harada, S.; Yamamoto, H.; Hosono, R. Biological responses in Caenorhabditis elegans to high magnetic fields. *Experientia* **1995,** *51* (3), 284-288.

39. Kimura, T.; Takahashi, K.; Suzuki, Y.; Konishi, Y.; Ota, Y.; Mori, C.; Ikenaga, T.; Takanami, T.; Saito, R.; Ichiishi, E.; Awaji, S.; Watanabe, K.; Higashitani, A. The effect of high strength static magnetic fields and ionizing radiation on gene expression and DNA damage in Caenorhabditis elegans. *Bioelectromagnetics* **2008,** *29* (8), 605-614.

40. Lee, C. H.; Chen, H. M.; Yeh, L. K.; Hong, M. Y.; Huang, G. S. Dosage-dependent induction of behavioral decline in Caenorhabditis elegans by long-term treatment of static magnetic fields. *J Radiat Res* **2012,** *53* (1), 24-32.

41. Vidal-Gadea, A. G.; Ward, K. A.; Truong, N.; Parikh, A.; Beron, C.; Pierce-Shimomura, J. T. Magnetic orientation in C. elegans is mediated by a pair of magnetosensitive neurons. *(in preparation)* **2014**.

42. van West, P.; Morris, B. M.; Reid, B.; Appiah, A. A.; Osborne, M. C.; Campbell, T. A.; Shepherd, S. J. Oomycete plant pathogens use electric fields to target roots. *Mol Plant Microbe Interact* **2002,** *15* (8), 790-798.

43. Nuccitelli, R. A role for endogenous electric fields in wound healing. *Curr Top Dev Biol* **2003,** *58,* 1-26.

44. Tai, G.; Reid, B.; Cao, L.; Zhao, M. Electrotaxis and wound healing: experimental methods to study electric fields as a directional signal for cell migration. *Methods Mol Biol* **2009,** *571,* 77-97.

45. Messerli, M. A.; Graham, D. M. Extracellular electrical fields direct wound healing and regeneration. *Biol Bull* **2011,** *221* (1), 79-92.

46. Jaffe, L. F.; Nuccitelli, R. Electrical controls of development. *Annu Rev Biophys Bioeng* **1977,** *6*, 445-476.

47. McCaig, C. D. Studies on the mechanism of embryonic frog nerve orientation in a small applied electric field. *J Cell Sci* **1989,** *93* (Pt 4), 723-730.

48. Song, B.; Gu, Y.; Pu, J.; Reid, B.; Zhao, Z.; Zhao, M. Application of direct current electric fields to cells and tissues in vitro and modulation of wound electric field in vivo. *Nat Protoc* **2007,** *2* (6), 1479-1489.

49. Zhao, M.; Song, B.; Pu, J.; Wada, T.; Reid, B.; Tai, G.; Wang, F.; Guo, A.; Walczysko, P.; Gu, Y.; Sasaki, T.; Suzuki, A.; Forrester, J. V.; Bourne, H. R.; Devreotes, P. N.; McCaig, C. D.; Penninger, J. M. Electrical signals control wound healing through phosphatidylinositol-3-OH kinase-gamma and PTEN. *Nature* **2006,** *442* (7101), 457-460.

50. Ozkucur, N.; Monsees, T. K.; Perike, S.; Do, H. Q.; Funk, R. H. Local calcium elevation and cell elongation initiate guided motility in electrically stimulated osteoblast-like cells. *PLoS One* **2009,** *4* (7), e6131.

51. Cohen, D. J.; Nelson, W. J.; Maharbiz, M. M. Galvanotactic control of collective cell migration in epithelial monolayers. *Nat Mater* **2014,** *13* (4), 409-417.

52. Cortese, B.; Palamà, I. E.; D'Amone, S.; Gigli, G. Influence of electrotaxis on cell behaviour. *Integr Biol (Camb)* **2014,** *6* (9), 817-830.

53. Zupanc, G. K. H.; Bullock, T. H. From Electrogenesis to Electroreception: An Overview. In *Electroreception;* Bullock, T. H., Hopkins, C. D., Popper, A. N., Fay, R. R., Eds.; Springer Science+Business Media, Inc.: New York, NY, 2005; pp 5-46.

54. Coplin, S. P.; Whitehead, D. The functional roles of passive electroreception in non-electric fishes. *Anim Biol* **2004,** *54* (1), 1-25.

55. Albert, J. S.; Crampton, W. G. Electroreception and Electrogenesis. In *The Physiology of Fishes;* Lutz, P. L., Ed.; CRC Press: Boca Raton, FL, 2006; pp 429-470.

56. Scheich, H.; Langner, G.; Tidemann, C.; Coles, R. B.; Guppy, A. Electroreception and electrolocation in platypus. *Nature* **1986,** *319* (6052), 401-402.

57. Pettigrew, J. D. Electroreception in monotremes. *J Exp Biol* **1999,** *202* (Pt 10), 1447-

1454.

58. Czech-Damal, N. U.; Liebschner, A.; Miersch, L.; Klauer, G.; Hanke, F. D.; Marshall, C.; Dehnhardt, G.; Hanke, W. Electroreception in the Guiana dolphin (Sotalia guianensis). *Proc R Soc B* **2012,** *279* (1729), 663-668.

59. Clarke, D.; Whitney, H.; Sutton, G.; Robert, D. Detection and Learning of Floral Electric Fields by Bumblebees. *Science* **2013,** *340* (6128), 66-69.

60. Caveness, F. E.; Panzer, J. D. Nemic galvanotaxis. *Proceedings of the Helminthological Society* **1960,** *27* (1), 73-74.

61. Gupta, S. P. Galvanotactic reaction of infective larvae of Trichostrongylus retortaeformis. *Exp Parasitol* **1962,** *12*, 118-119.

62. Shapiro-Ilan, D. I.; Campbell, J. F.; Lewis, E. E.; Elkon, J. M.; Kim-Shapiro, D. B. Directional movement of steinernematid nematodes in response to electrical current. *J Invertebr Pathol* **2009,** *100* (2), 134-137.

63. Shapiro-Ilan, D. I.; Lewis, E. E.; Campbell, J. F.; Kim-Shapiro, D. B. Directional movement of entomopathogenic nematodes in response to electrical field: effects of species, magnitude of voltage, and infective juvenile age. *J Invertebr Pathol* **2012,** *109* (1), 34-40.

64. Sukul, N. C.; Croll, N. A. Influence of Potential Difference and Current on the Electrotaxis of Caenorhaditis elegans. *J Nematol* **1978,** *10* (4), 314-317.

65. Gabel, C. V.; Gabel, H.; Pavlichin, D.; Kao, A.; Clark, D. A.; Samuel, A. D. T. Neural circuits mediate electrosensory behavior in Caenorhabditis elegans. *The Journal of Neuroscience* **2007,** *27* (28), 7586-7596.

66. Jones, F. G. W. Some observations and reflections on host finding by plant nematodes. *Meded Lanbl Hoogesd Gent* **1960,** *25* (3-4), 1009-1024.

67. Rezai, P.; Siddiqui, A.; Selvaganapathy, P. R.; Gupta, B. P. Electrotaxis of Caenorhabditis elegans in a microfluidic environment. *Lab Chip* **2010,** *10*, 220-226.

68. Rezai, P.; Siddiqui, A.; Selvaganapathy, P. R.; Gupta, B. P. Behavior of Caenorhabditis elegans in alternating electric field and its application to their localization and control. *Appl Phys Lett* **2010,** *96* (15), 153702.

69. Rezai, P.; Salam, S.; Selvaganapathy, P. R.; Gupta, B. P. Effect of pulse direct current signals on electrotactic movement of nematodes Caenorhabditis elegans and Caenorhabditis briggsae. *Biomicrofluidics* **2011,** *5* (4), 044116.

70. Tong, J.; Rezai, P.; Salam, S.; Selvaganapathy, P. R.; Gupta, B. P. Microfluidic-based electrotaxis for on-demand quantitative analysis of Caenorhabditis elegans' locomotion. *J Vis Exp* **2013,** *75,* e50226.

71. Rezai, P.; Salam, S.; Selvaganapathy, P. R.; Gupta, B. P. Electrical sorting of Caenorhabditis elegans. *Lab Chip* **2012,** *12* (10), 1831-1840.

72. Cookson, M. R. α-Synuclein and neuronal cell death. *Mol Neurodegener* **2009,** *4,* 9.

73. Salam, S.; Ansari, A.; Amon, S.; Rezai, P.; Selvaganapathy, P. R.; Mishra, R. K.; Gupta, B. P. A microfluidics set up to study neuronal degeneration and identification of neuroprotective compounds in C. elegans. *Worm* **2013,** *2* (3), e24558.

74. Runkel, E. D.; Baumeister, R.; Schulze, E. Mitochondrial stress: Balancing friend and foe. *Exp Gerontol* **2014,** [Epub ahead of print].

75. Calì, T.; Ottolini, D.; Brini, M. Mitochondria, calcium, and endoplasmic reticulum stress in Parkinson's disease. *Biofactors* **2011,** *37* (3), 228-240.

76. Liu, D.; Zhang, M.; Yin, H. Signaling pathways involved in endoplasmic reticulum stress-induced neuronal apoptosis. *Int J Neurosci* **2013,** *123* (3), 155-162.

77. Mercado, G.; Valdés, P.; Hetz, C. An ERcentric view of Parkinson's disease. *Trends Mol Med* **2013,** *19* (3), 165-175.

78. Roussel, B. D.; Kruppa, A. J.; Miranda, E.; Crowther, D. C.; Lomas, D. A.; Marciniak, S. J. Endoplasmic reticulum dysfunction in neurological disease. *Lancet Neurol* **2013,** *12* (1), 105-118.

79. Stefani, I. C.; Wright, D.; Polizzi, K. M.; Kontoravdi, C. The role of ER stress-induced apoptosis in neurodegeneration. *Curr Alzheimer Res* **2012,** *9* (3), 373-387.

80. Tonkiss, J.; Calderwood, S. K. Regulation of heat shock gene transcription in neuronal cells. *Int J Hyperthermia* **2005,** *21* (5), 433-444.

81. Jung, A. E.; Fitzsimons, H. L.; Bland, R. J.; During, M. J.; Young, D. HSP70 and constitutively active HSF1 mediate protection against CDCrel-1-mediated toxicity.

Mol Ther **2008,** *16* (6), 1048-1055.

82. Fujikake, N.; Nagai, Y.; Popiel, H. A.; Okamoto, Y.; Yamaguchi, M.; Toda, T. Heat shock transcription factor 1-activating compounds suppress polyglutamine-induced neurodegeneration through induction of multiple molecular chaperones. *J Biol Chem* **2008,** *283* (38), 26188-26197.

83. Liangliang, X.; Yonghui, H.; Shunmei, E.; Shoufang, G.; Wei, Z.; Jiangying, Z. Dominant-positive HSF1 decreases alpha-synuclein level and alpha-synuclein-induced toxicity. *Mol Biol Rep* **2010,** *37* (4), 1875-1881.

84. Kilpatrick, K.; Novoa, J. A.; Hancock, T.; Guerriero, C. J.; Wipf, P.; Brodsky, J. L.; Segatori, L. Chemical induction of Hsp70 reduces α-synuclein aggregation in neuroglioma cells. *ACS Chem Biol* **2013,** *8* (7), 1460-1468.

85. Jiang, Y. Q.; Wang, X. L.; Cao, X. H.; Ye, Z. Y.; Li, L.; Cai, W. Q. Increased heat shock transcription factor 1 in the cerebellum reverses the deficiency of Purkinje cells in Alzheimer's disease. *Brain Res* **2013,** *1519*, 105-111.

86. Altun, Z. F.; Hall, D. H. Handbook of C. elegans Anatomy, 2005. WormAtlas. http://www.wormatlas.org/ver1/handbook/contents.htm.

Figures

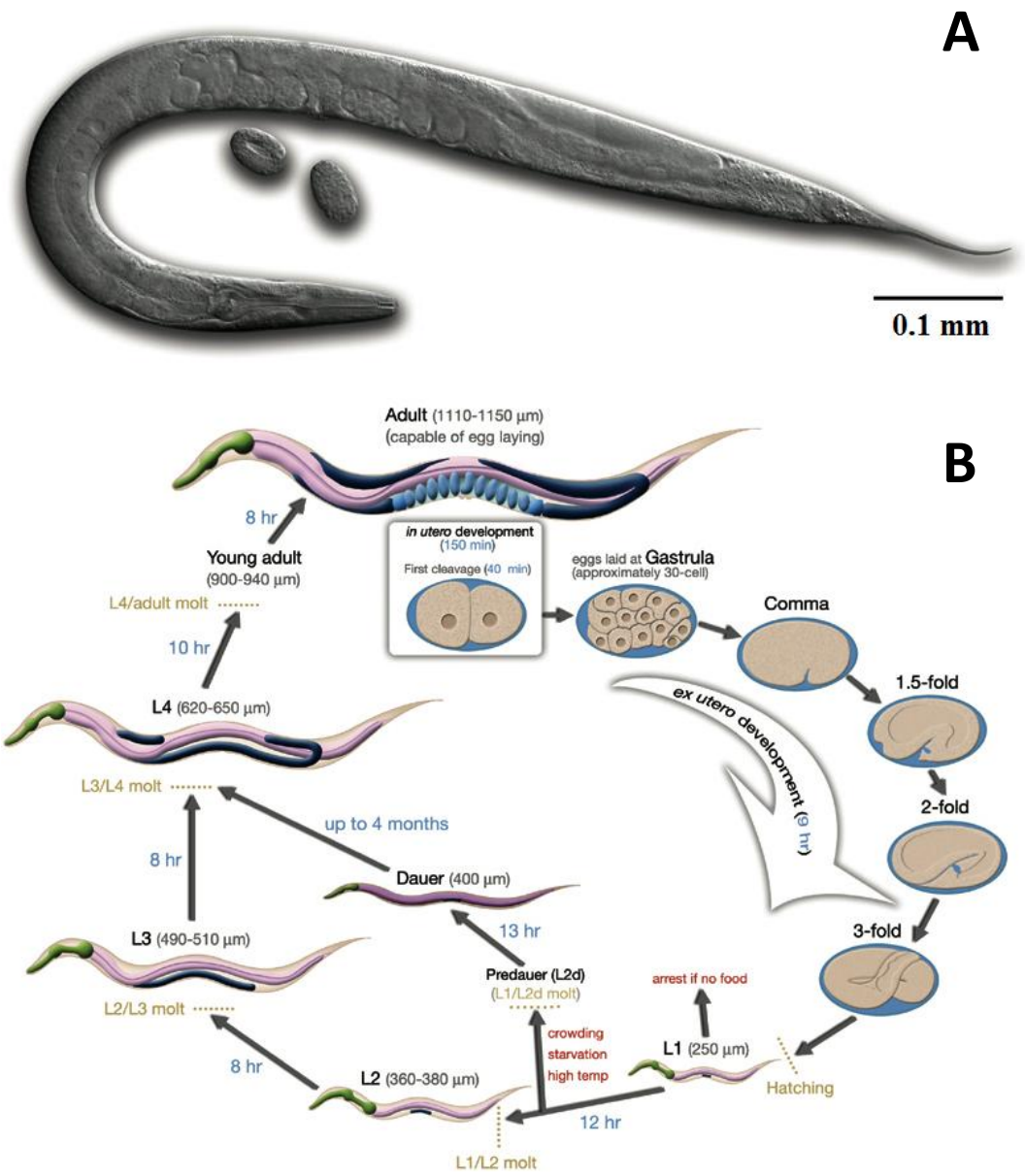

Figure 1. *C. elegans* and its life cycle. (A) DIC image of adult hermaphrodite, left lateral side. (B) Developmental stages and durations at 22°C. Adapted from WormAtlas **(**86**)** with permission from WormAtlas.

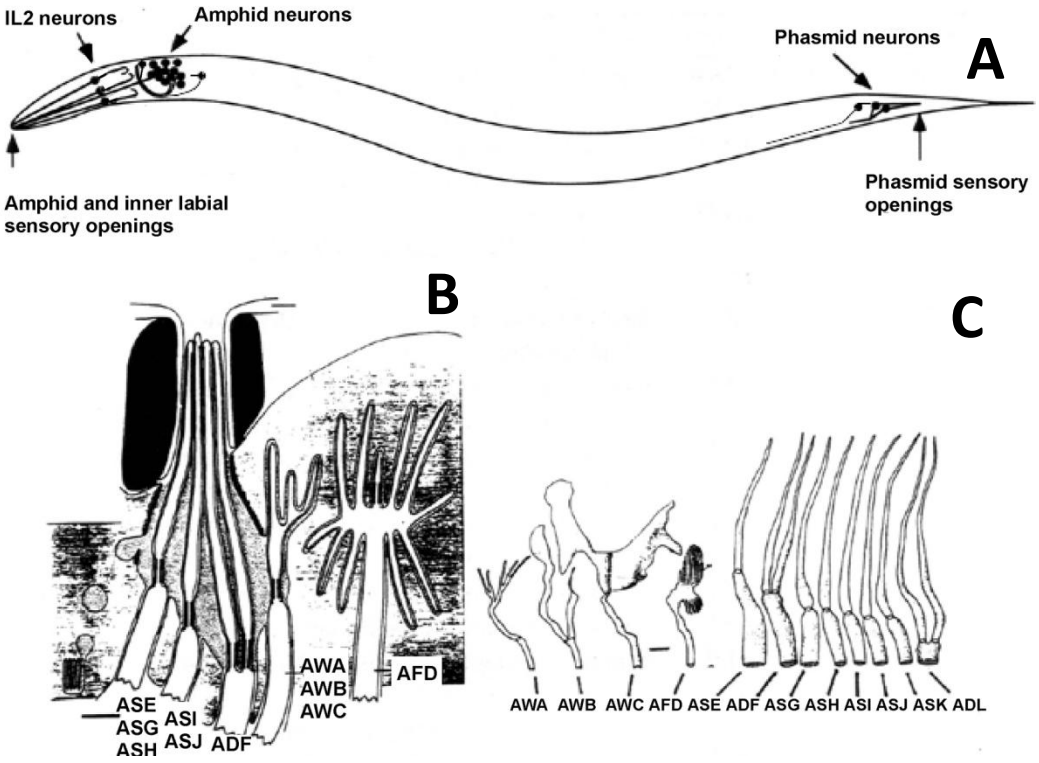

Figure 2. Structure of head and tail sensory organs in *C. elegans*. (A) Anatomical location of the amphids and phasmids. (B) Detailed structure of the amphid sensory opening showing ciliated nerve endings. (C) Detailed structure of the cilia in the 12 classes of amphid neurons. Adapted from WormBook **(**20**)** with permission from WormBook and Elsevier.

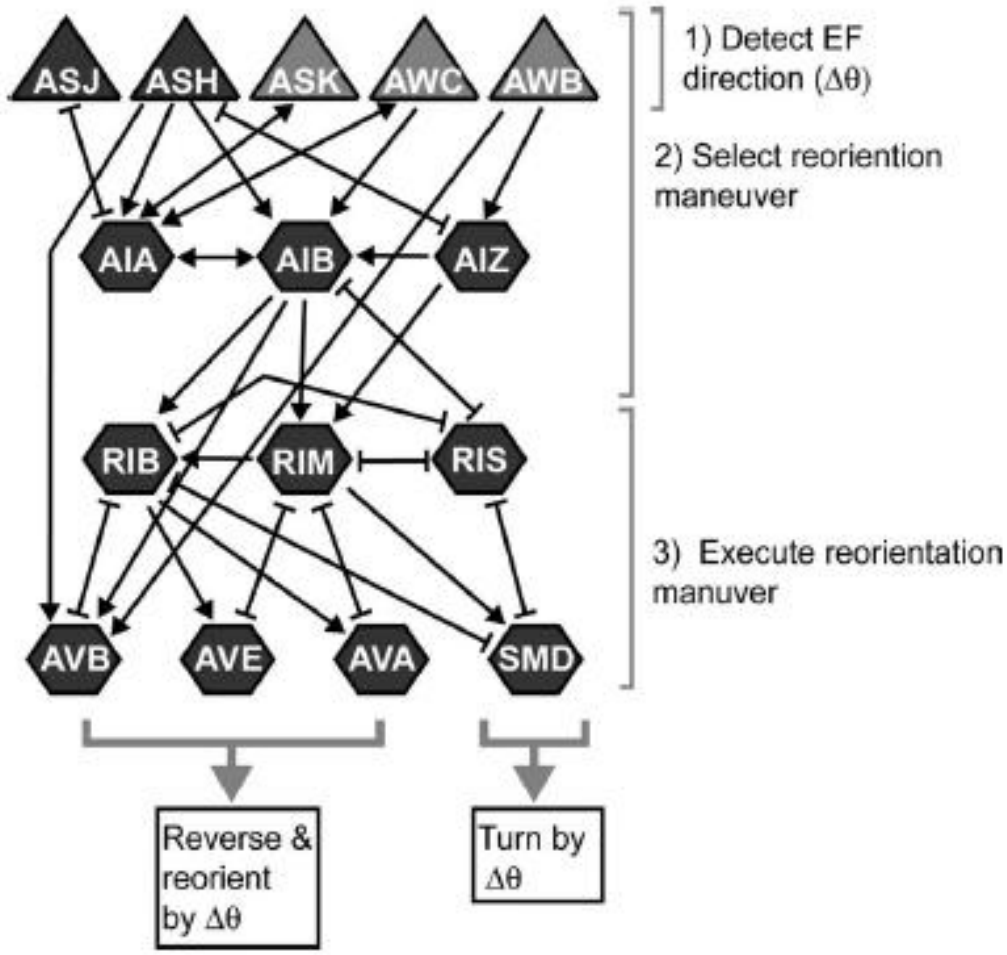

Figure 3. Neural circuits involved in electrosensation, as proposed by Gabel and colleagues **(**65**)**. Sensory neurons are represented as triangles, with those . Interneurons and command motor neurons are represented as hexagons. Pointed arrows indicate chemical synaptic connections between neurons. Flat-headed arrows indicate gap junctions. RIM and AVA appear to contribute to turns and reversals during electrosensory steering, respectively. Additional neurons show pathways that might connect ASJ, ASH, RIM, and AVA to motor output during electrotactic behavior. Adapted from Gabel and colleagues **(**65**)** with permission from SfN.

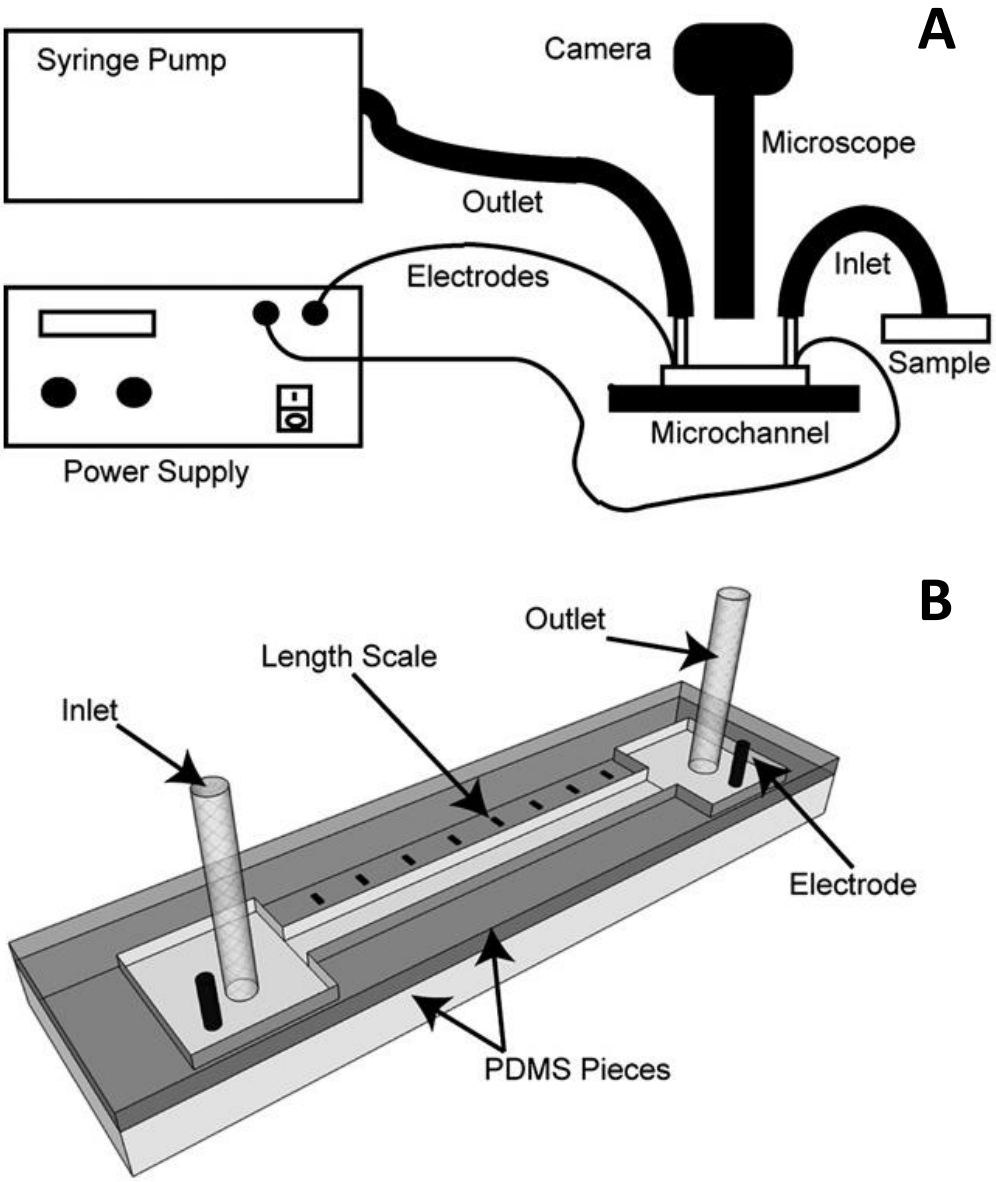

Figure 4. The microfluidic electrotaxis platform. (A) Worms are aspirated into the channel with a syringe or pump, electric field is generated by a power supply, and worm response is recorded with a microscope-mounted camera. (B) Sealed PDMS microchannel with electrodes and inlet/outlet tubes embedded in reservoir areas. Adapted from the original article by Rezai and colleagues **(**67**)** with permission from RSC.

Chapter 2-Microfluidic-based electrotaxis for on-demand quantitative analysis of *Caenorhabditis elegans*' locomotion

Citation & Author Contributions

JT served as the lead investigator and main author of this article, under the guidance of senior authors PRS and BPG. JT was directly involved in all steps including initial project formulation, assay optimization, data collection, data analysis (including implementation of newly developed software for automated analysis), and final dissemination. The second co-author PR was the original developer of the devices and assay described in this article and contributed to writing of the manuscript. The third co-author SS also contributed to writing of the manuscript.

> **Tong, J.**; Rezai, P.; Salam, S.; Selvaganapathy, P.R.; Gupta, B.P. Microfluidic-based electrotaxis for on-demand quantitative analysis of *Caenorhabditis elegans*' locomotion. *J Vis Exp* **2013,** *75,* e50226. doi: 10.3791/50226.

Reproduced in the current thesis document with permission from JoVE: http://www.jove.com/publish/submission-faq

Microfluidic-based electrotaxis for on-demand quantitative analysis of *Caenorhabditis elegans*' locomotion

Justin Tong, Pouya Rezai, Sangeena Salam, P Ravi Selvaganapathy, Bhagwati P Gupta

Justin Tong
Department of Biology, McMaster University
1280 Main St W, Hamilton, ON, Canada L8S4L8
tongjw@mcmaster.ca

Pouya Rezai
Department of Engineering, McMaster University
1280 Main St W, Hamilton, ON, Canada L8S4L8
rezaip@mcmaster.ca

Sangeena Salam
Department of Biology, McMaster University
1280 Main St W, Hamilton, ON, Canada L8S4L8
salamsd@mcmaster.ca

P Ravi Selvaganapathy
Department of Engineering, McMaster University
1280 Main St W, Hamilton, ON, Canada L8S4L8
selvaga@mcmaster.ca

Bhagwati P Gupta
Department of Biology, McMaster University
1280 Main St W, Hamilton, ON, Canada L8S4L8
guptab@mcmaster.ca

Corresponding author:

Bhagwati P Gupta

Phone: 905-525-9140 x26451

Fax: 905-522-6066

Keywords:

C. elegans, microfluidics, electrotaxis, locomotion, swimming, movement, neurodegeneration, neuronal signaling, dopamine, behavior

***Short Abstract*:** (50 words maximum)

A semi-automated micro-electro-fluidic method to induce on-demand locomotion in *Caenorhabditis elegans* is described. This method is based on the neurophysiologic phenomenon of worms responding to mild electric fields ("electrotaxis") inside microfluidic channels. Microfluidic electrotaxis serves as a rapid, sensitive, low-cost, and scalable technique to screen for factors affecting neuronal health.

***Long Abstract*:** (150 words minimum, 400 words maximum)

The nematode *Caenorhabditis elegans* is a versatile model organism for biomedical research because of its conservation of disease-related genes and pathways as well as its ease of cultivation. Several *C. elegans* disease models have been reported, including neurodegenerative disorders such as Parkinson's disease (PD), which involves the degeneration of dopaminergic (DA) neurons [1]. Both transgenes and neurotoxic chemicals have been used to induce DA neurodegeneration and consequent movement defects in worms, allowing for investigations into the basis of neurodegeneration and screens for neuroprotective genes and compounds [2, 3].

Screens in lower eukaryotes like *C. elegans* provide an efficient and economical means to identify compounds and genes affecting neuronal signaling. Conventional screens are typically performed manually and scored by visual inspection; consequently, they are time-consuming and prone to human errors. Additionally, most focus on cellular level analysis while ignoring locomotion, which is an especially important parameter for movement disorders.

We have developed a novel microfluidic screening system (**Fig. 1**) that controls and quantifies *C. elegans*' locomotion using electric field stimuli inside microchannels. We have shown that a Direct Current (DC) field can robustly induce on-demand locomotion towards the cathode ("electrotaxis") [4]. Reversing

the field's polarity causes the worm to quickly reverse its direction as well. We have also shown that defects in dopaminergic and other sensory neurons alter the swimming response [5]. Therefore, abnormalities in neuronal signaling can be determined using locomotion as a read-out. The movement response can be accurately quantified using a range of parameters such as swimming speed, body bending frequency and reversal time.

Our work has revealed that the electrotactic response varies with age. Specifically, young adults respond to a lower range of electric fields and move faster compared to larvae [4]. These findings led us to design a new microfluidic device to passively sort worms by age and phenotype [6].

We have also tested the response of worms to pulsed DC and Alternating Current (AC) electric fields. Pulsed DC fields of various duty cycles effectively generated electrotaxis in both *C. elegans* and its cousin *C. briggsae* [7]. In another experiment, symmetrical AC fields with frequencies ranging from 1Hz to 3KHz immobilized worms inside the channel [8].

Implementation of the electric field in a microfluidic environment enables rapid and automated execution of the electrotaxis assay. This approach promises to facilitate high-throughput genetic and chemical screens for factors affecting neuronal function and viability.

***PROTOCOL*:**

1.) Photolithography for Master Mold Fabrication

1.1) Bathe a 3-inch silicon wafer in acetone for 30sec and then methanol for 30sec. Rinse with de-ionized water for 5min.

1.2) Dry the wafer's surface with a N_2 blow gun. Heat the wafer on a hotplate at 140ºC for 2min.

1.3) Plasma oxidize the surface of the silicon wafer (1 min. 50W).

1.4) Spin-coat the wafer's surface with 3mL SU-8 100 photoresist (40sec, 1,750rpm).

1.5) Pre-bake the coated wafer on a hotplate at 65ºC for 10min, then ramp the temperature up to 95ºC over 2min. Maintain this setting for an additional 1h.

1.6) Align a photomask containing the desired channel design. Expose the resist to 550-600mJ/cm^2 of UV light (350-400nm). Photomasks can be designed in AutoCAD and printed on a transparency with high resolution printing.

1.7) Post-bake the wafer on a hotplate at 65ºC for 1min and 95ºC for 10min, ramping the temperature as before.

1.8) Immerse the wafer in SU-8 developer solution for 10-15min. Check for completion of development by rinsing with isopropanol. If a white precipitate appears, continue developing. The master mold is shown in **Fig. 2A**.

2.) Soft Lithography for Microchannel Fabrication

2.1) Mix 35ml polydimethylsiloxane (PDMS) elastomer base with 3.5mL PDMS curing agent.

2.2) Place the fabricated master mold (pattern facing up) and a blank silicon wafer into Petri dishes lined with aluminum foil.

2.3) Pour 20mL PDMS prepolymer into the master mold dish and 15mL into the second dish. Eliminate air pockets underneath the wafers by gently pressing on them with a disposable wooden applicator.

2.4) Cover both dishes and set aside for a day to cure. Alternatively, for faster curing, remove air bubbles from the PDMS using a vacuum degasifier and then leave the dishes on a hotplate at 80°C for 2h.

2.5) Remove the foil and peel the PDMS from the wafers.

2.6) Use the Harris Uni-Core (2.5mm) to punch fluid access ports at both ends of the channel. Cut the channel and blank PDMS into similarly sized strips.

2.7) Load the channel, the blank PDMS strip and a glass slide (75×25 mm^2) into a plasma oxidizer, likely located in a cleanroom. Expose to oxygen plasma for 40sec at 40W power.

2.8) Stick the channel piece and glass slide to opposite sides of the blank strip. Set aside for 2h to complete the bonding.

2.9) Attach plastic tubing (inner diameter 1/32”, outer diameter 3/32”), each at least six inches long, to the punched reservoirs using PDMS prepolymer. Affix a

fluidic plastic connector to one or both tubes to allow syringe attachment, or use commercially available fittings.

2.10) Place the assembly onto a hotplate at 120ºC. Insert 3" lengths of 22 gauge insulated copper wire into each reservoir, between the inlet tube and the channel, and secure with PDMS prepolymer. The finished product is shown in **Fig. 2B**.

3.) Electrotaxis Experiment

3.1) Place the microchannel on the stage (preferably XY-movable) of a microscope with a mounted camera connected to a monitor (**Fig. 1**).

3.2) Connect the power supply or amplifier's output wires to the microchannel's electrodes. A simple DC power supply is sufficient if only a DC signal is desired, but an amplifier connected to a function generator allows application of pulsed DC and AC signals as well.

3.3) Attach the microchannel's output tube to a disposable syringe. Submerge the mouth of the inlet tube in M9 physiological buffer and gently aspire liquid into the channel by applying a negative pressure inside the syringe (either manually or using a syringe pump). When the inlet and outlet tubes are both filled with M9, disconnect the syringe from the tube. Level both tubes to the same height to prevent hydrostatically driven flow.

3.4) Apply a DC voltage to the channel and ensure that resistance (R=V/I) is around 0.6MΩ (for a 50mm long, 0.3mm wide and ~0.1mm deep microchannel).

3.5) If satisfied with the channel's integrity, follow the above steps to load worms from a diluted suspension into the channel.

3.6) Disconnect the syringe and hydrostatically manipulate the flow by adjusting the tubes' relative height. Use this method to place a worm in the center of the channel and then lay both tubes flat at the same elevation.

3.7) Set the power supply to the appropriate voltage: 4-12V/cm for L3 stage animals, 4-10V/cm for L4s, and 2-4V/cm for young adults. Activate the electric signal and allow 1min of pre-exposure for the worm to acclimatize to the field. The worm should begin moving towards the cathode. When the minute has passed, use the camera to begin recording.

3.8) For AC and pulsed DC experiments, the maximum responsive electric field can be adopted from above and frequency and duty cycle of the signal can be modulated as desired [7, 8].

3.9) When experiment is finished, remove all liquid (and worms) from the channel, rinse it with de-ionized water, and leave the device on a hotplate at 125°C to dry.

3.10) Extract locomotory data from recorded videos manually using NIH ImageJ (*http://rsbweb.nih.gov/ij/*) or custom MATLAB-based worm tracking software.

***REPRESENTATIVE RESULTS*:** A representative video of a wild-type young adult nematode's electrotaxis and its position and velocity outputs from the worm tracking software are shown in **Supplementary Video 1** and **Fig. 3**. The movement analysis software itself does not recognize the direction of field polarity and the time of polarity reversal; rather, this information must be obtained from the source video. This could be done using an audio or visual cue in the video or writing down experimental conditions and manipulations.

Electrotaxis speed data from a set of wild-type (N2) and transgenic animals (NL5901) are displayed in **Fig. 4**. The NL5901 animals carry human □-*synuclein* gene under the control of *unc-54* (myosin heavy chain gene) promoter. The expressed □-*synuclein* in body wall muscles aggregates [9] and our results show that it causes abnormalities in the electrotactic response. The speed of NL5901 worms is significantly slower than wild type. To plot the graph, we calculated the speed of individual worms and plotted results in a box plot using Minitab statistical software (*http://www.minitab.com*). In addition to speed, other parameters of movement, such as turning response (time taken to complete the reversal in response to electric field polarity change) and body bending frequency (average number of sine waves per second), can also be analyzed as described elsewhere [5].

The electrotaxis protocol works best with a synchronized population, which can be obtained via treatment with a bleach solution (sodium hypochlorite and 4N sodium hydroxide in a 2:3 volume ratio) [10]. All data presented here was obtained from synchronized populations to rule out age- and stage-dependent variation. While we have used young adults (69 hrs post-L1 at 20^0C), other stages (L2 onwards) can also be tested.

Tables and Figures:

Figure 1: Schematic of microfluidic screening platform for nematode electrotaxis assay.

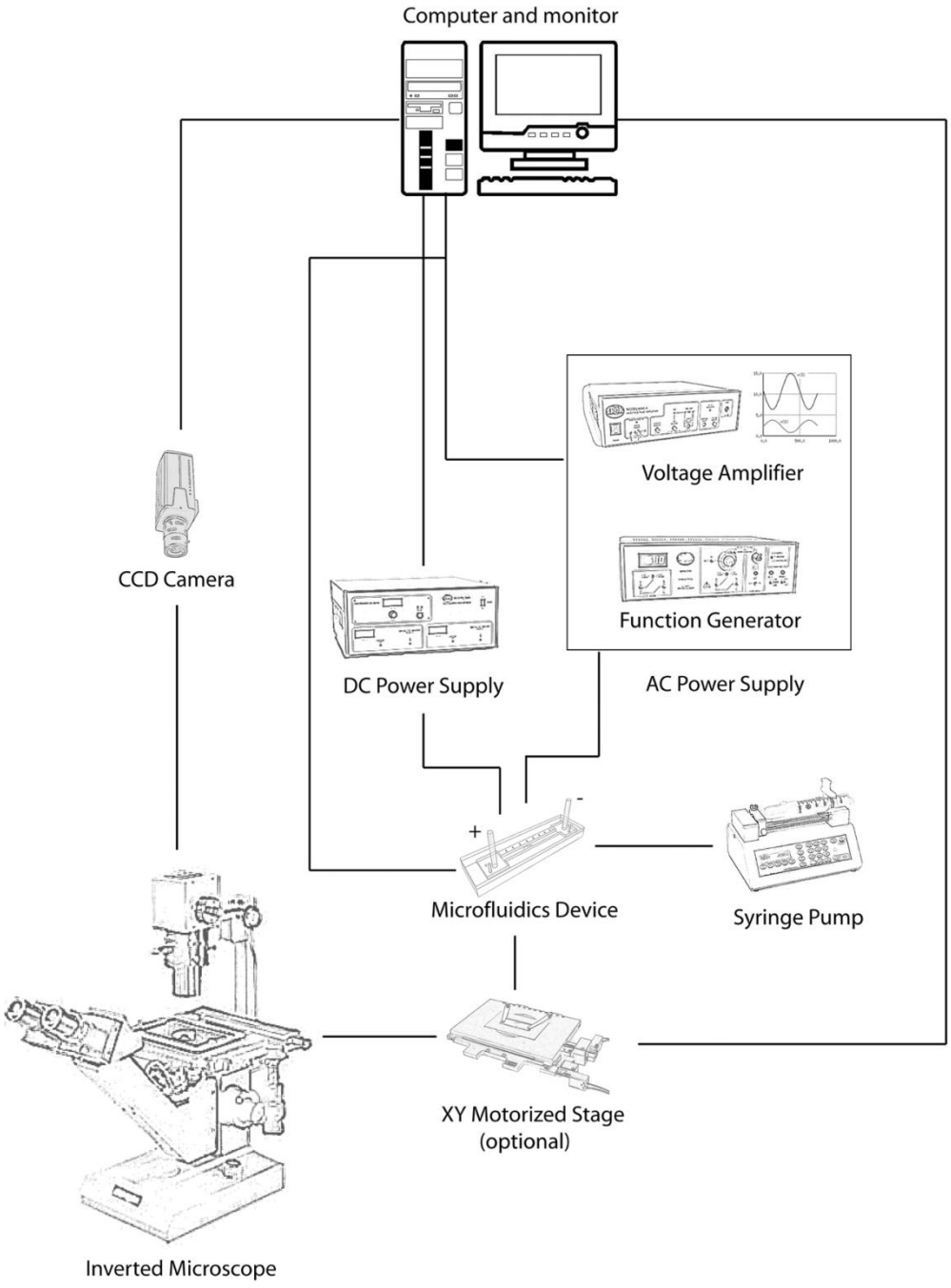

Figure 2: Master mold (A) and fully assembled PDMS microchannel device (B).

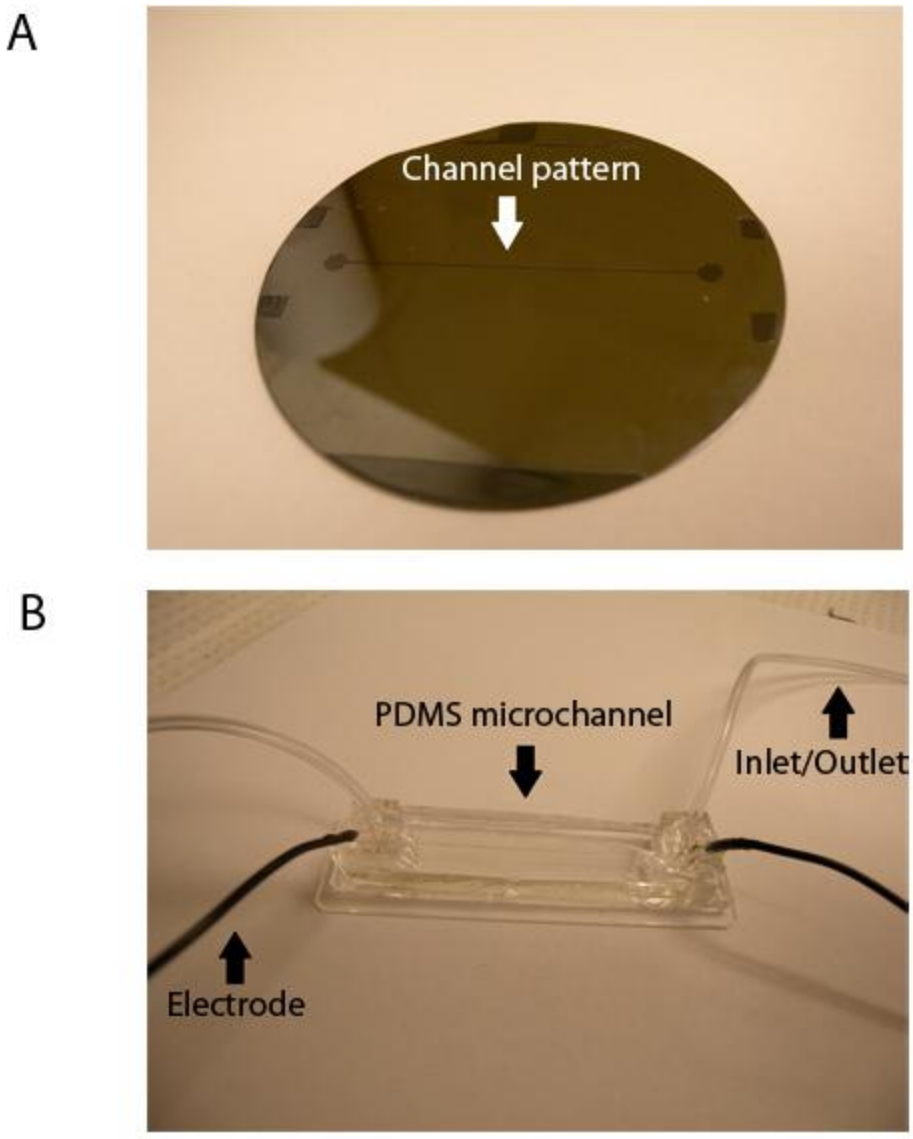

Figure 3: Position vs. time (A) and instantaneous velocity (B) outputs of custom worm tracking program. Source video is Supplementary Video 1 above. The program calculates the velocity curve from the position-time curve but disregards the spikes when calculating average speed.

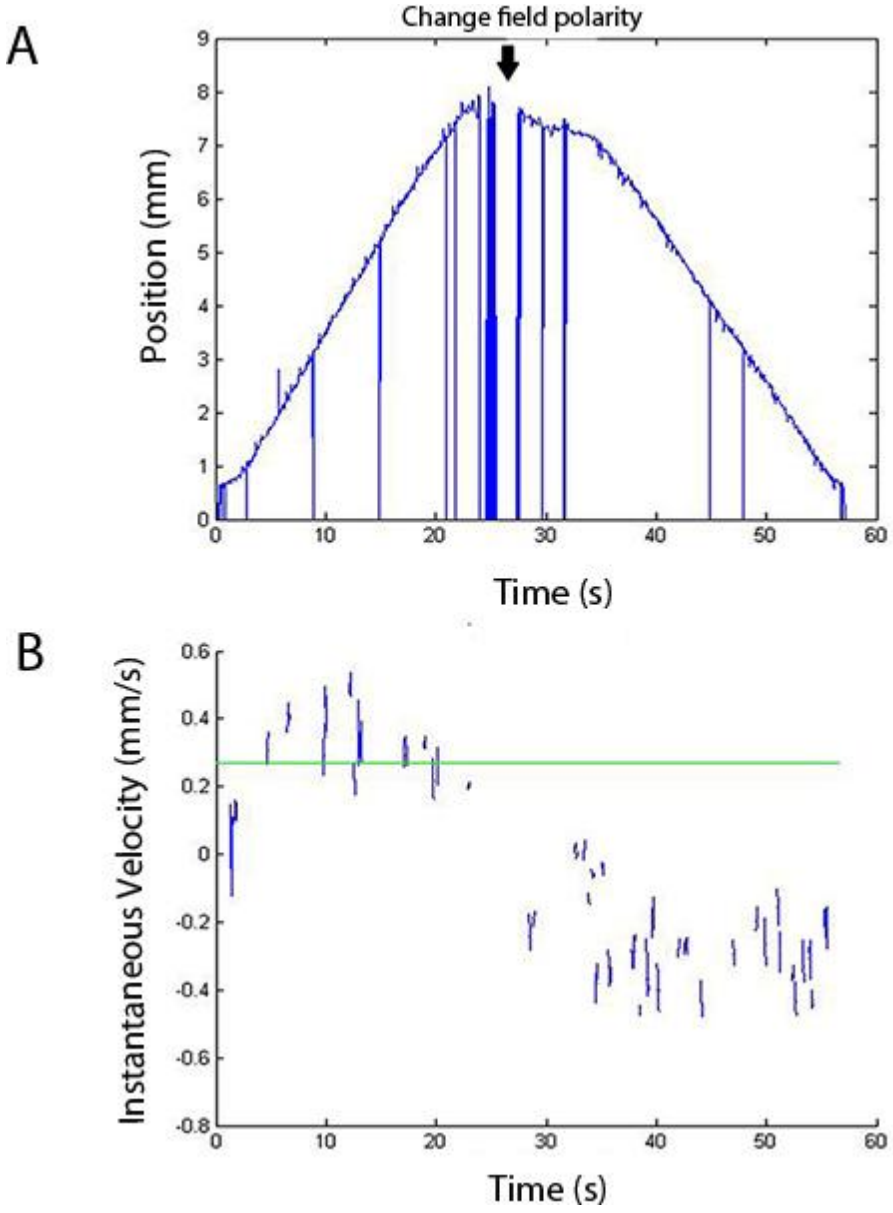

Figure 4: Electrotaxis speed of wild-type control N2 and transgenic NL5901 worms. NL5901 worms are significantly slower than control with p>0.0001. Significance is determined using the non-parametric Mann-Whitney test. n = 10 for N2 and n = 23 for NL5901.

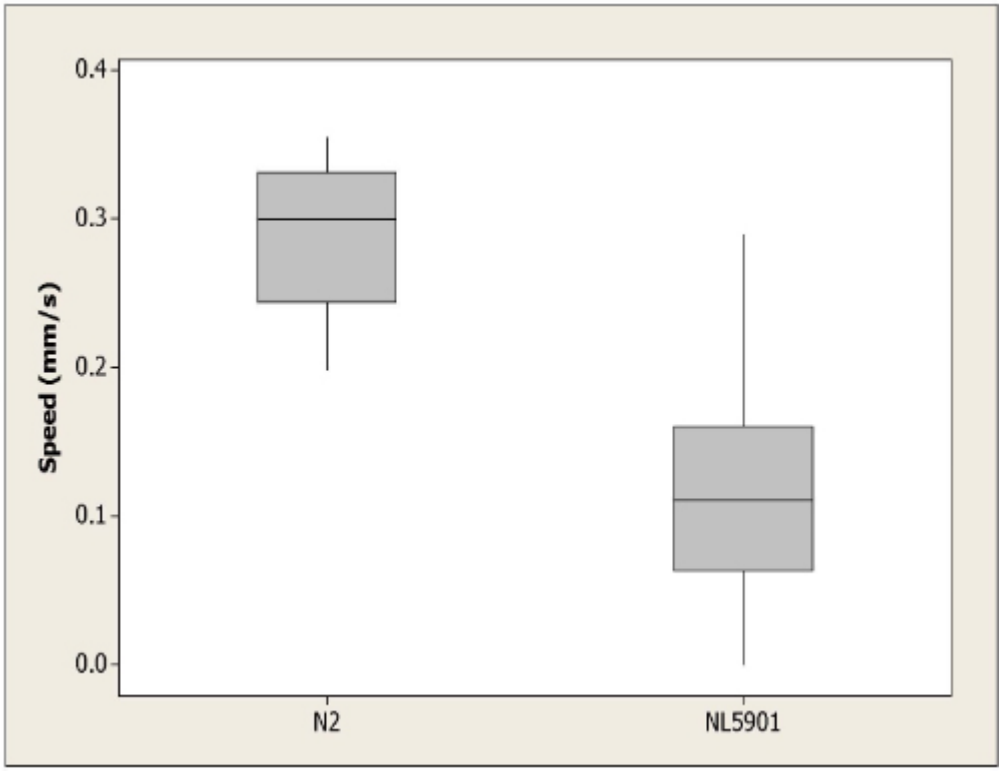

Supplementary Video 1: Electrotactic behaviour of young adult nematode in a microfluidic channel. Video begins with cathode to the right. Appearance of glass pipette indicates impending polarity reversal; subsequent removal of the pipette signals moment of reversal.

***DISCUSSION*:** Taking advantage of the behavioural phenomenon first described by Gabel and colleagues and building on the dielectrophoretic manipulation work of Chuang and colleagues [11, 12], our microfluidic-based electrotaxis assay provides an easy, robust and sensitive method to probe neuronal activity in worms using movement as an output. The analysis of movement parameters allows quantitative comparison between different genotypes. The precision of microchannel fabrication and electric field application together provide both a controllable environment and a means to communicate with the worm for locomotion control. Different electric signal wave shapes have different behavioural reflections in the worm and have been used to both stimulate and inhibit locomotion.

The single-channel design of the present microfluidic device requires that only a single worm be scored at a time. For this, worm solution must be sufficiently diluted with M9 buffer before attempting to load worms into the channel. It is important to point out that channel operations can be complicated by the presence of air bubbles and other irregularities affecting the hydrostatic pressure. This could be eliminated by flushing the channel with M9 and manipulating the elevation of the inlet and outlet tubes.

The assay described here can be improved further. A multi-channel microfluidic chip could accelerate worm screening, although it will require integration of other control mechanisms such as worm loading, positioning and tracking. Further automation of the electrotaxis protocol, especially computer-controlled flow management, will increase efficiency. These enhancements are currently under development in our laboratory.

Extraction of locomotion data from electrotaxis videos was originally performed manually using ImageJ, which is a slow and tedious process. To increase efficiency and eliminate human error, we have begun to use a worm tracking program adapted from an original MATLAB-based package developed at California Institute of Technology [13]. The software currently processes single-worm videos. The latest version is suitable for a wide range of assays including

chemically-treated worms and neuronal and muscle mutants. One of its limitations is that spontaneous reversals, observed in certain neuronal mutants (e.g., *osm-5*) [5], are not interpreted correctly. Such worms must be analyzed manually.

Limitations notwithstanding, microfluidic electrotaxis can be applied in myriad contexts, including drug discovery assays with worm models of movement-related disorders. Considering its amenability to parallelization, electrotaxis is particularly well suited for high-throughput screening applications. Genetic and age-dependent analysis of electrotactic behaviour and neuronal degeneration may also be studied with this system. Additionally, worms may be sorted by age or phenotype to form synchronized samples or to identify new mutants for forward genetic screens [6, 14].

ACKNOWLEDGEMENTS:

The authors would like to thank the Natural Sciences and Engineering Research Council of Canada, Canada Research Chairs Program, Canadian Institutes of Health Research, and Ontario Ministry of Research and Innovation through their Early Researchers Award Program for financial support.

DISCLOSURES: The microfluidic electrotaxis assay technology has been filed for patent in the United States of America and Canada.

Table of Specific Reagents and Equipment:

Name of the reagent	Company	Catalogue number	Comments (optional)
Acetone	CALEDON Labs	1200-1-30	
Methanol	CALEDON Labs	***6700-1-30***	
Isopropanol	CALEDON Labs	***8600-1-40***	
SU-8	Microchem Corp.	Y131273	SU-8 100
SU-8 Developer	Microchem Corp.	Y020100	
92x16mm Petri Dish	Sarstedt	82.1473.001	
Sylgard 184 Silicone Elastomer Kit	Dow Corning		Contains elastomer base and curing agent
Function generator	Tektronix Inc.		Model AFG3022B
Amplifier	Trek Inc.		Model 2210-CE
Syringe pump	Harvard Apparatus	70-4506	Model 11 ELITE
Hotplate	Fisher Scientific	11675916Q	Model HP131725Q

REFERENCES

[1] Kuwahara, T., Koyama, A., et al. Familial Parkinson mutant α-synuclein causes dopamine neuron dysfunction in transgenic *Caenorhabditis elegans*. *J. Biol. Chem.* **281** (1), 334-340 (2006).

[2] Kuwahara, T., Koyama, A., et al. A systematic RNAi screen reveals involvement of endocytic pathway in neuronal dysfunction in a-synuclein *transgenic C. elegans*. *Hum. Mol. Genet.* **17** (19), 2997-3009 (2008).

[3] Su, L. J., Auluck, P. K., et al. Compounds from an unbiased chemical screen reverse both ER-to-Golgi trafficking defects and mitochondrial dysfunction in Parkinson's disease models. *Dis. Model Mech.* **3** (3-4), 194-208 (2010).

[4] Rezai, P., Siddiqui, A., Selvaganapathy, P. R., & Gupta, B. P. Electrotaxis of *Caenorhabditis elegans* in a microfluidic environment. *Lab Chip*. **10** (2), 220-226 (2010).

[5] Salam, S., Ansari, A., et al. A microfluidics set up to study neuronal degeneration and identification of neuroprotective compounds in *C. elegans*. (submitted).

[6] Rezai, P., Salam, S., Selvaganapathy, P. R., & Gupta, B. P. Electrical sorting of *Caenorhabditis elegans*. *Lab Chip*. **12** (10), 1831-1840 (2012).

[7] Rezai, P., Salam, S., Selvaganapathy, P. R., & Gupta, B. P. Effect of pulse direct current signals on electrotactic movement of nematodes *Caenorhabditis elegans* and *Caenorhabditis briggsae*. *Biomicrofluidics*. **5** (4), 044116 (2011).

[8] Rezai, P., Siddiqui, A., Selvaganapathy, P. R., & Gupta, B. P. Behavior of *Caenorhabditis elegans* in alternating electric field and its application to their localization and control. *Appl. Phys. Lett.* **96** (15), 153702 (2010).

[9] van Ham, T. J., Thijssen, K. L., Breitling, R., Hofstra, R. M., Plasterk, R. H., & Nollen, E. A. *C. elegans* model identifies genetic modifiers of alpha-synuclein inclusion formation during aging. *PLoS Genet.* **4**, e1000027 (2008).

[10] Brenner, S. The genetics of *Caenorhabditis elegans*. *Genetics.* **77** (1), 71-94 (1974).

[11] Gabel, C. V., Gabel, H., Pavlichin, D., Kao, A., Clark, D. A., & Samuel, A. D. Neural circuits mediate electrosensory behavior in *Caenorhabditis elegans*. *J. Neurosci.* **27** (28), 7586-7596 (2007).

[12] Chuang, H.-S., Raizen, D. M., Lamb, A., Dabbish, N., & Bau, H. H. Dielectrophoresis of *Caenorhabditis elegans*. *Lab Chip* **11** (4), 599-604 (2011).

[13] Cronin, C.J., Mendel, J.E., Mukhtar, S., Kim, Y-M., Stirbl, R.C., Bruck, J., & Sternberg, P.W. An automated system for measuring parameters of nematode sinusoidal movement. *BMC Genet*. **6**:5 (2005).

[14] Manière, X., Lebois, F., Matic, I., Ladoux, B., Di Meglio J-M., & Hersen, P. Running worms: *C. elegans* self-sorting by electrotaxis. *PLoS One*, **6** (2), e16637 (2011).

Significance

This work represents the optimization of the processes of microchannel fabrication and electrotaxis speed measurement, especially using software-automated methods. This article was the first to report the use of our custom Matlab-based software to analyze electrotactic swimming and therefore set the stage for higher-throughput applications of the microfluidic electrotaxis platform, such as those described in the following chapters.

Chapter 3-Chronic exposure to metal salts induces defects in the electrotactic swimming behaviour of the nematode *C. elegans*

Citation & Author Contributions

This study was carried out by JT under the supervision of PRS, RKM, and BPG. JT was responsible for all data collection, analysis, and reporting for dissemination. PR supplied microfluidic devices and consultation.

> **Tong, J.**; Rezai, P.; Selvaganapathy, P.R.; Mishra, R.K.; & Gupta, B.P. Chronic exposure to metal salts induces defects in the electrotactic swimming behaviour of the nematode *Caenorhabditis elegans*. *J Appl Toxicol* (submitted, July 2014).

Chronic exposure to metal salts induces defects in the electrotactic swimming behavior of the nematode *Caenorhabditis elegans*

Justin Tong[1], *Pouya Rezai*[2†], *P. Ravi Selvaganapathy*[2], *Ram K. Mishra*[3], *Bhagwati P. Gupta*[1]

[1]Department of Biology, McMaster University, Hamilton, ON

[2]Department of Mechanical Engineering, McMaster University, Hamilton, ON

[3]Department of Psychiatry and Behavioural Neurosciences, McMaster University, Hamilton, ON

Short title: Metal salts induce electrotactic swimming defects in *C. elegans*

Corresponding author: guptab@mcmaster.ca

Present addresses: †Department of Mechanical Engineering, York University, Toronto, ON

Key words: *C. elegans*, microfluidics, electrotaxis, bioindicator, metals

ABSTRACT

We examined the effects of chronic exposure to various environmental toxicants on the nematode *C. elegans*' electrotactic behavior using a specially designed microfluidic channel device. Nine commonly used chemicals including industrial solvent, heavy metal, and herbicide, were tested. The results provide the first evidence that electrotactic swimming behavior is particularly susceptible to knockdown by metal salts. Specifically, $AgNO_3$, $CuSO_4$, $HgCl_2$, and MeHgCl induced significant swimming speed deficits at ecotoxicologically relevant concentrations. A comparison with traditional assays that measured fecundity, growth, and lifespan revealed that electrotactic speed shows a comparable level of sensitivity as a toxicity endpoint. *In vivo* measurements of metal concentrations following exposure suggest that bioaccumulation may be a factor determining metals' capacity to cause electrotactic deficits. In conclusion, our work demonstrates that the electrotactic swimming behavior of *C. elegans* is susceptible to metal exposure. The speed and sensitivity of the microfluidic assay makes it a promising non-invasive approach to detect environmental toxicants and examine their effects on locomotory behavior in multicellular eukaryotes.

SHORT ABSTRACT

We present a novel application of a microfluidic *C. elegans* electrotaxis platform for the detection of metal salt toxicity. Results show that worms' electrotactic swimming behavior is particularly sensitive to metal salts among environmental toxicants. Comparison with fecundity, growth, and lifespan assays reveals a similar level of sensitivity in the electrotaxis assay. *In vivo* measurements of metal concentrations following exposure suggest bioaccumulation may influence metals' capacity to cause electrotactic deficits.

1. INTRODUCTION

The various activities of modern civilization produce a slew of chemical byproducts that gradually accumulate in the environment. In particular, metals have been known to reach concentrations that are hazardous to humans; though naturally present at low levels in ecosystems, their widespread use in paints, preservatives, and industrial processes has significantly increased the presence of some metals and their compounds (Craig, et al., 2003). One method of evaluating the threat posed by environmental contamination is found in whole-sample analysis with bioindicator animals, as was proposed by the US Environmental Protection Agency (EPA) in a bid to secure early warnings of potential environmental hazards (Weber, 1993).

The nematode *Caenorhabditis elegans* is well suited for this purpose because it balances ease of cultivation with conservation of disease-related genes and pathways. These animals are sensitive to most toxicants of interest, including metal salts, and have been used in acute aquatic toxicity tests since the 1980s (Williams and Dusenbery, 1988). A standardized method for soil toxicity tests using *C. elegans* has also been published in the American Society for Testing and Materials (ASTM) Guide E2172-01 (2002). Because its advantages as a model facilitate high-throughput experimentation, *C. elegans* has been employed in various toxicity studies ranging from mechanistic toxicology to environmental assessment to chemical and genetic screening (Leung, et al., 2008). At the same time, its sensitivity to a diverse range of toxicants renders it useful for assessing toxicity at environmentally relevant concentrations (Nouara, et al., 2013; Ju, et al., 2013; Wu, et al., 2012).

A number of effective test endpoints have been developed for toxicity analyses with *C. elegans*. LC_{50} (lethal concentration 50) of acute copper exposure in agar, liquid medium, and soil was established by Dusenbery and colleagues in a series of studies (Williams and Dusenbery, 1988; Williams and Dusenbery, 1990; Donkin and Dusenbery, 1993); however, more sensitive, sub-lethal assays were required to sense metals at concentrations more commonly found in the environment (Wang and Xing, 2008). Since then, endpoints such as brood size, growth, and lifespan have been utilized to address this deficiency (Harada, et al., 2006; Traunspurger, et al., 1997). Transgenic and fluorescent microscopy techniques have also been employed to visualize metal-induced damage (Chu and Chow, 2002; Du and Wang, 2008; Xing, et al., 2009). Moreover, locomotion behavior has shown promise as an indicator of neuronal toxicity, with slow and abnormally uncoordinated movement being associated with nervous defects (Wang and Xing, 2008; Williams and Dusenbery, 1990).

Microfluidics is well suited for nematode experiments of this nature due to the miniature scale, low expense, and design flexibility of microfluidic devices

(Crane, et al., 2010). Robust methods of inducing on-demand locomotion and maintaining directionality within a microfluidic environment have been developed recently by our group (Rezai, et al., 2010a; Rezai, et al., 2010b). The techniques are based on a phenomenon first described by Sukul and Croll (Sukul and Croll, 1978) whereby *C. elegans* alters its direction of movement in response to mild electric fields, a behavior known as "electrotaxis." By combining electrotaxis with microfluidic technology, it has been a simple matter to create an environment where the animal reliably chooses to swim toward the negative electrode in the presence of a direct current (DC) electric field (Rezai, et al., 2010b).

Cell ablation experiments conducted by Gabel and colleagues (2007) revealed that no single neuron is responsible for electrosensation, though several amphid sensory neurons including ASH and ASJ were shown to contribute. Moreover, ablating all dendrites in both amphid bundles was observed to severely disrupt electrosensory behavior, further implicating the importance of amphid neurons in electrosensation (Gabel, et al., 2007). However, more work is required to fully explore the neuronal signaling and underlying mechanisms that mediate electrotaxis.

Since electrotaxis is mediated by neurons and muscles, abnormalities in the function of either cell type can be detected by the assay using locomotion, specifically swimming speed, as a read-out (Tong, et al., 2013). Such control over nematode locomotion makes the microfluidic electrotaxis assay a valuable technique for toxicity screening.

In the present study, we used a novel microfluidic approach to evaluate the deleterious effects of chronic exposure to a range of chemicals on the electrotaxis movement behavior of *C. elegans.* The chemicals include inorganic and organic metals ($AgNO_3$, $CuSO_4$, $HgCl_2$, and MeHgCl), synthetic xenoestrogens (bisphenol A [BPA] and nonylphenol [NP]), a herbicide (paraquat [PQ]), a narcotic (tricaine mesylate [MS-222]), and an industrial solvent (toluene). Ag is known to be toxic to many taxa, causing developmental deformities in zebrafish (Bar-Ilan, et al., 2009), neurotoxicity in mice (Rahman, et al., 2009), and mitochondrial damage to human cells (Asharani, et al., 2009). Cu is comparatively less malignant as it is in fact an essential trace element in plants and animals, having a natural biological role as a component of various oxidases and other enzymes (Halfdanarson, et al., 2008). However, chronic excesses of Cu caused by regular ingestion (e.g. when cooking with copper cookware) or by Cu retention (i.e. Wilson's disease) have been linked to brain and liver damage (Ala, et al., 2007). Hg and its compounds are notorious for their extreme toxicity, having been employed as murder and assassination tools at various points in history. While the targets of Hg are quite diverse, including the respiratory and gastrointestinal tracts, Hg is most infamous for its neurotoxic properties: even acute exposures can induce an assortment of cognitive, personality, sensory, and

motor abnormalities, possibly culminating in coma and death (Clarkson and Magos, 2006). A large fraction of the Hg that enters aquatic ecosystems undergoes methylation to assume its organic form MeHg, which represents a major modern concern surrounding the fish industry (Forsyth, et al., 2004). BPA is a compound used in epoxy resins and certain plastics, including food packaging, that exhibits estrogen hormone-like properties at high concentrations with toxic effects in both animal models and human placental cell cultures (Kim, et al., 2001; Benachour and Aris, 2009). Able to migrate from polymer to food at high temperatures, BPA has been detected in over 90% of American urine samples (Benachour and Aris, 2009). NP is a family of compounds that, like BPA, are considered xenoestrogens and exhibit a number of toxic properties. NP has been shown to affect mitochondrial membrane permeability, contribute to dysregulation of Ca^{2+} transport in skeletal muscle, and increase proliferation of mammary gland cells (Soares, et al., 2008). Many industrial surfactants are in fact NP ethoxylates, which release NP into riverbeds and soil upon degradation; subsequently, humans may be exposed through contaminated drinking water and/or produce (Soares, et al., 2008). PQ is a herbicide that has been linked to Parkinson's disease (Blesa, et al., 2012), routinely employed in research to induce oxidative stress in invertebrate models and cell cultures. MS-222 is a muscle relaxant licensed in the North America and Europe for anesthesia and euthanasia of fin fish intended for human consumption. It prevents the generation of action potentials in motor neurons by blocking Na^{+} channels (Wayson, et al., 1976). Toluene is a volatile, widely used industrial solvent with neurological effects resembling those of ethanol, including confusion, nausea, and memory loss. It acts on a diverse group of ligand-gated ion channels such as NMDA and $GABA_A$ receptors (Win-Shwe and Fujimaki, 2010). Together, these compounds provide a cross-section of environmental pollutants to investigate the impact of toxicants on electrotaxis behavior using our microfluidic assay.

Our results show that among the chemicals tested, only the metal salts, especially those of Ag and Hg, induced significant electrotaxis abnormalities in *C. elegans* at concentrations that do not produce obvious plate-level phenotypes. We also determined *in vivo* concentrations of metals and found high levels of bioaccumulation in the cases of Ag and Hg, which may contribute to electrotactic deficits. These findings provide the first evidence for metal toxicants causing electrotaxis defects in *C. elegans*. Our assay provides a quantitative measurement of chemicals' effects on movement behavior, which complements other common endpoints such as brood size, growth, and lifespan to enable a better understanding of the harmful impact of toxicants on multicellular eukaryotes.

2. MATERIALS AND METHODS

2.1 Strains and culturing

This study used N2 Bristol *C. elegans*, originally obtained from the Caenorhabditis Genetics Center (University of Minnesota, St. Paul, MN), for all behavioral and brood size experiments. Nematodes were grown and maintained at 20°C on Modified Youngren's Only Bactopeptone (MYOB) agar plates containing *Escherichia coli* OP50 culture using previously described methods (Brenner, 1974; Church, et al., 1995). All experiments used age-synchronous populations obtained by bleach treatment (Stiernagle, 2006).

2.2 Chemicals and treatments

$AgNO_3$, $CuSO_4 \cdot 5H_2O$, $HgCl_2$, MeHgCl, BPA, NP, PQ, and MS-222 were obtained from Sigma-Aldrich (St. Louis, MO, USA); toluene was obtained from Caledon (Georgetown, ON, Canada). Three concentration levels of $AgNO_3$, $CuSO_4$, and $HgCl_2$ were selected according to previous investigations (Chu and Chow, 2002; Wang and Xing, 2008): 5 μM, 50 μM, and 150 μM. These concentrations are higher than those found in healthy ecosystems but characteristic of soil in heavily metal-polluted ecosystems (Ebrahimpour and Mushrifah, 2008; Al Omron, et al., 2012). For all other chemicals used in this study, we chose to use the following concentrations: 2 μM for MeHgCl, 20 μM for BPA, 10 μM for NP, 125 μM for PQ, 200 μM for MS-222, and 400 mM for toluene. We defined appropriate concentrations as the highest concentrations of each compound at which chronic exposure would not produce obvious plate-level phenotypes such as lethality, larval arrest or significant developmental delay. These concentrations were determined by beginning with concentrations that have previously been used in *C. elegans* research, then increasing or decreasing the concentration depending on whether an obvious phenotype was observed. A complete listing of all concentrations tested in this way is shown in Table S3.

With the exception of toluene treatment, all toxicants were first prepared as 200x solutions in 100% DMSO, then diluted 10x with water. 500 μL of the resultant 20x solutions in 10% DMSO was then spread evenly across the surface of plates containing 10 mL of MYOB agar (Harada, et al., 2006), finally resulting in 1x concentrations of toxicant and 0.5% DMSO. In the case of toluene, which is immiscible in both DMSO and water, toxicant solution was prepared at 1x concentration in 100% soybean oil; 2 mL of this solution was then spread onto plates already containing *C. elegans*, a protocol that allows animals to live and develop normally at the interface of agar and oil (Kokel and Xue, 2006).

2.3 Electrotaxis assay

Microfluidic channels were fabricated as previously described (Rezai, et al., 2010b). The mold, channel, and other components of the electrotaxis platform are shown in Figures S1 and S2 (see Supporting Information). In preparation for the assay, nematodes were washed off their culture plates, cleaned, and suspended in M9 buffer. Animals were then aspirated into the channel using the syringe pump. Individual animals were isolated by adjusting the tubes' relative height to hydrostatically manipulate the flow of M9 through the channel. Both tubes were then laid flat at the same elevation to eliminate pressure-induced flow. Next, a 3 V/cm DC electric field was applied and the animal's resultant behavior recorded by camera. Locomotory data was later extracted from recorded videos either manually using NIH ImageJ (*http://rsbweb.nih.gov/ij/*) or automatically with custom MATLAB-based tracking software.

Toxicant-exposed animals were grown for 69 h at 20°C before scoring. At least three batches of 10 animals each were scored for each condition. Speed data was normalized to the median of the control.

2.4 Brood size assay

Reproductive capacity of toxicant-exposed animals was determined by counting the hatched progeny of isolated hermaphrodites. Five L4-stage larvae were picked onto fresh spiked MYOB plates and incubated for an additional 96 h at 20°C for maturation and egg-laying; afterwards, the number of offspring was estimated by suspending the population in M9 and counting the animals in aliquots of the suspension. In the cases of 50 and 150 μM Ag and Hg, nematodes were grown for 2 weeks instead of 6 days to account for these animals' slower growth, and progeny were counted and removed from plates daily. The resultant progeny on two batches of four plates per test condition were quantified in this way.

2.5 Growth assay

Body length of metal-exposed nematodes was determined after 69 h of growth at 20°C on toxicant-spiked MYOB plates containing food. Measurements were made from photographs of animals anesthetized through placement in a 15-μL drop of 30 mM NaN_3 in M9, which lay on a solidified pad of 4% agar on a glass slide. Photographs were taken and analyzed with a Hamamatsu ORCA-AG camera on a Nikon Eclipse 80i Nomarski microscope, using NIS-Elements BR software version 3.0 (www.nis-elements.com). At least two batches of 10 animals each were measured for each test condition.

2.6 Lifespan assay

Two batches of 20 age-synchronous L1 larvae per condition were transferred into four fresh spiked MYOB plates (five animals per plate) and grown at 20°C. Viability of animals was checked each day under a stereomicroscope. If immobile, animals were checked for viability by tapping the plate and gently touching their bodies with a platinum pick. Nematodes were transferred to fresh spiked MYOB plates after 120 h, 168 h, and 216 h to prevent contamination of parent animals by offspring.

2.7 Determination of metal content

Approximately 10,000 age-synchronous L1 larvae per condition were transferred into fresh spiked MYOB plates and grown at 20°C for 69 h, at the conclusion of which both live and dead animals were collected and washed twice with deionized water. Two biological replicates were prepared for each exposure. Untreated worms were used as controls. The pelleted pool of worms was frozen at -80°C for further processing at Actlabs (Ancaster, ON, Canada). Each sample was weighed into a 50-mL centrifuge tube followed by the addition of 2 mL of concentrated HNO_3. Centrifuge tubes were placed in a boiling water bath for 1 h to digest samples. The fully digested content in each tube was then diluted to 50 mL with water and analyzed by inductively coupled plasma-mass spectrometry (ICP-MS) using QOP Hydrogeo Rev. 6.6. In addition to testing worms, we also measured metal concentrations in the exposure media.

2.8 Data analysis

Electrotaxis assays were carried out for up to 5 min. Animals were allowed to travel a minimum distance of 5 mm in one direction, towards the cathode, after which the field polarity was reversed to induce a turning response. Electrotaxis speed data was plotted in box plots and compared with the non-parametric Mann-Whitney test. Lifespan data was assessed with the Kaplan-Meier method and compared with the log-rank test. All other data was analyzed with Student's *t*-test. All tests were performed using the Systat SigmaPlot statistical software package version 11.0 (*www.sigmaplot.com)* with significance set at $P < 0.05$. For all assays, data from all repeats were pooled and analyzed together.

3. RESULTS

3.1 Metal salts cause defects in electrotactic response

To evaluate the ability of our microfluidic electrotaxis assay to detect the toxic effects of metal exposure, we loaded *C. elegans* grown on toxicant-polluted plates into our microchannel and measured their speed upon activation of the electric field. We first tested a relatively low concentration (5 μM) of Ag, Cu, and Hg salts, none of which cause obvious plate-level defects (see Methods for details). Animals continuously exposed to 5 μM Ag displayed discontinuous locomotion with frequent pauses and spontaneous turns in the microfluidic channel assay, resulting in slow overall movement (38% speed reduction; Figure 1A). Hg exposures at 5 μM produced locomotory phenotypes similar to those following Ag exposure, also manifesting as significantly retarded electrotaxis speed (36% speed reduction; Figure 1A). Unlike Ag and Hg, Cu exposures did not produce any significant difference at 5 μM (Figure 1A).

Next, we tested higher concentrations of the three metal salts. Ag and Hg at 50 μM each caused major growth defects, including variable developmental delay, as well as locomotion deficiencies on the plate level. Due to these abnormalities, the electrotaxis phenotype of these animals was not analyzed further (data not shown). Cu, on the other hand, did not cause either plate-level phenotypes or electrotaxis defects at 50 μM (Figure 1B). However, when increased 3-fold (150 μM), Cu did cause 23% reduction in electrotaxis speed (Figure 1B), although plate-level phenotypes were still absent.

Overall, these results suggest that electrotaxis speed is a useful endpoint for assessing the toxicity from chronic exposures to Ag and Hg at low concentrations (5 μM) and Cu at relatively high concentrations (150 μM).

3.2 Electrotactic response is particularly sensitive to metal salts

To further characterize the susceptibility of the electrotactic response to chemical exposure, we proceeded to test a diverse set of additional environmental pollutants (MeHg, BPA, NP, PQ, MS-222, and toluene) as described in Introduction. To this end, we first determined appropriate concentrations at which to test each compound, using previously used concentrations as a starting point. For each chemical, four different concentration points were evaluated for suitability for the electrotaxis assay (see Methods and Supporting Information, Table S3). Concentrations were considered appropriate when they did not cause obvious plate-level phenotypes such as significant developmental delay.

We found that among this panel of chemicals, tested at appropriate concentrations, only MeHg (at 2 μM) produced electrotactic swimming speed deficits (65% speed reduction; Figure 2). The electrotactic responses following exposure to the other chemicals were indistinguishable from those of untreated controls (Figure 2). Combined with our observations from Ag, Cu, and inorganic Hg salts, these results suggest that *C. elegans*' electrotactic swimming is particularly vulnerable to metal salts.

3.3 Deficits in reproduction, growth, and lifespan induced by chronic exposure to metal salts

To correlate the electrotaxis phenotype with other biological endpoints following exposure to toxicants, we measured brood size, body length and lifespan. The brood size quantification is displayed in Figure 3. The results show that Ag inhibited reproduction at the lowest concentration of 5 μM (36% brood size reduction) (Figure 3A), which is consistent with previous findings (Roh, et al., 2009). At 50 μM, both Ag- and Hg-exposed animals produced significantly fewer progeny than control (Ag 50 μM: 99% brood size reduction, Hg 50 μM: 87% brood size reduction). At 150 μM, animals exposed to Ag or Hg did not produce progeny at all while animals exposed to Cu produced somewhat fewer progeny (18% brood size reduction). Figure 3B shows that among all other toxicants examined, only MeHg (64% brood size reduction) and toluene (33% brood size reduction) had an effect on reproduction at the concentrations examined.

In the cases of Ag, Cu, and Hg, we also measured body length and lifespan. Figure 4 shows that Ag and Hg induced growth defects in a dose-dependent manner (Ag 50 μM: 39% length reduction, Ag 150 μM: 56% length reduction, Hg 50 μM: 62% length reduction, Hg 150 μM: 77% length reduction) while Cu had only a slight effect at the highest concentration of 150 μM (8% length reduction). Figure 5A shows that chronic Ag exposure significantly reduced *C. elegans*' lifespan at both 50 μM (40% lifespan reduction) and 150 μM (87% lifespan reduction). However, Cu did not significantly affect lifespan at any concentration used in this study (Figure 5B). This finding is consistent with observations made by Harada and colleagues (2006), who did not see a clear separation of survivorship from control until Cu concentrations were increased to 1mM. Hg exposure at 5 μM and 50 μM also did not significantly reduce lifespan; however, most animals exposed to 150 μM Hg perished shortly after plating (87% lifespan reduction; Figure 5C). We also observed significant lifespan extension in animals exposed to 100 μM Hg (53% lifespan extension; Figure 5C).

3.4 Metals accumulate in animals cultured on agar containing metal salts

To evaluate the efficiency of our exposure paradigm, we used ICP-MS to measure metal content in exposure media and *C. elegans* for selected treatments after 69 h of worm growth. The highest exposures that were tested in the electrotaxis assay were selected for each metal: Ag 50 μM (~5.4 μg/mL), Cu 150 μM (~9.5 μg/mL), Hg 50 μM (~10.0 μg/mL), MeHg 2 μM (~0.4 μg Hg/mL). Our results show that while Ag is fully recoverable from the media, Cu and Hg are somewhat less recoverable (86% for $CuSO_4$, 71% for $HgCl_2$, and 37% for MeHgCl) (Figure 6), possibly due to speciation and/or unexpected precipitation. Speciation measurements would be an interesting extension of this research; however, such information could not be collected in this study due to small sample size.

Interestingly, metal content was significantly higher in worms in case of Ag (8-fold) and Hg (6-fold for $HgCl_2$ and 88-fold for MeHgCl) than in the exposure media (Figure 6), indicating that metal toxicants accumulate inside worms' bodies when present in their external environment. We observed slight accumulation of Cu (1.8-fold); however, it was not statistically significant. Overall, these results clearly demonstrate efficient uptake of metal toxicants in our method of exposure.

4. DISCUSSION

Because the phenomenon of movement requires the integration of processes at multiple levels, locomotory behavior can be easily altered by chemical insults such as toxic metal exposure. Previous works have shown that acute doses of metal salts at non-lethal concentrations not only inhibit growth and reproduction (Harada, et al., 2006; Guo, et al., 2009), but also induce locomotory behavioral defects (Wang and Xing, 2008; Anderson, et al., 2004; Yang, et al., 2012). Some of these past studies compared parameters of movement quality, such as head thrash and body bend frequency (Wang and Xing, 2008), while others compared movement speed (Anderson, et al., 2004). In both assays, however, the absence of a constant stimulus meant that animals were free to perform random behaviors, potentially complicating the scoring process. Left to their own devices, *C. elegans* arbitrarily exhibit pauses, reorientations, omega turns, and backward locomotion, creating complex patterns abundant in background noise (data not shown). We sought to address this issue by incorporating mild electric fields and linear microchannels into the assay, resulting in tightly-controlled stimulation which produces directional locomotion (Rezai, et al., 2010b). Because the electrotactic response is so highly stereotyped, neuromuscular defects are readily apparent during the procedure. We have successfully used this technique to sort nematodes

by age and phenotype (Rezai, et al., 2012) as well as to screen mutant and drug-treated animals for defective dopamine signaling (Salam, et al., 2013).

Furthermore, the nature of microfluidics renders the assay highly amenable to parallelization: while up to twenty nematodes can be assayed per hour using the simple single-channel design described in the Materials and Methods section, throughput can be increased by incorporating multichannels as well as automated detection approaches. These advantages stand to further increase the value of microfluidic electrotaxis as a tool for toxicological research with *C. elegans*.

Following Hg exposure we observed severe brood size defects at 150 μM but none at 5 μM (Figure 3A). This pattern differs from the findings of Guo and colleagues (2009) who reported intermediate phenotypes from 2.5 μM to 100 μM. The discrepancy may be due to the difference in exposure paradigm, as Guo and colleagues performed their exposures in an acute fashion and in liquid medium. We opted to use agar as our exposure medium in order to better simulate nematodes' natural environment, as *C. elegans* does not live in liquid. Furthermore, a recent study by Vidal-Gadea and colleagues suggests that in at least some cases, plate-based exposures provide superior bioavailability relative to liquid exposures because *C. elegans* does not drink, limiting exposure in liquid to absorption through the cuticle (Vidal-Gadea et al., 2012).

Given that Cu plays a role in normal biological function as an essential component of cytochrome c oxidase, superoxide dismutase, and other conserved enzymes (Halfdanarson, et al., 2008), it is not surprising that Cu displayed lower potency as a toxicant compared to Ag and Hg. However, the observation of lifespan reduction from 50 μM Ag but not 50 μM Hg was unexpected. Curiously, when we examined the additional condition of 100 μM Hg, exposed animals actually exhibited extended lifespans in addition to exacerbated growth defects relative to animals exposed to 50 μM (data not shown). Although more work would be required to establish this effect as hormetic, such a finding is consistent with previously reported hormesis-like phenomena in Hg-exposed *C. elegans*: Helmcke and Aschner (Helmcke and Aschner, 2010) showed that sub-lethal exposure to MeHg fortified animals against subsequent exposure. Meanwhile, hormetic effects of inorganic Hg have been reported in other systems, including animal, plant, and microbial models (Calabrese and Baldwin, 2003; Schmidt, et al., 2004). Similar hormetic effects have not been reported for Ag, whose inability to induce hormesis may explain why Ag exposure shortens nematode lifespan in a dose-dependent manner while Hg's effect on lifespan is biphasic.

Our analysis of metal concentrations inside worms revealed significant bioaccumulation of Ag (for $AgNO_3$ salt) and Hg (for $HgCl_2$ and MeHgCl salts), but much less in the case of Cu (for $CuSO_4$ salt). Consistent with our results, increased Hg content was previously reported in worms following longer MeHgCl

exposures (Helmcke, et al., 2009). We postulate that metal salts' capacity to bioaccumulate has a direct impact on their toxicity, which is supported by Cu's lesser and MeHg's greater tendencies to accumulate (Figure 6) in light of their lesser and greater respective impacts on behavior and other phenotypes. As Cu is a physiological mineral, there are endogenous mechanisms in place to regulate its homeostasis, including metallochaperones like CUTC-1 (Calafato, et al., 2008). MeHg, meanwhile, is known to molecularly mimic methionine and enter cells via the large amino acid transporter, LAT1 (Helmcke, et al., 2009), which promotes its accrual. This might explain in part why we observed over 10-fold higher accumulation of metal in case of MeHgCl exposure compared to other metal salt treatments.

In conclusion, we have shown for the first time that exposure to the metal salts $AgNO_3$, $CuSO_4$, $HgCl_2$ or MeHgCl compromises *C. elegans*' electrotactic response, whereas a variety of other environmental toxicants do not. To do so, we developed a new semi-automated electro-microfluidic technique that measures the electrotactic swimming response of animals, serving as an indirect output of the health of the neuronal and muscular systems involved in locomotion. Thus, any impact of chemicals on these two systems can be quantified in a rapid and sensitive manner. Considering that electrotaxis is mediated by sensory neurons, it would be interesting in the future to correlate our data with specific neuronal defects to probe the mechanisms by which metal exposure disrupts electrotactic movement. In preliminary studies we have observed some neuronal defects (see Supporting Information Figure S4), but more detailed investigation will be required to evaluate metals' effects on neurons. The results from our assay are consistent with those of other established toxicological protocols and demonstrate the suitability and reliability of this microfluidic approach in *C. elegans*-based environmental toxicology studies.

ACKNOWLEDGEMENTS

Many thanks to Dr. Joanna Wilson and Dr. Chris Wood for helpful comments and feedback. We are also grateful to Dr. Chris Wood for providing the $AgNO_3$, $CuSO_4$, $HgCl_2$, and MS-222, and to Dr. James McNulty for providing the toluene. Actlabs was employed to conduct ICP-MS experiments. All strains used in this study were originally acquired from the *Caenorhabditis* Genetics Center, supported by the National Institutes of Health's National Center for Research Resources. This work was funded by the Ontario Ministry of Research and Innovation and the Collaborative Health Research Projects award, co-funded by the Natural Sciences and Engineering Research Council of Canada and the Canadian Institutes of Health Research.

ASSOCIATED CONTENT

Supporting Information: Details on fabrication of microfluidic channels, the necessary components of our electrotaxis platform, and additional phenotypic data collected from animals exposed to toxicants. This material is available free of charge on the *Journal of Applied Toxicology* website.

REFERENCES

Al Omron AM, El-Maghraby, SE, Nadeem, MA, El-Eter, AM, Al-Mohani, H. 2012. Long term effect of irrigation with the treated sewage effluent on some soil properties of Al-Hassa Governorate, Saudi Arabia. *J. Saudi Soc. Agric. Sci.* **11**:15-18. DOI: 10.1016/j.jssas.2011.04.004.

Ala A, Walker AP, Ashkan K, Dooley JS, Schilsky ML. 2007. Wilson's disease. *Lancet* **369**(9559):397-408. DOI: 10.1016/S0140-6736(07)60196-2.

Anderson GL, Cole RD, Williams PL. 2004. Assessing behavioral toxicity with *Caenorhabditis elegans*. *Environ. Toxicol. Chem.* **23**:1235-1240.

Asharani PV, Hande MP, Valiyaveettil S. 2009. Anti-proliferative activity of silver nanoparticles. *BMC Cell Biol.* **10**:65. DOI: 10.1186/1471-2121-10-65.

ASTM (American Society for Testing and Materials). 2002. Standard guide for conducting laboratory soil toxicity tests with the nematode *Caenorhabditis elegans*. In *Annual Book of ASTM Standards*, ASTM. ASTM: Philadelphia; 1606-1616.

Bar-Ilan O, Albrecht RM, Fako VE, Furgeson DY. 2009. Toxicity assessments of multisized gold and silver nanoparticles in zebrafish embryos. *Small,* **5**(16):1897-1910. DOI: 10.1002/smll.200801716.

Benachour N, Aris A. 2009. Toxic effects of low doses of Bisphenol-A on human placental cells. *Toxicol. Appl. Pharmacol.* **241**(3):322-328. DOI: 10.1016/j.taap.2009.09.005.

Blesa J, Phani S, Jackson-Lewis V, Przedborski S. 2012. Classic and new animal models of Parkinson's disease. *J. Biomed. Biotechnol.* **2012**:845618. DOI: 10.1155/2012/845618.

Brenner S. 1974. The genetics of *Caenorhabditis elegans*. *Genetics,* **77**(1):71-94.

Calabrese EJ, Baldwin LA. 2003. Inorganics and Hormesis. *Crit. Rev. Toxicol.* **33**(3-4):215-304.

Calafato S, Swain S, Hughes S, Kille P, Stürzenbaum SR. 2008. Knock down of *Caenorhabditis elegans cutc-1* exacerbates the sensitivity toward high levels of copper. *Toxicol. Sci.* **106**(2):384-391. DOI: 10.1093/toxsci/kfn180.

Chu KW, Chow KL. 2002. Synergistic toxicity of multiple heavy metals is revealed by a biological assay using a nematode and its transgenic derivative. *Aquat. Toxicol.* **61**:53-64.

Church DL, Guan KL, Lambie EJ. 1995. Three genes of the MAP kinase cascade, *mek-2, mpk-1/sur-1* and *let-60* ras, are required for meiotic cell cycle progression in *Caenorhabditis elegans*. *Development,* **121**:2525-2535.

Clarkson TW, Magos L. 2006. The toxicology of mercury and its chemical compounds. *Crit. Rev. Toxicol.* **36**(8):609-662.

Craig PJ, Eng G, Jenkins RO. 2003. Occurrence and pathways of organometallic compounds in the environment—general considerations. In *Organometallic Compounds in the Environment*, Craig PJ (ed). John Wiley & Sons: Chichester; 1-55.

Crane MM, Chung K, Stirman J, Lu H. 2010. Microfluidics-enabled phenotyping, imaging, and screening of multicellular organisms. *Lab Chip* **10**:1509-1517. DOI: 10.1039/b927258e.

Donkin SG, Dusenbery DB. 1993. A soil toxicity test using the nematode *Caenorhabditis elegans* and an effective method of recovery. *Arch. Environ. Contam. Toxicol.* **25**:145-151.

Du M, Wang D. 2008. The neurotoxic effects of heavy metal exposure on GABAergic nervous system in nematode *Caenorhabditis elegans*. *Environ. Toxicol. Pharmacol.* **27**(3):314-320. DOI: 10.1016/j.etap.2008.11.011.

Ebrahimpour M, Mushrifah I. 2008. Heavy metal concentrations in water and sediments in Tasik Chini, a freshwater lake, Malaysia. *Environ. Monit. Assess.* **141**(1-3):297-307. DOI: 10.1007/s10661-007-9896-7.

Forsyth D, Casey V, Dabeka RW, McKenzie A. 2004. Methylmercury levels in predatory fish species. *Food Addit. Contam.* **21**(9):849-856. DOI: 10.1080/02652030400004259.

Gabel CV, Gabel H, Pavlichin D, Kao A, Clark DA, Samuel AD. 2007. Neural circuits mediate electrosensory behavior in *Caenorhabditis elegans*. *J. Neurosci.* **27**(28):7586-7596. DOI: 10.1523/JNEUROSCI.0775-07.2007.

Guo Y, Yang Y, Wang D. 2009. Induction of reproductive deficits in nematode *Caenorhabditis elegans* exposed to metals at different developmental stages. *Reprod. Toxicol.* **28**(1):90-5. DOI: 10.1016/j.reprotox.2009.03.007.

Halfdanarson TR, Kumar N, Li C, Phyliky RL, Hogan WJ. 2008. Hematological manifestations of copper deficiency: a retrospective review. *Eur. J. Haematol.* **80**(6):523-531. DOI: 10.1111/j.1600-0609.2008.01050.x.

Harada H, Kurauchi M, Hayashi R, Eki T. 2006. Shortened lifespan of nematode *Caenorhabditis elegans* after prolonged exposure to heavy metals and detergents. *Ecotoxicol. Environ. Saf.* **66**(3):378-383. DOI: 10.1016/j.ecoenv.2006.02.017.

Helmcke KJ, Aschner M. 2010. Hormetic effect of methylmercury on *Caenorhabditis elegans*. *Toxicol. Appl. Pharmacol.* **248**(2):156-164. DOI: 10.1016/j.taap.2010.07.023.

Helmcke K, Syversen T, Miller DM, Aschner M. 2009. Characterization of the effects of methylmercury on *Caenorhabditis elegans*. *Toxicol. Appl. Pharmacol.* **240**(2):265-272. DOI: 10.1016/j.taap.2009.03.013.

Ju J, Ruan Q, Li X, Liu R, Li Y, Pu Y, Lihong Y, Wang, D. (2013). Neurotoxicological evaluation of microcystin-LR exposure at environmental relevant concentrations on nematode *Caenorhabditis elegans*. *Environ. Sci. Pollut. Res. Int.* **20**(3):1823-1830. DOI: 10.1007/s11356-012-1151-2.

Kim JC, Shin HC, Cha SW, Koh WS, Chung MK, Han SS. 2001. Evaluation of developmental toxicity in rats exposed to the environmental estrogen bisphenol A during pregnancy. *Life Sci.* **69**(22):2611-2625.

Kokel D, Xue D. 2006. A class of benzenoid chemicals suppresses apoptosis in *C. elegans*. *Chembiochem.* **7**(12):2010-2015. DOI: 10.1002/cbic.200600262.

Leung MC, Williams PL, Benedetto A, Au C, Helmcke KJ, Aschner M, Meyer JN. 2008. *Caenorhabditis elegans*: An Emerging Model in Biomedical and Environmental Toxicology. *Toxicol. Sci.* **106**(1):5-28. DOI: 10.1093/toxsci/kfn121.

Nouara A, Wu Q, Li Y, Tang M, Wang H, Zhao Y, Wang D. 2013. Carboxylic acid functionalization prevents the translocation of multi-walled carbon nanotubes at predicted environmentally relevant concentrations into targeted organs of nematode *Caenorhabditis elegans*. *Nanoscale* **5**(13):6088-6096. DOI: 10.1039/c3nr00847a.

Rahman MF, Wang J, Patterson TA, Saini UT, Robinson BL, Newport GD, Murdock RC, Schlager JJ, Hussain SM, Ali SF. 2009. Expression of genes related to oxidative stress in the mouse brain after exposure to silver-25 nanoparticles. *Toxicol. Lett.* **187**(1):15-21. DOI: 10.1016/j.toxlet.2009.01.020.

Rezai P, Salam S, Selvaganapathy PR, Gupta BP. 2012. Electrical sorting of *Caenorhabditis elegans*. *Lab Chip* **12**(10):1831-1840. DOI: 10.1039/c2lc20967e.

Rezai P, Siddiqui A, Selvaganapathy PR, Gupta BP. 2010a. Behavior of *Caenorhabditis elegans* in alternating electric field and its application to their localization and control. *Appl. Phys. Lett.* **96**(15):153702. DOI: 10.1063/1.3383223.

Rezai P, Siddiqui A, Selvaganapathy PR, Gupta BP. 2010b. Electrotaxis of *Caenorhabditis elegans* in a microfluidic environment. *Lab Chip* **10**:220-226. DOI: 10.1039/b917486a.

Roh JY, Sim SJ, Yi J, Park K, Chung KH, Ryu DY, Choi J. 2009. Ecotoxicity of silver nanoparticles on the soil nematode *Caenorhabditis elegans* using functional ecotoxicogenomics. *Environ. Sci. Technol.* **43**(10):3933-3940.

Salam S, Ansari A, Amon S, Rezai P, Selvaganapathy PR, Mishra RK, Gupta BP. 2013. A microfluidics set up to study neuronal degeneration and identification of neuroprotective compounds in *C. elegans*. *Worm* **2**(3):e24558. DOI: 10.4161/worm.24558.

Schmidt CM, Cheng CN, Marino A, Konsoula R, Barile FA. 2004. Hormesis effect of trace metals on cultured normal and immortal human mammary cells. *Toxicol. Ind. Health* **20**(1-5):57-68. DOI: 10.1191/0748233704th192oa.

Soares A, Guieysse B, Jefferson B, Cartmell E, Lester JN. 2008. Nonylphenol in the environment: A critical review on occurrence, fate, toxicity and treatment in wastewaters. *Environ. Int.* **34**(7):1033-1049. DOI: 10.1016/j.envint.2008.01.004.

Stiernagle T. 2006. *Maintenance of C. elegans.* DOI: 10.1895/wormbook.1.101.1.

Sukul NC, Croll NA. 1978. Influence of Potential Difference and Current on the Electrotaxis of *Caenorhaditis elegans*. *J. Nematol.* **10**(4):314-317.

Tong J, Rezai P, Salam S, Selvaganapathy PR, Gupta BP. 2013. Microfluidic-based electrotaxis for on-demand quantitative analysis of *Caenorhabditis elegans*' locomotion. *J. Vis. Exp.* **75**:e50226. DOI: 10.3791/50226.

Traunspurger W, Haitzer M, Höss S, Beier S, Ahlf W, Steinberg C. 1997. Ecotoxicological assessment of aquatic sediments with *Caenorhabditis elegans* (nematode) -- a method testing liquid medium and whole-sediment samples. *Environ. Toxicol. Chem.* **16**:245-250.

Vidal-Gadea A, Davis S, Becker L, Pierce-Shimomura JT. 2012. Coordination of behavioral hierarchies during environmental transitions in *Caenorhabditis elegans*. *Worm* **1**(1):5-11. DOI: 10.4161/worm.19148.

Wang D, Xing X. 2008. Assessment of locomotion behavioral defects induced by acute toxicity from heavy metal exposure in nematode *Caenorhabditis elegans*. *J. Environ. Sci.* **20**:1132-1137.

Wayson KA, Downes H, Lynn RK, Gerber N. 1976. Studies on the comparative pharmacology and selective toxicity of tricaine methanesulfonate: metabolism as a basis of the selective toxicity in poikilotherms. *J. Pharmacol. Exp. Ther.* **198**(3):695-708.

Weber CI. 1993. *Methods for measuring the acute toxicity of effluents to freshwater and marine organisms* (4th ed.). US Environmental Protection Agency: Cincinnati.

Williams PL, Dusenbery DB. 1988. Using the nematode *Caenorhabditis elegans* to predict mammalian acute lethality to metallic salts. *Toxicol. Ind. Health* **4**(4):469-478.

Williams PL, Dusenbery DB. 1990. A promising indicator of neurobehavioral toxicity using the nematode *Caenorhabditis elegans* and computer tracking. *Toxicol. Ind. Health*, **6**:425-440.

Win-Shwe TT, Fujimaki H. 2010. Neurotoxicity of toluene. *Toxicol. Lett.* **198**(2):93-99. DOI: 10.1016/j.toxlet.2010.06.022.

Wu Q, Qu Y, Li X, Wang D. 2012. Chromium exhibits adverse effects at environmental relevant concentrations in chronic toxicity assay system of nematode *Caenorhabditis elegans*. *Chemosphere* **87**(11):1281-1287. DOI: 10.1016/j.chemosphere.2012.01.035.

Xing X, Du M, Zhang Y, Wang D. 2009. Adverse effects of metal exposure on chemotaxis towards water-soluble attractants regulated mainly by ASE sensory neuron in nematode *Caenorhabditis elegans*. *J. Environ. Sci.* **21**:1684-1694. DOI: 10.1016/S1001-0742(08)62474-2.

Yang X, Gondikas AP, Marinakos SM, Auffan M, Liu J, Hsu-Kim H, Meyer JN. 2012. Mechanism of Silver Nanoparticle Toxicity Is Dependent on Dissolved Silver and Surface Coating in *Caenorhabditis elegans*. *Environ. Sci. Technol.* **46**(2):1119-27. DOI: 10.1021/es202417t.

FIGURES

Figure 1. Electrotaxis of animals chronically exposed to Ag, Cu, or Hg. Boxes represent measurements from 25th to 75th percentiles, central horizontal lines represent medians, vertical lines extend to 10th and 90th percentiles, and dots represent outliers. (A) Defects manifesting as slower swimming speeds appear in animals grown on plates containing 5 µM Ag ($P < 0.01$) or 5 µM Hg ($P < 0.01$), but not 5 µM Cu ($P > 0.05$). Note that the median speeds of Ag- and Hg-treated animals lie well below the 25th percentile of control animals. (B) Cu-induced electrotaxis speed defects do not appear with exposure concentrations of 5 µM ($P > 0.05$) or 50 µM ($P > 0.05$), but do appear at 150 µM ($P < 0.01$).

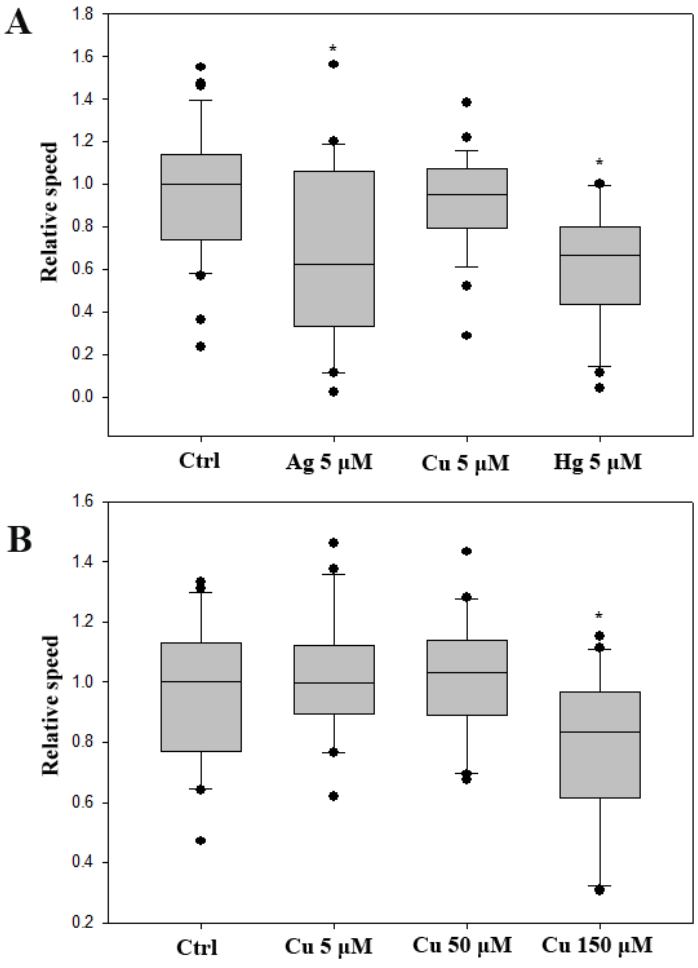

Figure 2. Electrotaxis of animals chronically exposed to MeHg, BPA, NP, PQ, MS-222, or toluene. Refer to Figure 1 for the description of the box plot. (A) Defects manifesting as slower swimming speeds appear in animals grown on plates containing 2 µM MeHg ($P < 0.01$) but not other DMSO-soluble toxicants at concentrations that do not produce obvious plate-level phenotypes ($P > 0.05$). Note that the 90th percentile of MeHg-treated animals lies well below the 10th percentile of control animals. (B) Chronic exposure to 400 mM toluene in oil does not produce electrotactic defects relative to animals exposed to oil alone ($P > 0.05$).

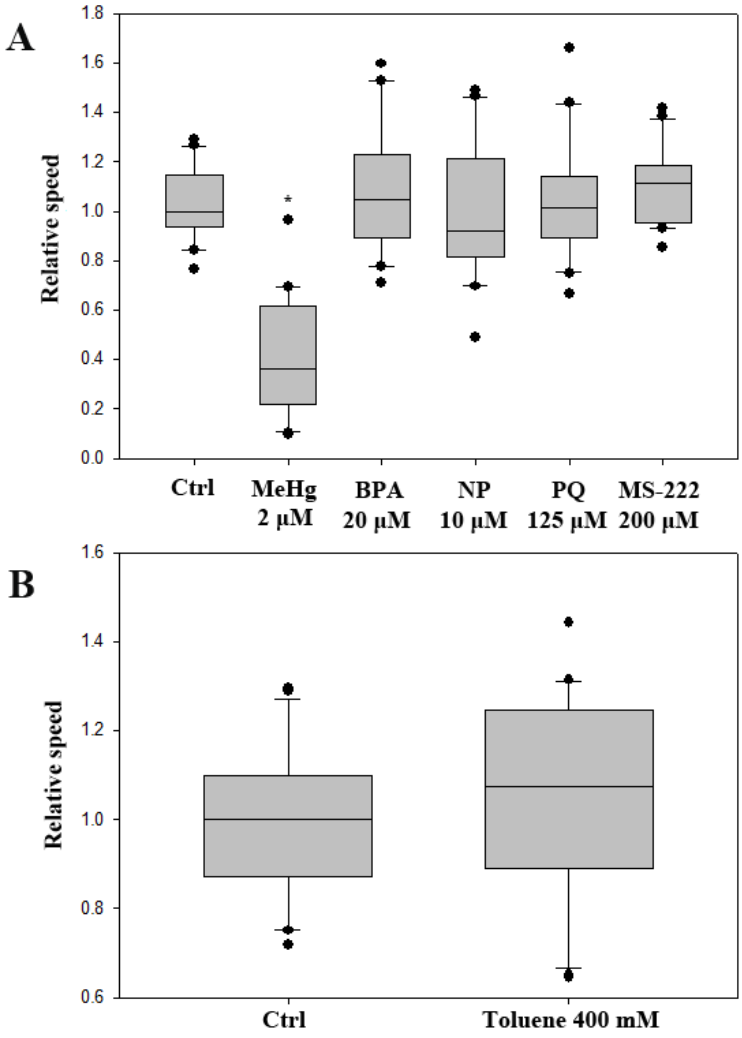

Figure 3. Influence of chronic toxicant exposure on reproductive capacity of *C. elegans*. (A) Brood size was significantly reduced by chronic exposure to Ag 5 µM ($P < 0.01$), Ag 50 µM ($P < 0.01$), Ag 150 µM ($P < 0.01$), Cu 150 µM ($P < 0.05$), Hg 50 µM ($P < 0.01$), and Hg 150 µM ($P < 0.01$), but not Cu 50 µM ($P > 0.05$), Cu 5 µM ($P > 0.05$), or Hg 5 µM ($P > 0.05$). (B) Brood size was significantly reduced by chronic exposure to MeHg 2 µM ($P = 0.01$) and toluene 400 mM ($P = 0.01$), but not other toxicants at concentrations that do not produce obvious plate-level phenotypes ($P > 0.05$).

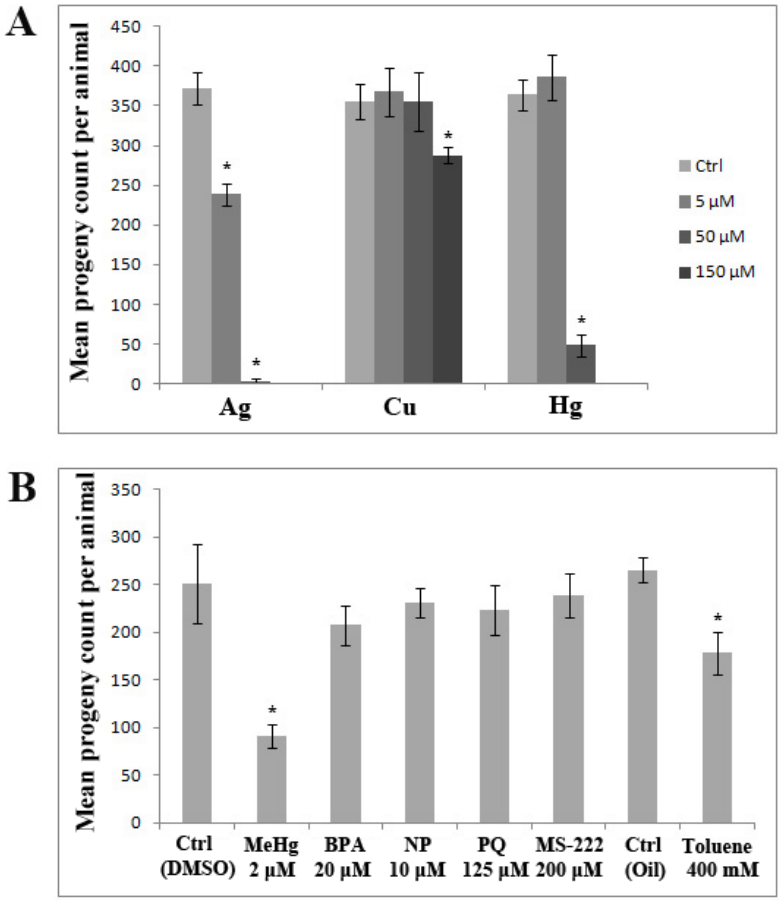

Figure 4. Influence of chronic metal exposure on growth of *C. elegans*. Growth was significantly stunted by chronic exposure to Ag 50 µM ($P < 0.01$), Ag 150 µM ($P < 0.01$), Cu 150 µM ($P < 0.01$), Hg 50 µM ($P < 0.01$), and Hg 150 µM ($P < 0.01$) but not Ag 5 µM ($P > 0.05$), Cu 5 µM ($P > 0.05$), Cu 50 µM ($P > 0.05$), or Hg 5 µM ($P > 0.05$).

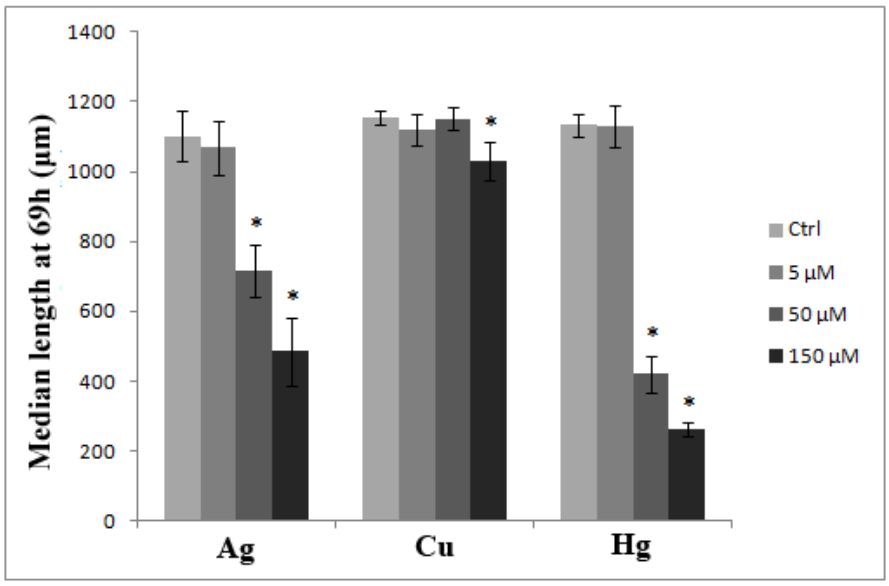

Figure 5. Influence of chronic metal exposure on lifespan of wild-type *C. elegans*. (A) Lifespan is significantly reduced at 150 µM ($P < 0.01$) and 50 µM ($P < 0.01$) Ag, but not 5 µM Ag ($P > 0.05$). (B) Lifespan is not significantly reduced by any concentration of Cu used in this study ($P > 0.05$ in all cases). (C) Lifespan is severely reduced by 150 µM Hg ($p < 0.01$), but not significantly by 50 µM ($P > 0.05$) or 5 µM ($P > 0.05$); lifespan is extended by 100 µM Hg ($p < 0.01$).

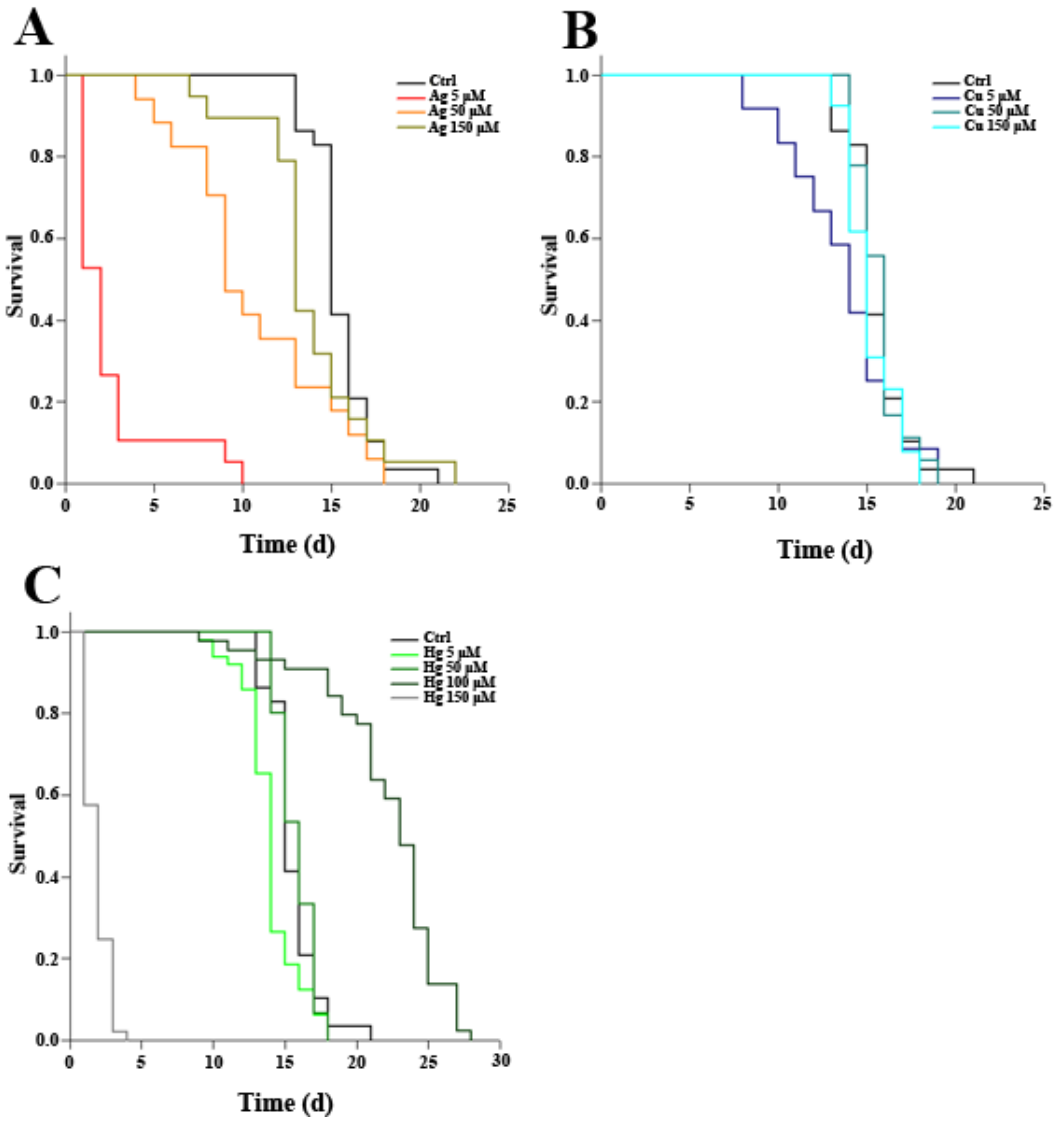

Figure 6. Metal content in culture substrate and *C. elegans* following 69 h metal salt exposure. Elemental content was measured as a function of total sample volume. Metal content in worms is significantly higher than in culture substrate following treatment with Ag 50 µM ($p < 0.01$), Hg 50 µM ($p < 0.01$), or MeHg 2 µM ($p < 0.01$), but not Cu 150 µM ($p = 0.247$).

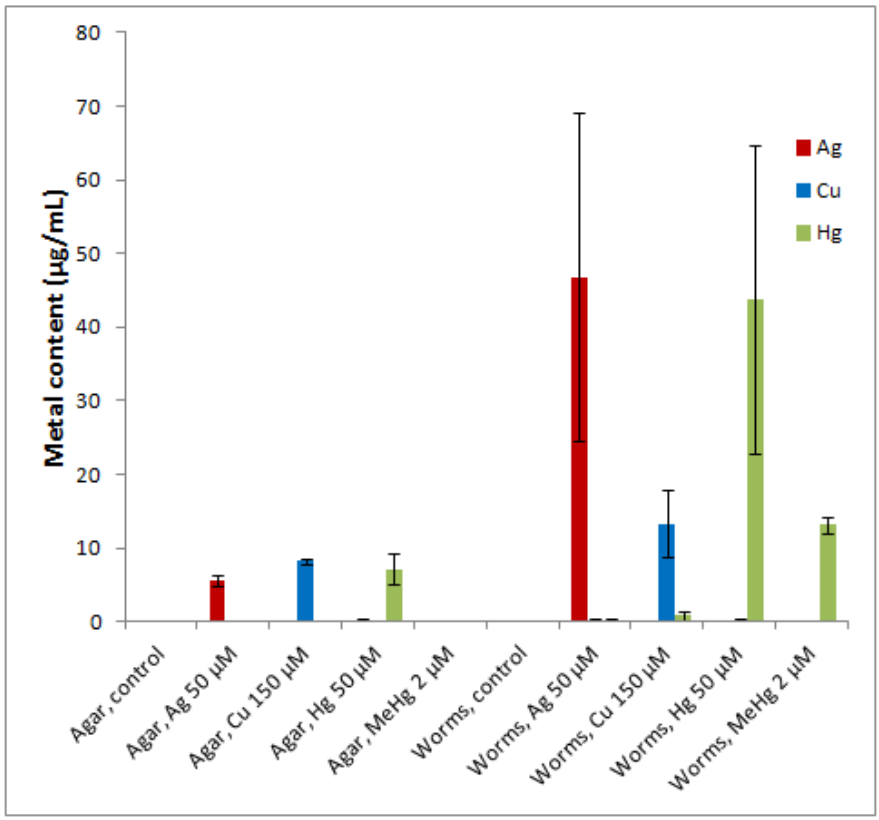

Supporting Information

S1. Microchannel fabrication

The channel design was printed on a transparency sheet using high-resolution photoplotting to create a photomask, which was then used in conjunction with SU-8 100 negative photoresist (MicroChem Corp., MA, USA) to lithographically pattern the design onto a silicon wafer (Figure S1A). Microchannels were then casted by pouring polydimethylsiloxane (PDMS) pre-polymer (Sylgard 184 Kit, Dow Corning Corp., MI, USA; 10:1 ratio of base and cross-linker) onto the resultant master mold and allowing 24 h for curing. The channel was then excised from the PDMS replica and fluid access ports were punched into each end. Next, the channel, a blank PDMS strip and a glass slide were oxidized via exposure to oxygen plasma for 40 s at 40 W power and stuck together to seal the microchannel. Lastly, plastic tubing and insulated copper wire were affixed to the punched reservoirs and secured with PDMS pre-polymer. The final assembly is shown in Figure S1B. An animal performing electrotaxis inside a microchannel is shown in Figure S1C.

S2. Electrotaxis experimental setup

In addition to the PDMS microchannel, the electrotaxis assay requires a syringe pump, power supply, microscope, camera, and monitor. The syringe pump is

attached to one of the inlet/outlet tubes of the microchannel device to facilitate sample loading at the other tube. The power supply is connected via insulated copper wiring to the electrodes of the microchannel device to provide animals with electrical stimulus. The microscope, camera, and monitor allow visualization and recording of the electrotaxis experiment. A schematic of the setup is shown in Figure S2.

S3. Plate-level phenotypes of toxicant exposure at various concentrations

Before electrotaxis experiments were conducted for MeHg, BPA, NP, PQ, MS-222, and toluene exposure, appropriate concentrations were first determined for each of these chemicals. These concentrations were determined as described in Materials and Methods. A complete listing of all concentrations tested for induction of plate-level phenotypes is shown in Table S3.

S4. ASEL and GABAergic neuronal damage induced by chronic exposure to Ag, Cu, and Hg

For neuronal phenotype analyses animals were examined under a Nomarski fluorescence microscope. Adults were anesthetized in a 15-µL drop of 30 mM NaN_3 in M9 buffer, which lay on a solidified pad of 4% agar on a glass slide. Epifluorescence was visualized with a Hamamatsu ORCA-AG camera, a Nikon

Eclipse 80i microscope, a GFP or YFP filter (31044V2 CY GFP C61331), and NIS-Elements BR software version 3.0 (*www.nis-elements.com*).

Two transgenic strains, OH123 *gcy-7*::GFP (otIs1) and EG1285 *unc-47*::GFP (oxIs12), expressing GFP in subsets of neurons, were examined. *gcy-7*::GFP is expressed in specific amphid sensory neuron ASEL and *unc-47*::GFP is expressed in GABAergic motor neurons. Both markers revealed abnormal neuronal morphologies following metal exposure. The phenotype is observed as wrinkles in the ASEL dendrites in the case of *gcy-7*::GFP (Figure S4B), as previously reported by Xing and colleagues (2009a). The GABAergic motor neurons in *unc-47*::GFP showed missing portions of dendrites following exposure to Hg and Ag, as revealed by gaps in fluorescence (Figure S4D). A similar phenotype for GABAergic motor neurons was previously reported following Pb, Cu, and Hg exposure (Xing, et al., 2009b; Du and Wang, 2008).

SUPPLEMENTARY FIGURES

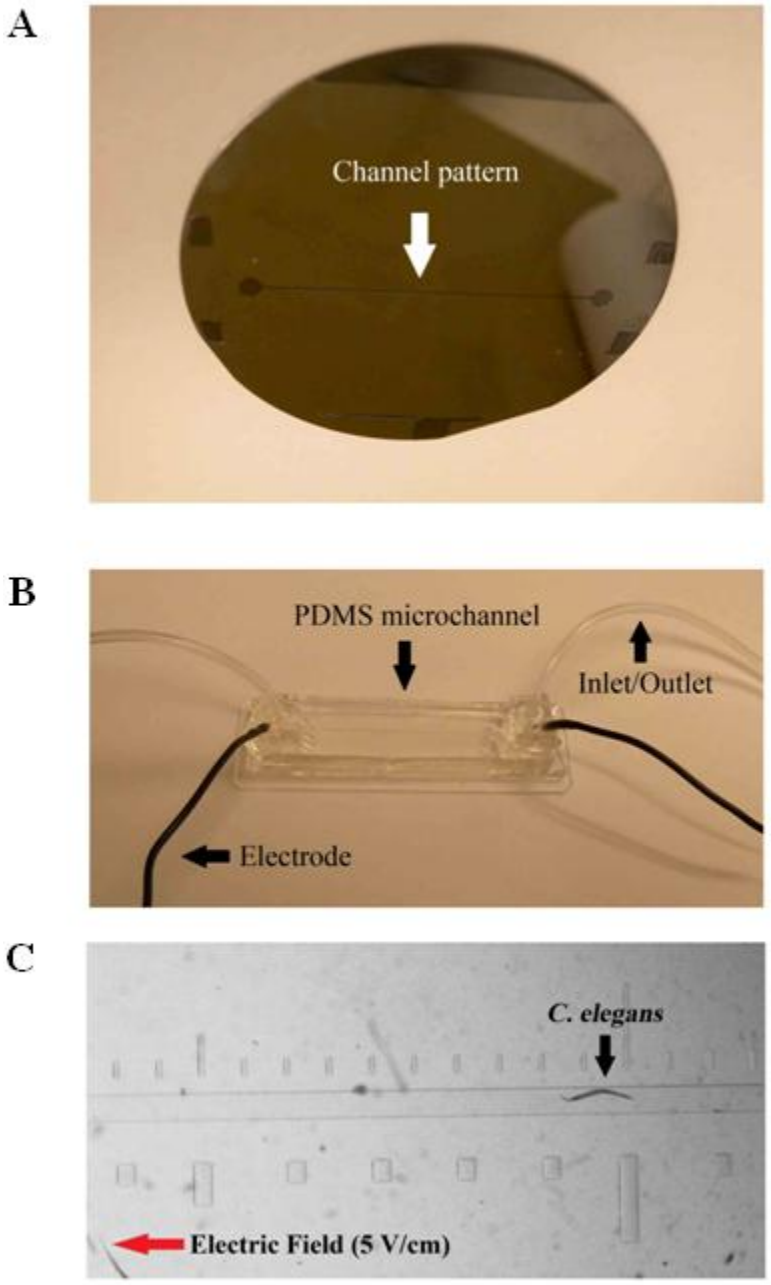

Figure S1. (A) Silicon master mold, produced via photolithography and used to cast microchannels from PDMS. (B) Fully assembled microchannel device.

Microchannels used in the present study are linear and measure 5 cm long x 300 μm wide x 80 μm deep. (C) Interior of microchannel. Red arrow indicates position of cathode/direction of electrotaxis.

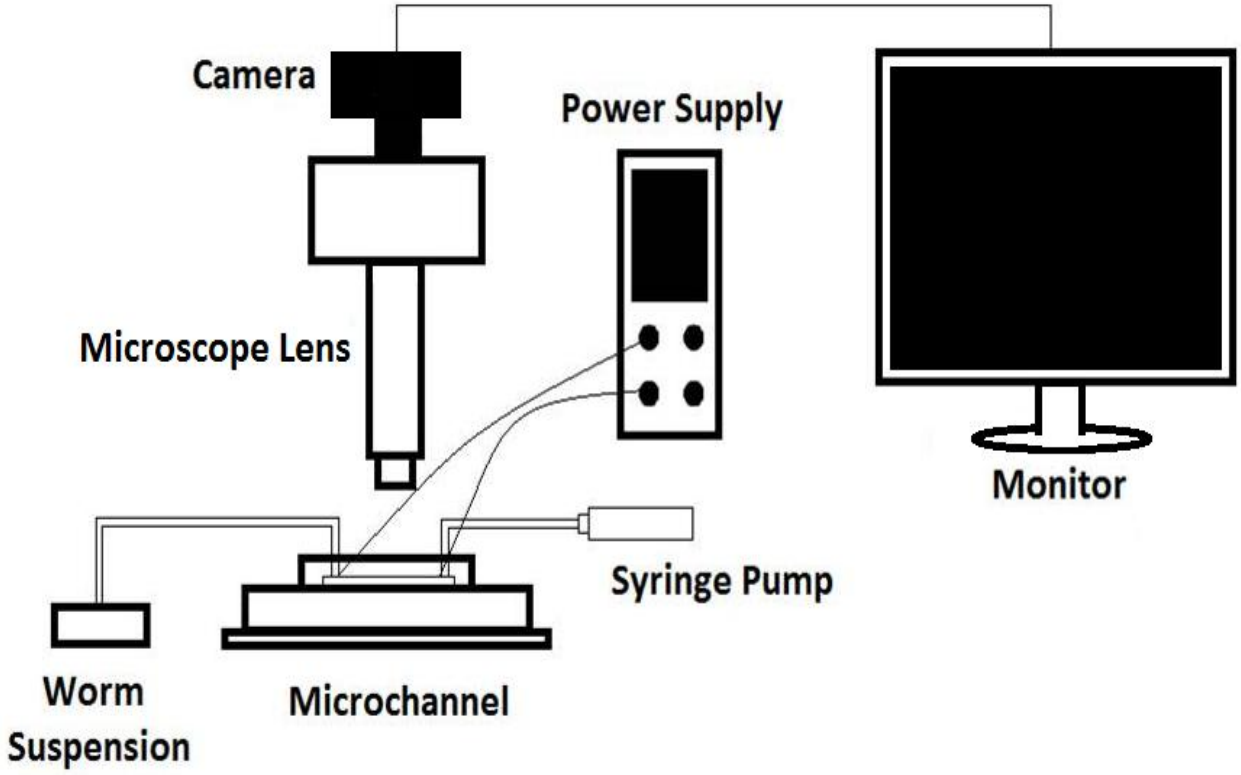

Figure S2. Schematic of the experimental setup for the electrotaxis assay.

MeHg	**2 µM**	**4.5 µM**	**9 µM**	**18 µM**
	Slight developmental delay	Significant developmental delay	Significant developmental delay	L1 arrest

BPA	**5 µM**	**10 µM**	**20 µM**	**40 µM**
	No obvious phenotype	No obvious phenotype	No obvious phenotype	Asynchrony

NP	**2.5 µM**	**5 µM**	**10 µM**	**20 µM**
	No obvious phenotype	No obvious phenotype	No obvious phenotype	Significant developmental delay

PQ	**50 µM**	**75 µM**	**125 µM**	**250 µM**
	No obvious phenotype	No obvious phenotype	Slight developmental delay	Significant developmental delay

MS-222	**100 µM**	**200 µM**	**400 µM**	**800 µM**
	No obvious phenotype	No obvious phenotype	Significant developmental delay	L1 arrest

Toluene	**100 mM**	**200 mM**	**400 mM**	**800 mM**
	No obvious phenotype	Slight developmental delay	Slight developmental delay	Significant developmental delay

Table S3. Listing of all concentrations tested during determination of appropriate toxicant concentration for electrotaxis experiments. Developmental delays of more than 10% were considered significant. Shaded cells indicate the concentrations settled upon for use in electrotaxis experiments.

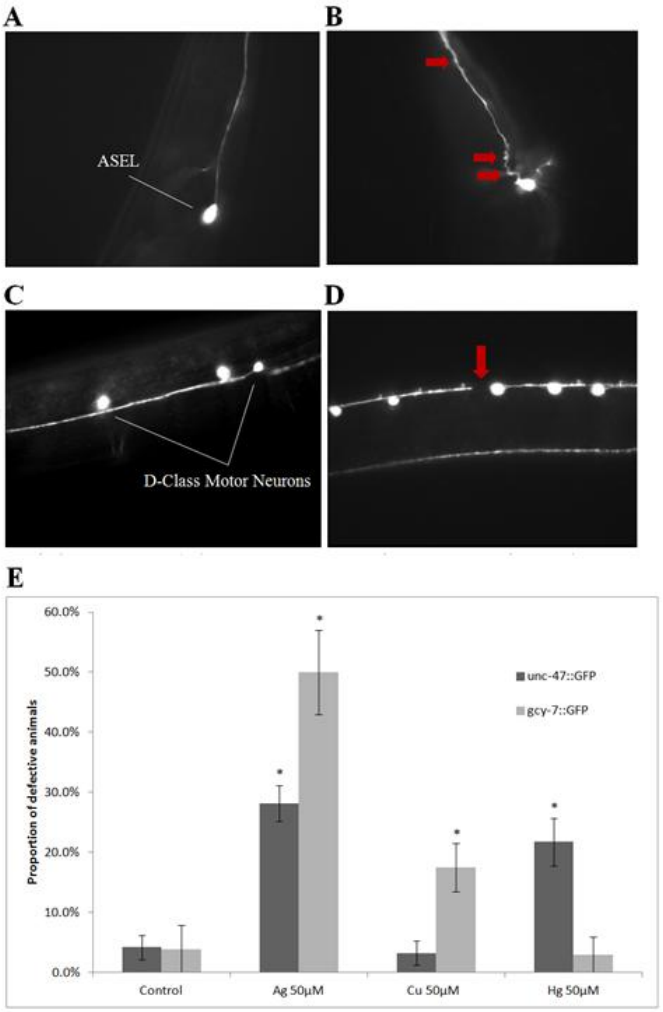

Figure S4. (A) Untreated OH123 animals express *gcy-7*::GFP in the ASEL amphid chemosensory neuron. (B) OH123 animals grown on plates spiked with 50 μM Ag or Cu show abnormal ASEL dendrites (red arrows). (C) Untreated EG1285 animals express *unc-47*::GFP in all GABAergic neurons: 4 RMEs, AVL, and RIS in the head, 19 D-type motor neurons along the ventral cord, and DVB in the tail. (D) EG1285 animals grown on plates spiked with 50 μM Hg or Ag show gaps in the ventral cord (red arrow). (E) Quantification of aberrant fluorescence patterns in metal-exposed transgenic nematodes. The means of 4 different trials were plotted along with standard error. Asterisks (*) mark values that are significantly different from controls ($P < 0.05$).

SUPPLEMENTARY REFERENCES

Du M, Wang D. 2008. The neurotoxic effects of heavy metal exposure on GABAergic nervous system in nematode *Caenorhabditis elegans*. *Environ. Toxicol. Pharmacol.* **27**(3):314-320. DOI: 10.1016/j.etap.2008.11.011.

Xing X, Du M, Zhang Y, Wang D. 2009a. Adverse effects of metal exposure on chemotaxis towards water-soluble attractants regulated mainly by ASE sensory neuron in nematode *Caenorhabditis elegans*. *J. Environ. Sci.* **21**:1684-1694. DOI: 10.1016/S1001-0742(08)62474-2.

Xing X, Rui Q, Du M, Wang D. 2009b. Exposure to Lead and Mercury in Young Larvae Induces More Severe Deficits in Neuronal Survival and Synaptic Function than in Adult Nematodes. *Arch. Environ. Contam. Toxicol.* **56**:732–741. DOI: 10.1007/s00244-009-9307-x.

Significance

This study demonstrates the microfluidic electrotaxis assay's potential for toxicological applications by showing that the assay can detect the toxic effects of anthropogenic metallic contaminants added to worms' culture substrate. The sensitivity of our assay is revealed to be comparable to that of more traditional assays that measure fecundity, growth, and lifespan, supporting the practicality of electrotactic swimming as a toxicity endpoint in *C. elegans*. We also provide the first evidence for bioaccumulation of silver, copper, and inorganic mercury salts inside the bodies of *C. elegans* and postulate that a metal salt's capacity to bioaccumulate is associated with its impact on electrotactic behaviour.

Chapter 4-Modelling Parkinson's disease using the electrotactic swimming response of transgenic *C. elegans*

Citation & Author Contributions

This project was conducted by JT under the senior guidance of PRS, RKM, and BPG. JT was responsible for all data collection, analysis, and reporting for dissemination. Additional consultation was provided by SS and PR.

> **Tong, J.**; Salam, S.; Rezai, P.; Selvaganapathy, P.R.; Mishra, R.K.; & Gupta, B.P. Familial Parkinson mutant α-synuclein causes defective electrotactic swimming behaviour in transgenic *Caenorhabditis elegans*. (in prep, June 2014).

Familial Parkinson mutant α-synuclein causes defective electrotactic swimming behaviour in transgenic *Caenorhabditis elegans*

Justin Tong[1], Sangeena Salam[1], Pouya Rezai[2,3], P. Ravi Selvaganapathy[2], Ram K. Mishra[4], Bhagwati P. Gupta[1]*

[1]Department of Biology, McMaster University, Hamilton, ON

[2]Department of Mechanical Engineering, McMaster University, Hamilton, ON

[3]Department of Mechanical Engineering, York University, Toronto, ON

[4]Department of Psychiatry and Behavioural Neurosciences, McMaster University, Hamilton, ON

Key words: *C. elegans*, microfluidics, electrotaxis, Parkinson's disease, neurodegeneration, alpha-synuclein, curcumin

*Contact:

guptab@mcmaster.ca; Phone: 1-905-525-9140 x26451; Fax: 1-905-522-6066

ABSTRACT

Mutations in *SNCA* are the most common cause of familial Parkinson's disease (PD). The gene's protein product, α-synuclein (αSyn), is the major structural component of Lewy bodies and has been implicated in the Parkinson's disease-related degeneration of nigral dopamine (DA) neurons. Transgenic *Caenorhabditis elegans* expressing αSyn have been established as PD models and show aggregation of proteins into Lewy body-like cellular inclusions, DA neuronal damage, defects in motility and DA-mediated behaviours, and abnormal overall DA levels. In the present study, we expand upon the characterization of *C. elegans* αSyn models of PD. We have previously reported a versatile electro-microfluidic platform for inducing swimming behaviour in *C. elegans* on demand; here, we use the platform to demonstrate that αSyn-expressing worms show deficits in electrotactic swimming speed. When αSyn expression is restricted to DA neurons, slowness does not appear in young adulthood but rather appears as an acceleration of aging-related locomotory decline, coinciding with acceleration of aging-related DA neuronal degeneration. We further show that both the electrotaxis and neuronal phenotypes of worms expressing αSyn in DA neurons can be ameliorated by treatment with curcumin, a putative neuroprotective agent. These findings support the utility of the microfluidic electrotaxis assay for evaluating potential PD therapeutics and encourage further investigation into the use of curcumin as a preventative measure against PD.

1. INTRODUCTION

Parkinson's disease (PD) is a debilitating aging-related neurodegenerative disorder that afflicts roughly 1.5% of the North American population (***1***). The disease primarily manifests as motor symptoms including tremor, postural instability, rigidity, and bradykinesia, though neuropsychiatric disorders may also develop as PD progresses (***2***). From a pathological perspective, PD is caused by the progressive loss of dopamine (DA) neurons in the substantia nigra pars compacta (SNpc), which results in a decreased supply of DA to the striatum, under-activation of the movement-promoting direct striatal pathway mediated by D1 receptors, and over-activation of the movement-inhibiting indirect striatal pathway mediated by D2 receptors (***3***). The mechanisms underlying this neuronal loss, while incompletely understood, appear to be associated with the formation of proteinaceous intracellular inclusions called Lewy bodies (LBs), which are often

found inside the remaining SNpc DA neurons of PD patients. LBs contain a number of different proteins but mainly consist of α-synuclein (αSyn), a poorly characterized protein with unclear physiological function encoded by the *SNCA/PARK1/PARK4* gene.

The first causal PD gene to be identified, *SNCA* and its polymorphisms are responsible for the majority of dominant familial PD cases (***4***). Point mutations such as A53T and gene multiplications have both been associated with increased risk of PD, suggesting that both quality and quantity of αSyn affect its toxicity. The exact function of αSyn has not been elucidated, but the fact that it can associate with lipids and bind synaptic vesicles suggests involvement in vesicle trafficking; moreover, some studies suggest that it plays a role in the regulation of DA homeostasis in presynaptic vesicle recycling (***5***). Of note, while αSyn is not present in invertebrates, ectopic expression of αSyn limits cell growth in yeast and causes DA neurodegeneration in *Drosophila* and *Caenorhabditis elegans*, raising doubt regarding the degree to which the normal role of αSyn is relevant to its toxicity (***6***). However, the mechanisms by which αSyn contributes to DA cell death under pathological conditions are only slightly better understood than its usual function. As a matter of fact, there are several theories for why αSyn is toxic, ranging from mitochondrial dysfunction and impaired energy production to ER stress-induced apoptosis (***6***). Additionally, αSyn can form pore-like structures *in vitro*, and annular rings of αSyn have been isolated from brains of patients with multiple system atrophy (***7***). αSyn also displays a tendency to misfold and aggregate, and this tendency is exacerbated by certain point mutations as well as *SNCA* copy number variations; the resultant aggregation forms the principal structure of LBs. Furthermore, there is some indication that misfolded αSyn is released upon cell death and taken up by neighbouring cells, where it may spread its misfolded conformation in a prion-like fashion (***8***).

Aside from *SNCA*, there is a handful of other genes associated with risk of PD. Leucine-rich repeat kinase 2 (*LRRK2/PARK8*) encodes a large multi-domain protein with kinase and GTPase activity but unclear biological function, as until recently no physiological substrates had been identified. Mutations in *LRRK2* that bestow increased kinase activity, such as G2019S, result in accumulation of αSyn, DA neuronal damage, impairment of autophagy, and increased apoptosis (**6**). A recent study identified ribosomal proteins as major LRRK2 kinase targets, showed that blocking phosphorylation of small ribosomal subunit protein s15 rescues LRRK2 neurotoxicity, and demonstrated that pathogenic LRRK2 induces

an increase in bulk protein synthesis that is blocked by phosphodeficient s15; together, these findings link elevated LRRK2 kinase activity to PD pathogenesis via altered translation (***9***). Another important gene is parkin (*PRKN/PARK2*), which encodes an E3 ubiquitin ligase involved in protein degradation (**10**); however, most cases of *PRKN*-related parkinsonism do not present with LBs (**4**). Parkin also has a role in mitophagy, where it is responsible for ubiquitinating depolarized or otherwise damaged mitochondria to maintain cell integrity (**11**). Recruitment of parkin to such mitochondria requires the action of PTEN-induced kinase 1 (PINK1/PARK6), which has itself been implicated in cellular protection against oxidative stress, mitochondrial dysfunction, and apoptosis (**11**). Genome-wide association studies have uncovered a few other PD-related candidate genes, but further studies are required to clarify the roles of the encoded proteins.

Current treatments for PD are dominated by levodopa (L-DOPA), a DA precursor that crosses the blood-brain barrier; however, L-DOPA only temporarily reduces motor symptoms and gradually loses effectiveness as therapy continues (**12**). There exist DA agonists and inhibitors of DA metabolism that produce effects similar to those of L-DOPA, but side effects are significant and include drowsiness, hallucinations, insomnia, nausea, and constipation (**12**). Instead of simply raising DA levels, the ideal PD drug would prevent DA neuronal loss in the first place. While no such drug has yet been developed, compounds such as curcumin have shown some promise and warrant further investigation. Curcumin is a polyphenolic compound extracted from the South Asian spice turmeric (*Curcuma longa*) and appears to bear a broad range of protective properties, including anti-oxidant and anti-inflammatory activity (**13**,**14**). It has been reported to inhibit neurotoxin-induced DA neuron damage in rodents and αSyn aggregation in cell lines (**15**), but curcumin also increases lifespan of wild-type *C. elegans* (**16**), indicating that its therapeutic benefit may not be specific to PD-like conditions. Nonetheless, its further characterization as a potential neuroprotective agent should be pursued.

Although there is much that we still do not understand about PD-related processes, we have learned a great deal about its etiology, pathology, and molecular mechanisms from animal models (**17**). Model organisms have proven invaluable for PD studies due to their relatively simple nervous systems, accelerated disease progression, and amenability to experimental manipulation without ethical concerns. Alongside the rat, mouse, and fruit fly, the nematode *C. elegans* is one animal model that has been used extensively to study DA

neurodegeneration and explore possible avenues of neuroprotection. *C. elegans* is a particularly attractive model due to its genetic tractability, ease of culture, and short three-day life cycle, which all serve to greatly expedite the rate of discovery. Despite its relative simplicity, *C. elegans* shares roughly half of its genes with humans and utilizes many conserved processes (**18**), including both D1- and D2-mediated signaling pathways. Though the worm does not endogenously produce αSyn, transgenic *C. elegans* expressing human αSyn have been reported to display Lewy body-like cellular inclusions, DA neuronal damage, defects in motility and DA-mediated behaviours, and aberrant overall DA levels (**19**,**20**,**21**).

The worm's body is also appropriately sized for use in microfluidic systems, which have been used to study biological processes in live nematodes with great precision (**22**,**23**). Our group has previously shown that a mild direct current (DC) electric field stimulates *C. elegans* in a microfluidic environment to swim towards the cathode in a directed manner (**24**). Both robust and sensitive, this electrotactic behaviour provides a powerful non-invasive method to evaluate the functional output of nematode locomotory circuits under variable conditions such as exposure to metal salts (**25**) and various other stresses (**26**). We have also shown that electrotactic swimming speed deficits can be induced by exposure to DA neuron-specific neurotoxins including 6-hydroxydopamine (6-OHDA), 1-methyl-1,2,3,6-tetrahydropyridine (MPTP), and rotenone, implicating DA signaling in the electrotactic swimming response (**27**).

While our previous work characterized the electrotaxis of neurotoxin-based PD model worms, we now build upon that work by demonstrating that transgenic, αSyn-expressing PD model worms also exhibit electrotactic speed deficits. When αSyn expression is restricted to DA neurons, slowness does not appear in young adulthood but rather appears as an acceleration of aging-related locomotory decline, coinciding with acceleration of aging-related DA neuronal degeneration. We further show that both the electrotaxis and neurodegenerative phenotypes of worms expressing αSyn in DA neurons can be ameliorated by treatment with curcumin. These findings support the utility of the microfluidic electrotaxis assay for evaluating potential PD therapeutics and encourage further investigation into the use of curcumin as a preventative measure against PD.

2. MATERIALS AND METHODS

2.1 Strains and culturing

The following strains were employed and/or obtained in the present study. Where known, the locations of mutations and integrated transgenes are indicated.

N2 Bristol wild-type, DY328 *unc-119(ed4) III; bhEx120(unc-119(+) + dat-1::YFP)*, DY463 *unc-119(tm4063) III; bhEx172(unc-119(+) + dat-1::αSyn(A53T) + dat-1::YFP)*, DY416 *nre-1(hd20) lin-15b(hd126) X*, DY471 *nre-1(hd20) lin-15b(hd126) X; bhEx172(unc-119(+) + dat-1::αSyn(A53T) + dat-1::YFP)*, NL5901 *pkIs2386(unc-54::αSyn::YFP + unc-119(+))*, FX14480 *tmIs0910(unc-51::αSyn(A53T) + unc-51::EGFP)*, VM6365 *lin-15(n765) X; akEx387(lin-15(+) + dat-1::ICE + dat-1::GFP)*, DY482 *bhIs7(unc-119(+) + dat-1::αSyn(A53T) + dat-1::YFP)*, KU41 *lrk-2(km41) I*, DY488 *lrk-1(tm1898) I*, DY487 *cdnf(tm3603) IV*, DY481 *bhEx179(lin-11-int3::SNCA + lin-11-int3::GFP)*.

DY416 was backcrossed in-house from VH624 *rhIs13[unc-119::gfp + dpy-20(+)]; nre-1(hd20) lin-15B(hd126)*. DY471 was obtained by crossing DY416 with DY463. DY488 and DY487 were outcrossed in-house from FX01898 *lrk-1(tm1898)* and FX03603 *cdnf(tm3603)* respectively. DY482 was created from DY463 through integration of extrachromosomal arrays by gamma irradiation with 4000 Rad from a Co-60 source (**28**). All other DY-series strains were generated in-house through microinjection to create stable lines carrying extrachromosomal arrays (**29**). FX14480, FX01898, and FX03603 were obtained from Shohei Mitani's laboratory (Tokyo Women's Medical University, Tokyo, Japan). VM6365 was obtained from Andres Maricq's laboratory (University of Utah, Salt Lake City, UT, USA). KU41 was obtained from Kunio Matsumoto's laboratory (Nagoya University, Nagoya, Japan). VH624 and all other strains were originally obtained from the Caenorhabditis Genetics Center (University of Minnesota, St. Paul, MN, USA).

The general methods for culturing and genetic manipulations have been previously described (**30**). Nematodes were grown and maintained at 20°C on nematode growth medium (NGM) agar plates containing *E. coli* OP50 culture. Age-synchronous populations were obtained by bleach treatment (**31**).

For experiments on animals older than young adults, 5-fluoro-2'-deoxyuridine (FUdR, obtained from Sigma-Aldrich [St. Louis, MO, USA]) was used to prevent contamination by progeny. FUdR treatments were first prepared as a 400 μM stock solution in M9 buffer; subsequently, 1x treatment plates were produced by spreading 500 μL of the 400 μM solution across the surface of plates containing 10 mL of NGM agar. Worms were then grown on these FUdR-containing plates beginning in L4.

2.2 Molecular biology and generation of transgenics

The *dat-1::*YFP plasmid pGLC72 was created in our lab and reported previously (**27**). The *dat-1::*αSyn(A53T) plasmid was a gift from Takeshi Iwatsubo's laboratory (University of Tokyo, Tokyo, Japan), and its construction has been described (**19**). The *lin-11-int3::GFP* plasmid pGLC59 was built in our lab and will be described elsewhere. The *lin-11-int3::*αSyn(A53T) plasmid pGLC95 was also constructed in our lab and was made by amplifying the αSyn-coding region of the *dat-1::*αSyn(A53T) plasmid using primers GL860 (5'-AAACTGCAGCTATGGATGTATTCATGAAAGGACTTTCAAAGGCCAAGG-3') and GL861 (5'-AAAGTCGACTTAGGCTTCAGGTTCGTAGTCTTGATACCC-3'). The resulting PCR product was digested with PstI and SalI and subcloned into pGLC59.

Transgenic animals carrying extrachromosomal arrays were generated by a standard microinjection technique (**29**). The following concentrations of plasmids were injected as part of this study: pGLC72 (*dat-1::*YFP) 50 ng/µL, *dat-1::*αSyn(A53T) 10 ng/µL, pGLC59 (*lin-11-int3::*GFP) 50 ng/µL, pGLC95 (*lin-11-int3::*αSyn(A53T)) 10 ng/µL.

Outcrossed DY488 *lrk-1(tm1898)* was confirmed by PCR using primers GL917 (5'- ATCAGAAGCCGGGGACATGT-3') and GL918 (5'-ACGAGGGCTCTACGTGTCTA-3'). Outcrossed DY487 *cdnf(tm3603)* was confirmed by PCR using primers GL915 (5'- CTCGGTGCATCCCTTGCACA-3') and GL916 (5'- AGCCGACTCGTCCTTCTCAT-3').

2.3 Curcumin treatment

Curcumin was obtained from Sigma-Aldrich (St. Louis, MO, USA) and maintained as a 100 mM stock solution in 100% dimethylsulfoxide (DMSO). Treatments were prepared by mixing curcumin solution into liquid NGM agar at the time of pouring plates, for a final concentration of 500 µM curcumin and 0.5% DMSO.

2.4 RNAi

RNA interference (RNAi) was performed on plates containing 0.6% Na2HP04, 0.3% KH_2P0_4, 0.1 % NH_4CI, 0.5% casamino acids, 2% agar, 1 mM $CaCl_2$, 1 mM $MgS0_4$, 0.0005% cholesterol, 0.2% β-lactose, and 50 µg/mL

carbenicillin. Plates were seeded with 150 μL of HT115 bacterial culture that produces dsRNA of the gene of interest, which was grown overnight in LB media containing 100 μg/mL carbenicillin and 10 μg/mL tetracycline. Ten to 15 L4-stage worms were picked onto RNAi plates and the phenotypes of F1 progeny were examined.

2.5 Microchannel fabrication and electrotaxis

Electrotaxis assays were performed exclusively in PDMS microchannels that were first reported by Rezai and colleagues (**24**). Both the details of microchannel construction and a standard protocol for the electrotaxis assay proper have been previously published (**32**).

The channel design was printed on a transparency sheet using high-resolution photoplotting to create a photomask, which was then used in conjunction with SU-8 100 negative photoresist (MicroChem Corp., MA, USA) to lithographically pattern the design onto a silicon wafer. Microchannels were then casted by pouring polydimethylsiloxane (PDMS) pre-polymer (Sylgard 184 Kit, Dow Corning Corp., MI, USA; 10:1 ratio of base and cross-linker) onto the resultant master mold and allowing 24 h for curing. The channel was then excised from the PDMS replica and fluid access ports were punched into each end. Next, the channel, a blank PDMS strip and a glass slide were oxidized via exposure to oxygen plasma for 40 s at 40 W power and stuck together to seal the microchannel. Lastly, plastic tubing and insulated copper wire were affixed to the punched reservoirs and secured with PDMS pre-polymer.

In preparation for each electrotaxis assay, a syringe was attached to the outlet tube of the PDMS microchannel to facilitate worm loading at the inlet tube. A power supply was connected via insulated copper wiring to the electrodes of the microchannel device to provide worms with electrical stimulus. A microscope, camera and monitor allowed visualization and recording of the electrotaxis experiment.

Worms were washed off of their culture plates, cleaned, and suspended in M9 buffer. Animals were then aspirated into the channel using the syringe. Individual worms were isolated by adjusting the tubes' relative height to hydrostatically manipulate the flow of M9 through the channel. Both tubes were then laid flat at the same elevation to eliminate pressure-induced flow. Next, a 3 V/cm DC electric field was applied and the worm's resultant behaviour recorded by camera. Locomotory data was later extracted from recorded videos using custom MATLAB-based worm tracking software.

2.6 Fluorescence microscopy

Fluorescent reporter-expressing strains were mounted on 4% agar pads on glass slides and examined under Nomarski optics. To anesthetize animals, each pad contained a 15-μL drop of 30 mM NaN_3 in M9 buffer. Epifluorescence was visualized with a Hamamatsu ORCA-AG camera, a Nikon Eclipse 80i microscope, a GFP or YFP filter (31044V2 CY GFP C61331), and NIS-Elements BR software version 3.0 (*www.nis-elements.com*). Images were processed using NIH ImageJ (*http://rsbweb.nih.gov/ij*).

2.7 Basal slowing response

The following protocol was originally developed by Sawin and colleagues (***33***). Assay plates containing food were prepared by spreading *E. coli* HB101 in a ring with an outer diameter of approximately 3.5 cm and an inner diameter of approximately 1 cm onto an NGM agar plate, incubating overnight at 37°C, and then cooling to room temperature. Assay plates lacking food were also incubated at 37°C and cooled to room temperature before use.

For each assay trial, well-fed animals were washed twice in M9 buffer and then transferred to an assay plate in a drop of buffer. In the cases of assay plates with food, worms were placed in the bacteria-free circle at the center of the ring. The drop of buffer containing the worms was absorbed with tissue paper to allow animals to crawl onto the agar. After 5 min of acclimatization, the number of body bends propagated by each worm in a 20 s interval of continuous locomotion was recorded as its locomotory rate. The slowing rate was calculated as the ratio of the locomotory rate on assay plates with food to the locomotory rate on assay plates without food.

2.8 Data analysis

Electrotaxis speed data was analyzed using the non-parametric Mann-Whitney test. All other data was analyzed with Student's *t*-test. All tests were performed using the Systat SigmaPlot statistical software package version 11.0 (*www.sigmaplot.com*) with significance set at $P < 0.05$. For all assays, data from all repeats were pooled and analyzed together.

3. RESULTS

3.1 Ectopic expression of αSyn causes electrotactic defects

We began our investigation by determining whether broadly expressed αSyn could affect the electrotactic swimming behaviour of *C. elegans*. For these experiments, we employed NL5901 *unc-54::*αSyn(A53T)::YFP and FX14480 *unc-51::*αSyn(A53T) transgenic animals. To evaluate electrotactic behaviour, we loaded young adult worms into a microchannel and measured their speed upon electric field activation. As shown in **Figure 1**, NL5901 worms, which express αSyn in the body wall and other muscles, move significantly more slowly than N2 wild-type controls inside the electric field. FX14480 worms express αSyn pan-neuronally as well as in muscles; as expected, FX14480 animals show significant defects even compared to NL5901 (**Figure 1**). These findings indicate that overexpression of αSyn in *C. elegans* impairs its electrotactic swimming behaviour.

Genome-wide RNAi screens have identified a number of genetic modifiers of αSyn inclusion formation, among them *lagr-1* and *ymel-1* (**21**). *lagr-1* encodes an ortholog of human LASS1, a sphingolipid synthase, and *ymel-1* encodes an ortholog of human presenilin-associated metalloprotease (PAMP), a mitochondrial protease. We confirmed that RNAi knockdown of either gene exacerbates the formation of αSyn inclusion formation in NL5901 (**Supplementary Figure 1**, A-C), and further observed that RNAi against *lagr-1* or *ymel-1* worsens the locomotory phenotype of NL5901 in the electrotaxis assay (**Supplementary Figure 1**, D), implicating aggregation as a factor relevant to αSyn's effect on behaviour.

3.2 Expression of αSyn in DA neurons accelerates aging-related neurodegeneration, produces defective DA-mediated behaviours, and exacerbates aging-related declines in electrotactic speed

Because PD is primarily associated with DA neuronal death, we opted to focus the rest of our investigation on transgenic worms that express αSyn specifically in DA neurons, of which *C. elegans* contains only eight: 4 CEP and 2 ADE neurons in the head, and 2 PDE neurons in the tail region. To this end, we used microinjection to generate two independent *dat-1::*αSyn(A53T); *dat-1::*YFP lines, DY463 and DY465. Both strains are superficially indistinguishable from wild-type N2 animals at the plate level except for their expression of YFP in DA neurons. As the two lines are identical, we concentrated our remaining experiments on DY463. Although similar *C. elegans* PD models have been

generated and analyzed in the past (**19**,**20**), we first sought to establish that our in-house-generated line appropriately mimics PD in terms of DA neurodegeneration. This neuronal damage can be visualized using fluorescence microscopy, where it manifests as a decreased number of fluorescing cell bodies and/or punctate patterns in projections (**Figure 2**). Indeed, compared to DY328 *dat-1::*YFP controls, DY463 animals show significantly more neuronal damage, and the difference becomes more prominent with age (**Figure 3**).

There are several established behavioural assays for evaluating the state of the DA signaling system in *C. elegans*. We used one, the basal slowing response, to further characterize our DY463 transgenic line. The basal slowing response is a DA-dependent food-sensing behaviour in which worms decrease their rate of movement upon encountering a food source, likely an adaptive mechanism to increase the amount of time animals spend in the presence of food. This behaviour is triggered by worms' perception of a mechanical attribute of bacteria, which is mediated by mechanosensory DA neurons (**33**). As expected, ablation of DA neurons abolishes the response completely (**Figure 4**, A). We also observed abnormal phenotypes in DY463 during this assay. While both N2 and DY463 display a robust basal slowing response in young adulthood, this robustness weakens with age only in DY463 (**Figure 4**, B). This observation indicates that the DA signaling system is perturbed to the extent of behavioural manifestation in DY463.

Our next goal was to characterize the locomotory phenotype of DY463 *dat-1::*αSyn using microfluidic electrotaxis. As shown in **Figure 5**, young adult DY463 animals do not display electrotactic speeds that are significantly different from those of wild-type controls; however, differences appear with age. Although even N2 animals show a decline in motility as they grow older, this decline is more pronounced in DY463: indeed, 5-day-old DY463 animals swim with speeds similar to those of 7-day-old N2, and 7-day-old DY463 animals move like 9-day-old N2 (**Figure 5**, A). In contrast, no exacerbation of motor decline appears in DY481 *lin-11-int3::*αSyn transgenic animals, which express αSyn in ten non-DAergic amphid neurons including AVA, AVE, ADF, ASH, ADL, AWA, ASG, RIC, AIZ, and AVG (**Figure 5**, B), or in KU41 *lrk-1(km41)* mutants (**Supplementary Figure 2**). We note that the DY481 and KU41 electrotaxis data were conducted during the same experiment, and that **Figure 5** and **Supplementary Figure 2** therefore display the same control data. Overall, these results show that DY463 develops PD-like motor symptoms that are detectable via microfluidic electrotaxis as a result of αSyn expression in DA neurons, supporting the viability of using *dat-1::*αSyn transgenic animals as a baseline upon which to test potential PD therapeutic compounds with our electrotaxis platform.

3.3 Chronic curcumin treatment ameliorates αSyn-induced DA neurodegeneration and aging-related declines in electrotactic speed

Having established that DY463 *dat-1::*αSyn *C. elegans* simulate PD in terms of DA neurodegeneration and locomotion, we proceeded to use DY463 to evaluate the efficacy of curcumin as a neuroprotective agent. We first investigated curcumin's ability to rescue the accelerated DA neurodegenerative phenotypes of DY463 animals. As shown in **Figure 6**, chronic curcumin treatment has no apparent effect on αSyn-expressing DA neurons at 100 μM, but significantly reduces the frequency of dendritic damage at 500 μM. These findings suggest that curcumin can protect DA neurons against αSyn toxicity when administered at a sufficiently high dose.

Next, we assessed the effect of 500 μM curcumin on DY463 electrotaxis. Interestingly, while curcumin treatment has no effect on either N2 or DY463 at young adulthood, it completely rescues the electrotactic deficits that appear in 5-day-old DY463 worms (**Figure 7**, A). 9-day-old DY463 animals also derive significant benefit from curcumin in terms of electrotactic speed preservation, though some degree of locomotory depression relative to young adults remains (**Figure 7**, B). These observations indicate that curcumin can mitigate aging-related declines in motility in *dat-1::*αSyn transgenic worms. Together with the neuronal phenotype data, the results of these experiments support the therapeutic benefit of curcumin in the context of αSyn-induced DA neurodegeneration.

4. DISCUSSION

We have here characterized for the first time the electrotactic phenotypes of transgenic PD model *C. elegans* ectopically expressing αSyn(A53T). *dat-1::*αSyn animals in particular display aging-related speed deficits relative to age-matched controls, which do not appear in other transgenics and PD-related mutants (**Figure 5**; **Supplementary Figure 2**). We have also shown that curcumin can ameliorate the electrotactic swimming defects that develop in aging *dat-1::*αSyn transgenic animals. Given that this effect coincides with rescue of DA neurodegenerative phenotypes and does not impact speed of young adult (pre-symptomatic) worms, curcumin's rescue of electrotactic slowness in aging *dat-1::*αSyn animals appears to be a manifestation of its protective properties rather than a non-specific increase in locomotory rate.

Although no other research group to our knowledge has taken a microfluidic approach to PD-related research using *C. elegans*, several past studies have employed αSyn PD model worms. Lakso and colleagues were the first to establish αSyn-overexpressing *C. elegans* models and reported that while

pan-neuronal and motor neuronal expression of αSyn impairs thrashing rate of young adults in M9 buffer, DA neuronal expression of αSyn does not (**34**). These results concur with our observations that pan-neuronal expression of αSyn causes electrotactic swimming defects even in young adulthood while worms expressing αSyn in DA neurons only develop speed deficits in later life. Another study by Kuwahara and colleagues reported that worms expressing αSyn in DA neurons show defective basal slowing responses (**19**), which was also observed in the present study. An additional study by Cao and colleagues found that slightly aged *dat-1::*αSyn worms show not only basal slowing response impairment, but also decreases in general locomotion, measured as centroid velocity on a plate without stimulus (**20**). Although they did not take velocity measurements at different ages, and the scoring process was likely complicated by animals' freedom to perform random behaviours (arbitrary pauses, reorientations, omega turns, and reversals) in the absence of a constant stimulus, their observation of motor deficit agrees with the results from our microfluidic electrotaxis assay. Therefore, the behavioural data of the present study is highly consistent with that of the established literature. Some differences in neurodegenerative phenotype were observed, but on this point the past studies also disagree with each other: Lakso and colleagues reported both losses of cell bodies and damage to processes but no worsening of the phenotype with age (**34**), Kuwahara and colleagues reported losses of fluorescence in dendrites but not cell bodies (**19**), and Cao and colleagues reported both losses of cell bodies and damage to processes that do worsen with age (**20**). Our own findings bear most resemblance to the latter study. Regardless, it is likely that these discrepancies are due to minor variations between transgenic strains, as each group has generated its own.

There is also some disagreement regarding the changes in actual DA content that accompany αSyn-induced DA neurodegeneration. Kuwahara and colleagues found decreased DA in their *dat-1::*αSyn lines (**19**), which is intuitive in the context of DA cell death and consistent with striatal DA reduction in PD patients. However, Cao and colleagues reported increased DA in their *dat-1::*αSyn worms, hypothesizing that αSyn alters DA synaptic vesicle trafficking or packing to reduce the availability of DA synaptic vesicles at synapses while simultaneously stimulating DA synthesis through feedback control mechanisms (**20**). We therefore have plans to investigate the DA content of our own lines using high-performance liquid chromatography (HPLC), and have used gamma irradiation to integrate the *dat-1::*αSyn extrachromosomal array (creating the DY482 *bhIs7* strain) for this purpose.

Our findings regarding the ability of curcumin to mitigate αSyn-induced neuronal and behavioural defects are interesting in light of previous studies reporting that curcumin inhibits neurotoxin-induced DA neuron damage in rodents and αSyn aggregation in cell lines (**15**). Taken together, these data

strongly support further exploration of curcumin as a neuroprotective agent with potential applications for PD. To test whether curcumin's protective effect is specific to DA neurons, future experiments will investigate whether curcumin treatment can also rescue the electrotactic speed deficits of *unc-54::*αSyn and *unc-51::*αSyn transgenic animals. We are also interested in elucidating the mechanisms behind curcumin's action, which we plan to address with an RNAi screen. We have created a neuronal RNAi-hypersensitive strain (DY471 *nre-1(hd20) lin-15b(hd126); dat-1::αSyn; dat-1::YFP*) for this purpose.

Transgenic worms exhibiting functional disturbances caused by A53T αSyn expression in DA neurons promise to facilitate PD research. In addition to providing a platform on which to screen for molecules that block neuronal dysfunction and degeneration, such PD models may contribute to the illumination of the genetics underlying αSyn neurotoxicity. αSyn-expressing lines have been used in RNAi screens in the past to identify modifiers of αSyn-induced inclusion formation and abnormalities in neuronal function (**21**,**35**), but similar screens have yet to be performed in worms where αSyn expression is restricted to DA neurons. We have plans to pursue such an investigation in the future (again using DY471).

5. CONCLUSION

In summary, we have taken an electro-microfluidic approach to the characterization of transgenic PD model worms ectopically expressing αSyn, especially those expressing αSyn in DA neurons. We observed significant electrotactic speed defects that are ameliorated by chronic treatment with curcumin, a putative neuroprotective agent. These findings support the utility of the microfluidic electrotaxis platform for evaluating potential PD therapeutics and encourage further investigation into the use of curcumin as a preventative measure against PD.

Acknowledgements

Many thanks to fellow members of the Gupta laboratory for discussion and feedback. Many strains were acquired from the Caenorhabditis Genetics Center, which is supported by the National Institutes of Health's National Center for Research Resources. This work was funded by the Ontario Ministry of Research and Innovation and the Collaborative Health Research Projects award, co-funded by the Natural Sciences and Engineering Research Council of Canada and the Canadian Institutes of Health Research.

References

1. Lees, A. J.; Hardy, J.; Revesz, T. Parkinson's disease. *Lancet* **2009,** *373* (9680), 2055-2066.

2. Braak, H.; Ghebremedhin, E.; Rüb, U.; Bratzke, H.; Del Tredici, K. Stages in the development of Parkinson's disease-related pathology. *Cell Tissue Res* **2004,** *318* (1), 121-134.

3. Niccolini, F.; Su, P.; Politis, M. Dopamine receptor mapping with PET imaging in Parkinson's disease. *J Neurol* **2014,** [Epub ahead of print].

4. Saiki, S.; Sato, S.; Hattori, N. Molecular pathogenesis of Parkinson's disease: update. *J Neurol Neurosurg Psychiatry* **2012,** *83* (4), 430-436.

5. Bendor, J. T.; Logan, T. P.; Edwards, R. H. The function of α-synuclein. *Neuron* **2013,** *79* (6), 1044-1066.

6. Cookson, M. R. α-Synuclein and neuronal cell death. *Mol Neurodegener* **2009,** *4*, 9.

7. Pountney, D. L.; Lowe, R.; Quilty, M.; Vickers, J. C.; Voelcker, N. H.; Gai, W. P. Annular alpha-synuclein species from purified multiple system atrophy inclusions. *J Neurochem* **2004,** *90* (2), 502-512.

8. Brundin, P.; Li, J. Y.; Holton, J. L.; Lindvall, O.; Revesz, T. Research in motion: the enigma of Parkinson's disease pathology spread. *Nat Rev Neurosci* **2008,** *9* (10), 741-745.

9. Martin, I.; Kim, J. W.; Lee, B. D.; Kang, H. C.; Xu, J.-C.; Jia, H.; Stankowski, J.; Kim, M.-S.; Zhong, J.; Kumar, M.; Andrabi, S. A.; Xiong, Y.; Dickson, D. W.; Wszolek, Z. K.; Pandey, A.; Dawson, T. M.; Dawson, V. L. Ribosomal Protein s15 Phosphorylation Mediates LRRK2 Neurodegeneration in Parkinson's Disease. *Cell* **2014,** *157* (2), 472-485.

10. Shimura, H.; Hattori, N.; Kubo, S. I.; Mizuno, Y.; Asakawa, S.; Minoshima, S.; Shimizu, N.; Iwai, K.; Chiba, T.; Tanaka, K.; Suzuki, T. Familial Parkinson disease gene product, parkin, is a ubiquitin-protein ligase. *Nat Genet* **2000,** *25* (3), 302-305.

11. Doyle, K. M.; Kennedy, D.; Gorman, A. M.; Gupta, S.; Healy, S. J.; Samali, A. Unfolded proteins and endoplasmic reticulum stress in neurodegenerative disorders.

J Cell Mol Med **2011,** *15* (10), 2025-2039.

12. Goldenberg, M. M. Medical management of Parkinson's disease. *P T* **2008,** *33* (10), 590-606.

13. Kulkarni, S. K.; Dhir, A. An overview of curcumin in neurological disorders. *Indian J Pharm Sci* **2010,** *72* (2), 149-154.

14. Sookram, C.; Daya, R.; Tan, M.; Mah, J.; Mishra, R. K. Curcumin: Implications in the Treatment of Central Nervous System Disease. In *Curcumin: Biosynthesis, Medicinal Uses and Health Benefits;* Sasaki, J., Kichida, M., Eds.; Nova Publishers: Hauppauge, NY, 2012; pp 1-38.

15. Monroy, A.; Lithgow, G. J.; Alavez, S. Curcumin and neurodegenerative diseases. *Biofactors* **2013,** *39* (1), 122-132.

16. Liao, V. H.; Yu, C. W.; Chu, Y. J.; Li, W. H.; Hsieh, Y. C.; Wang, T. T. Curcumin-mediated lifespan extension in Caenorhabditis elegans. *Mech Ageing Dev* **2011,** *132* (10), 480-487.

17. Blesa, J.; Phani, S.; Jackson-Lewis, V.; Przedborski, S. Classic and new animal models of Parkinson's disease. *J Biomed Biotechnol* **2012,** *2012,* 845618.

18. Kaletta, T.; Hengartner, M. O. Finding function in novel targets: C. elegans as a model organism. *Nat Rev Drug Discov* **2006,** *5* (5), 387-398.

19. Kuwahara, T.; Koyama, A.; Gengyo-Ando, K.; Masuda, M.; Kowa, H.; Tsunoda, M.; Mitani, S.; Iwatsubo, T. Familial Parkinson mutant α-synuclein causes dopamine neuron dysfunction in transgenic Caenorhabditis elegans. *J Biol Chem* **2006,** *281* (1), 334-340.

20. Cao, P.; Yuan, Y.; Pehek, E. A.; Moise, A. R.; Huang, Y.; Palczewski, K.; Feng, Z. Alpha-synuclein disrupted dopamine homeostasis leads to dopaminergic neuron degeneration in Caenorhabditis elegans. *PLoS One* **2010,** *5* (2), e9312.

21. van Ham, T. J.; Thijssen, K. L.; Breitling, R.; Hofstra, R. M.; Plasterk, R. H.; Nollen, E. A. C. elegans model identifies genetic modifiers of alpha-synuclein inclusion formation during aging. *PLoS Genetics* **2008,** *4,* e1000027.

22. Chronis, N.; Zimmer, M.; Bargmann, C. I. Microfluidics for in vivo imaging of neuronal and behavioral activity in Caenorhabditis elegans. *Nat Meth* **2007,** *4,* 727-

731.

23. Chung, K.; Crane, M. M.; Lu, H. Automated on-chip rapid microscopy, phenotyping and sorting of C. elegans. *Nat Methods* **2008,** *5* (7), 637-643.

24. Rezai, P.; Siddiqui, A.; Selvaganapathy, P. R.; Gupta, B. P. Electrotaxis of Caenorhabditis elegans in a microfluidic environment. *Lab Chip* **2010,** *10*, 220-226.

25. Tong, J.; Rezai, P.; Selvaganapathy, P. R.; Mishra, R. K.; Gupta, B. P. Chronic exposure to metal salts induces defects in the electrotactic swimming behaviour of the nematode Caenorhabditis elegans. *(in preparation).*

26. Tong, J.; Sung, B.; Selvaganapathy, P. R.; Mishra, R. K.; Gupta, B. P. Paraquat, the heat shock response, and proteotoxic stress converge on the ER to modulate electrotactic swimming behaviour in Caenorhabditis elegans. *(in preparation).*

27. Salam, S.; Ansari, A.; Amon, S.; Rezai, P.; Selvaganapathy, P. R.; Mishra, R. K.; Gupta, B. P. A microfluidics set up to study neuronal degeneration and identification of neuroprotective compounds in C. elegans. *Worm* **2013,** *2* (3), e24558.

28. Evans, T. C. Transformation and microinjection, 2006. WormBook. http://wormbook.org/chapters/www_transformationmicroinjection/transformationmicroinjection.html.

29. Mello, C. C.; Kramer, J. M.; Stinchcomb, D.; Ambros, V. Efficient gene transfer in C.elegans: extrachromosomal maintenance and integration of transforming sequences. *EMBO J* **1991,** 3959-3970.

30. Brenner, S. The genetics of Caenorhabditis elegans. *Genetics* **1974,** *77* (1), 71-94.

31. Stiernagle, T. Maintenance of C. elegans, 2006. WormBook. http://wormbook.org/chapters/www_strainmaintain/strainmaintain.html.

32. Tong, J.; Rezai, P.; Salam, S.; Selvaganapathy, P. R.; Gupta, B. P. Microfluidic-based electrotaxis for on-demand quantitative analysis of Caenorhabditis elegans' locomotion. *J Vis Exp* **2013,** *75*, e50226.

33. Sawin, E. R.; Ranganathan, R.; Horvitz, H. R. C. elegans locomotory rate is modulated by the environment through a dopaminergic pathway and by experience through a serotonergic pathway. *Neuron* **2000,** *26* (3), 619-631.

34. Lakso, M.; Vartiainen, S.; Moilanen, A. M.; Sirviö, J.; Thomas, J. H.; Nass, R.; Blakely, R. D.; Wong, G. Dopaminergic neuronal loss and motor deficits in Caenorhabditis elegans overexpressing human alpha-synuclein. *J Neurochem* **2003,** *86* (1), 165-172.

35. Kuwahara, T.; Koyama, A.; Koyama, S.; Yoshina, S.; Ren, C.-H.; Kato, T.; Mitani, S.; Iwatsubo, T. A systematic RNAi screen reveals involvement of endocytic pathway in neuronal dysfunction in a-synuclein transgenic C. elegans. *Hum Mol Genet* **2008,** *17* (19), 2997-3009.

36. Hills, T.; Brockie, P. J.; Maricq, A. V. Dopamine and glutamate control area-restricted search behavior in Caenorhabditis elegans. *J Neurosci* **2004,** *24* (5), 1217-1225.

Figures

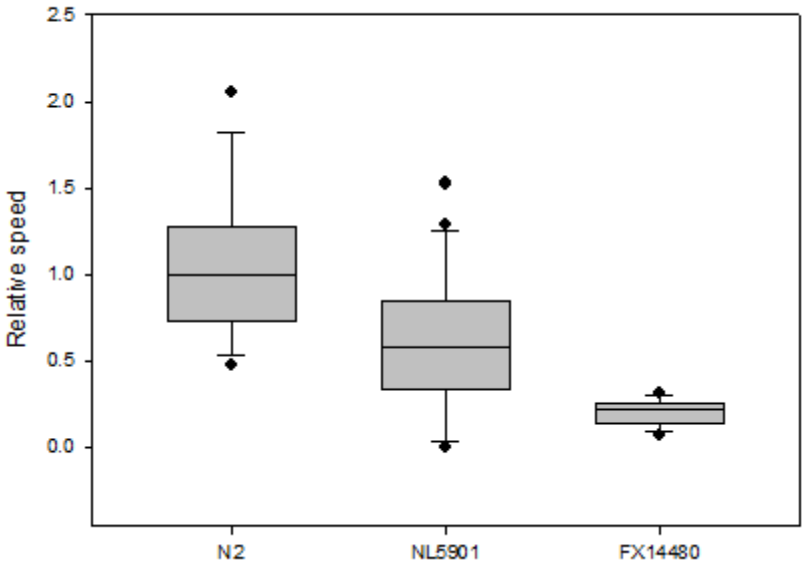

Figure 1. Transgenic animals expressing αSyn in muscles and neurons exhibit electrotactic swimming deficits in young adulthood. Boxes represent measurements from 25th to 75th percentiles, central horizontal lines represent medians, vertical lines extend to 10th and 90th percentiles, and dots represent outliers. NL5901 *unc-54::*αSyn ($p < 0.01$) transgenic animals show significant slowness relative to wild-type controls, and FX14480 *unc-51::*αSyn show even more severe defects than NL5901 ($p < 0.01$).

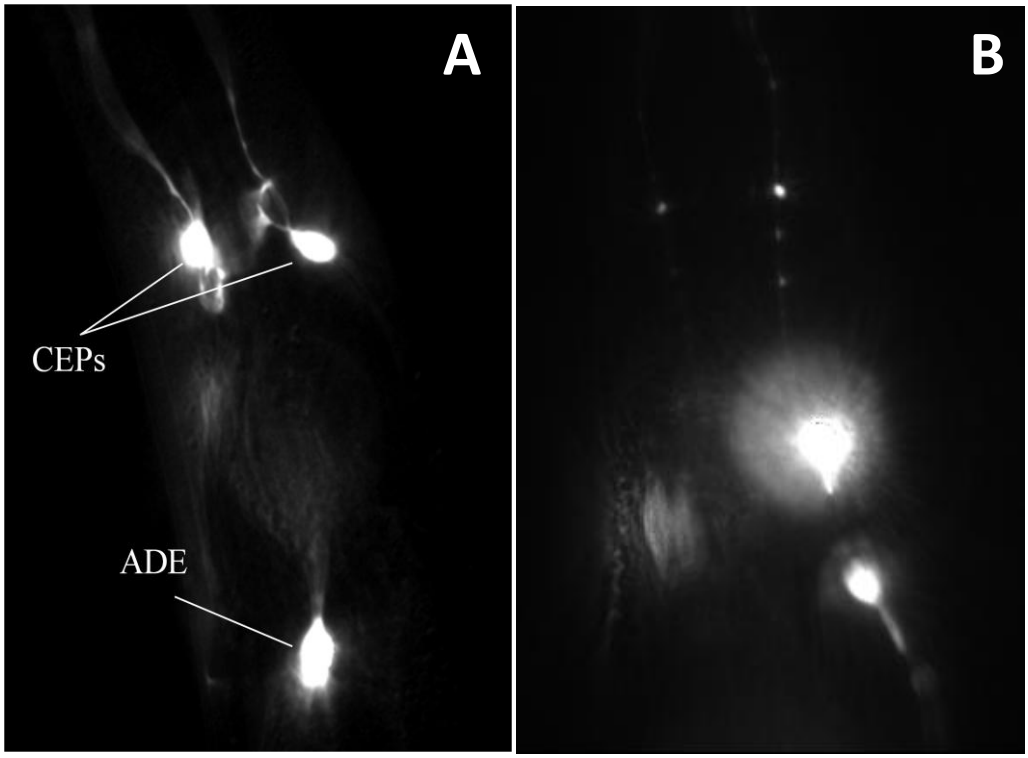

Figure 2. Degenerative phenotype of DAergic CEP and ADE neurons. (A) Healthy DA neurons in 5-day-old DY328 *dat-1::*YFP animals. (B) DA neurons bearing punctate-patterned dendrites in 5-day-old DY463 *dat-1::*αSyn; *dat-1::*YFP animals.

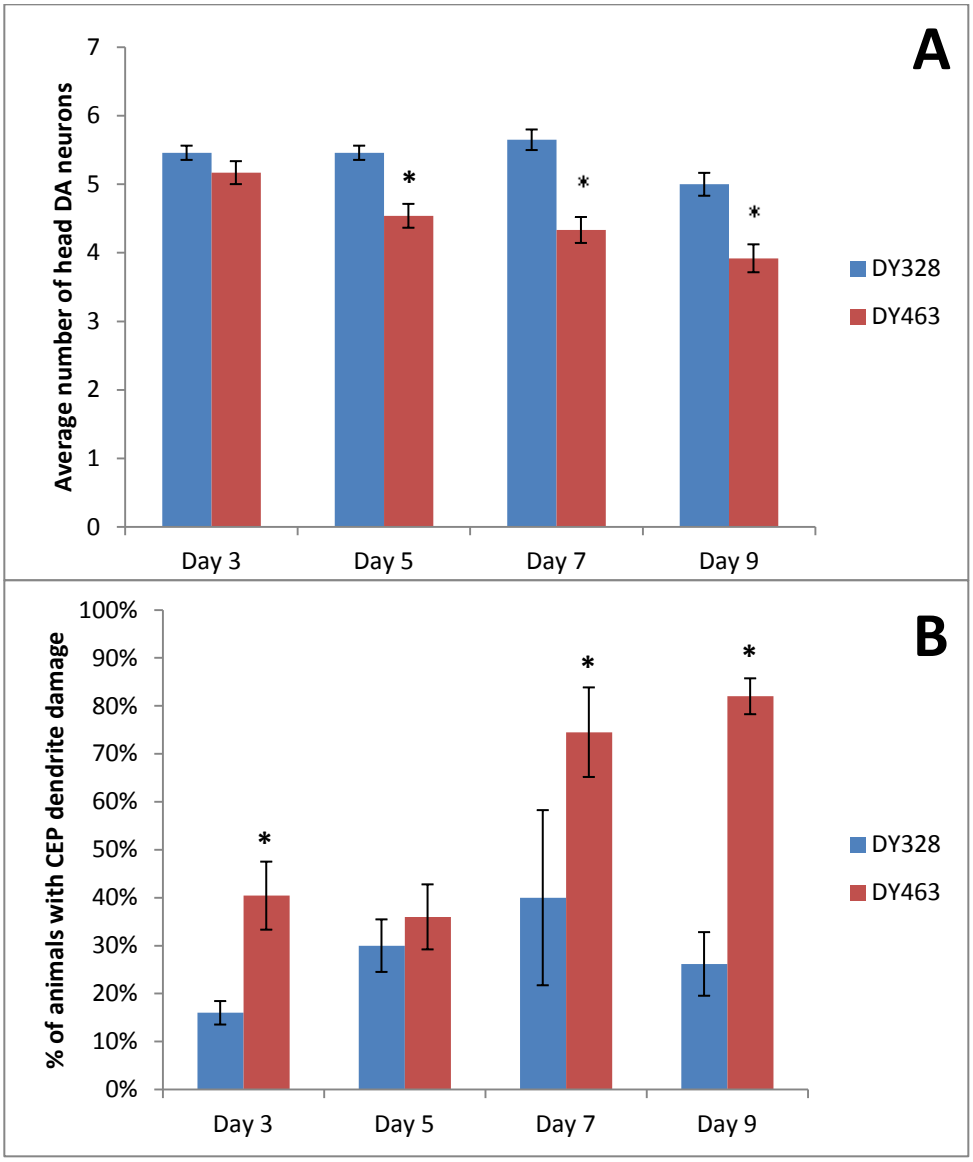

Figure 3. Transgenic animals expressing αSyn in DA neurons show accelerated aging-related neurodegeneration. Compared to DY328 *dat-1::*YFP controls, DY463 *dat-1::*αSyn; *dat-1::*YFP animals (A) lose DA neuronal cell bodies more quickly with age, and (B) develop DA dendritic damage more frequently. * denotes significant ($P < 0.05$) differences between DY328 and DY463.

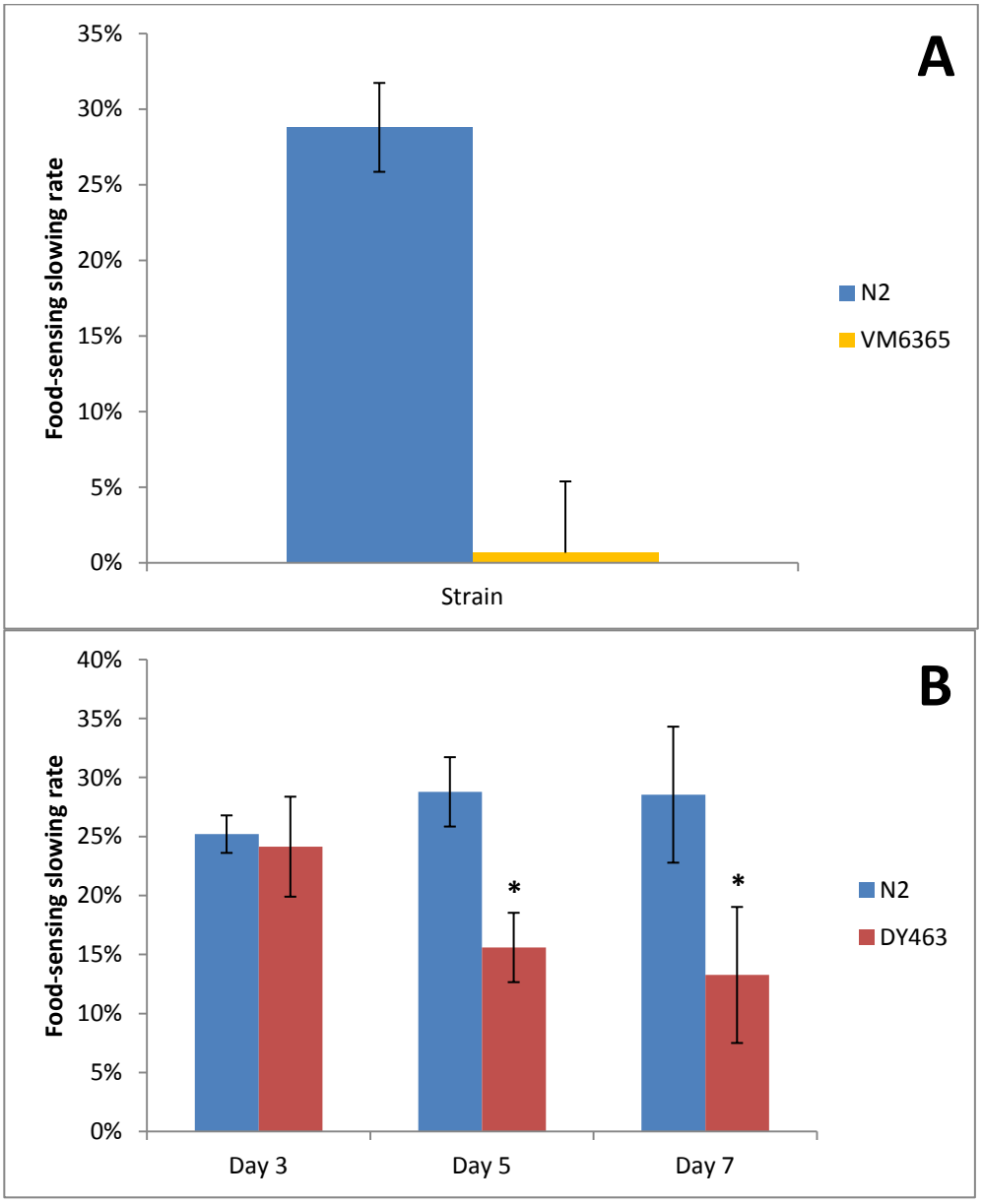

Figure 4. The basal slowing response requires DA signaling and is perturbed in transgenic animals expressing αSyn in DA neurons. (A) The basal slowing response is abolished in young adult VM6365 *dat-1::*ICE animals, which lose all DA neurons in early L1 **(***36***)**. (B) DY463 *dat-1::*αSyn animals develop basal slowing response deficits by Day 5 of life. Slowing rates were calculated as the percentage decrease of locomotory rate (counted as frequency of body bending)

on plates with bacteria as compared with that on plates without bacteria. * denotes significant ($P < 0.05$) differences between N2 and DY463.

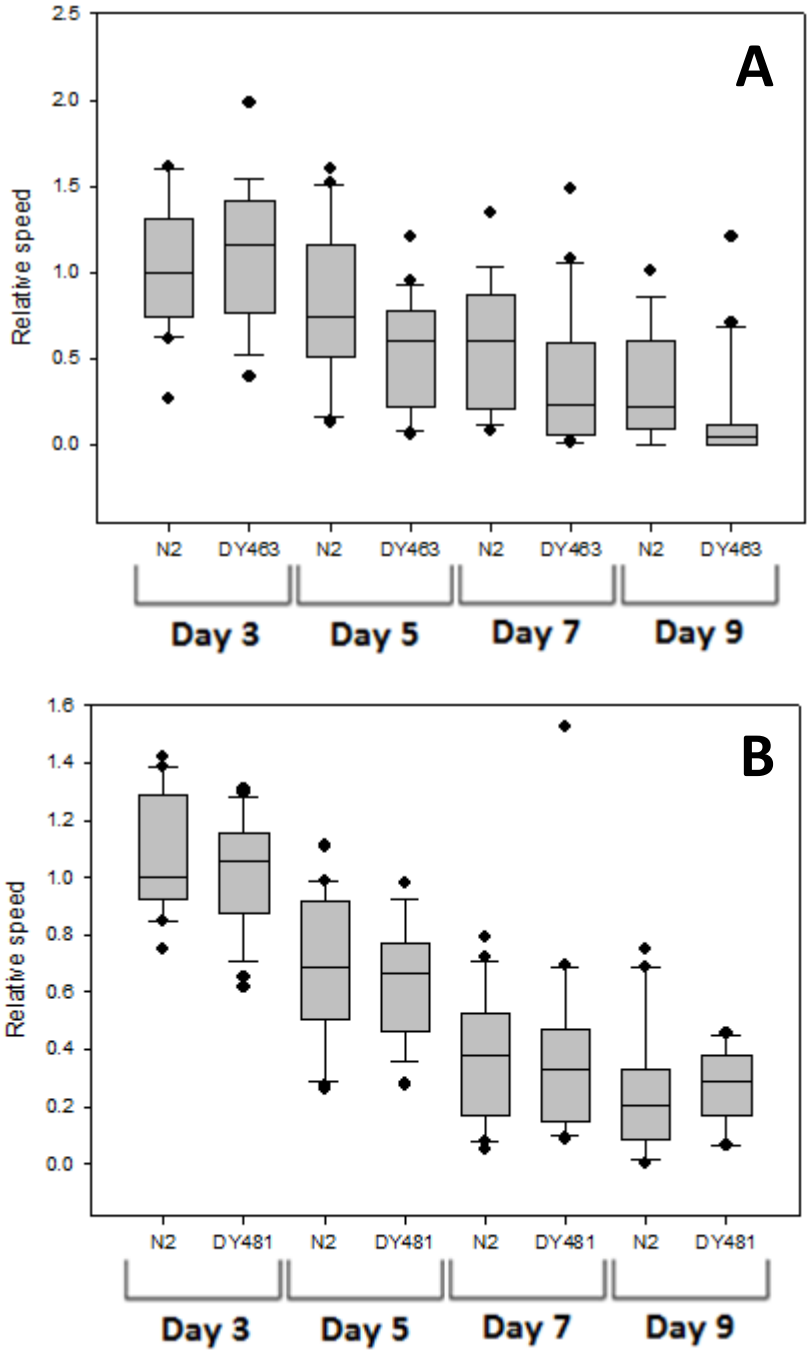

Figure 5. Transgenic animals expressing αSyn in DA neurons, but not other amphid neurons, exhibit aging-related declines in electrotactic speed. Refer to Figure 1 for description of box plot. (A) DY463 *dat-1::*αSyn animals do not differ from controls in young adulthood (Day 3, p = 0.759), but do show slowness relative to age-matched controls on Day 5 (p = 0.021), Day 7 (p = 0.047), and Day

9 ($p = 0.015$) of life. (B) DY481 *lin-11-int3::*αSyn animals, which express αSyn in a number of non-DAergic amphid neurons, do not show electrotactic defects relative to age-matched N2 controls ($P > 0.05$ in all cases).

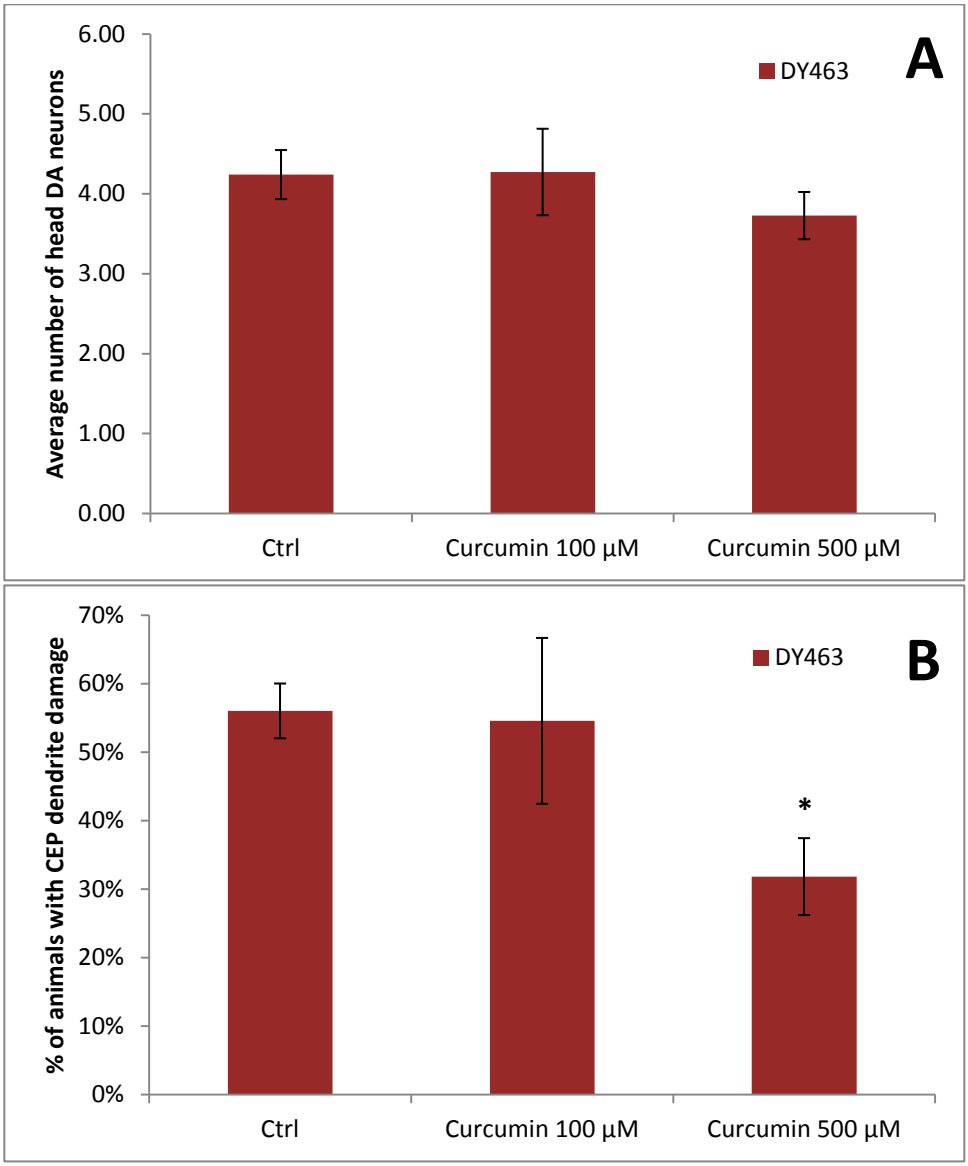

Figure 6. Chronic curcumin exposure ameliorates some neurodegenerative phenotypes of transgenic animals expressing αSyn in DA neurons. (A) Loss of DA neuronal cell bodies in 7-day-old DY463 *dat-1::*αSyn; *dat-1::*YFP animals is not affected by curcumin treatment at either 100 µM ($p = 0.479$) or 500 µM ($p = 0.118$). (B) Curcumin treatment does not affect frequency of dendritic damage in 7-day-old DY463 *dat-1::*αSyn; *dat-1::*YFP animals at 100 µM ($p = 0.410$) but significantly reduces frequency of dendritic damage at 500 µM ($p < 0.01$).

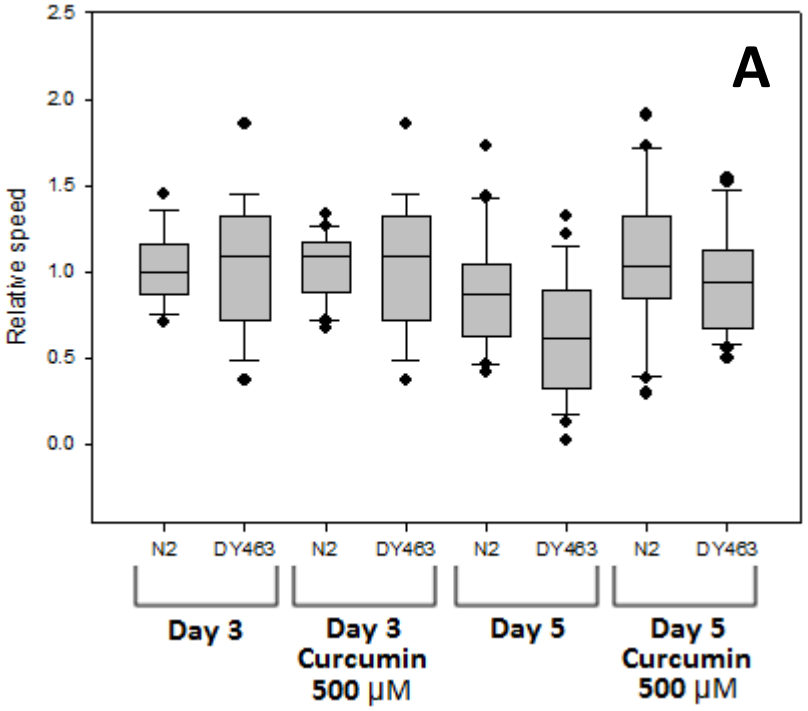
A
Relative speed
2.5
2.0
1.5
1.0
0.5
0.0
N2
DY463
N2
DY463
N2
DY463
N2
DY463
Day 3
Day 3
Curcumin
500 µM
Day 5
Day 5
Curcumin
500 µM

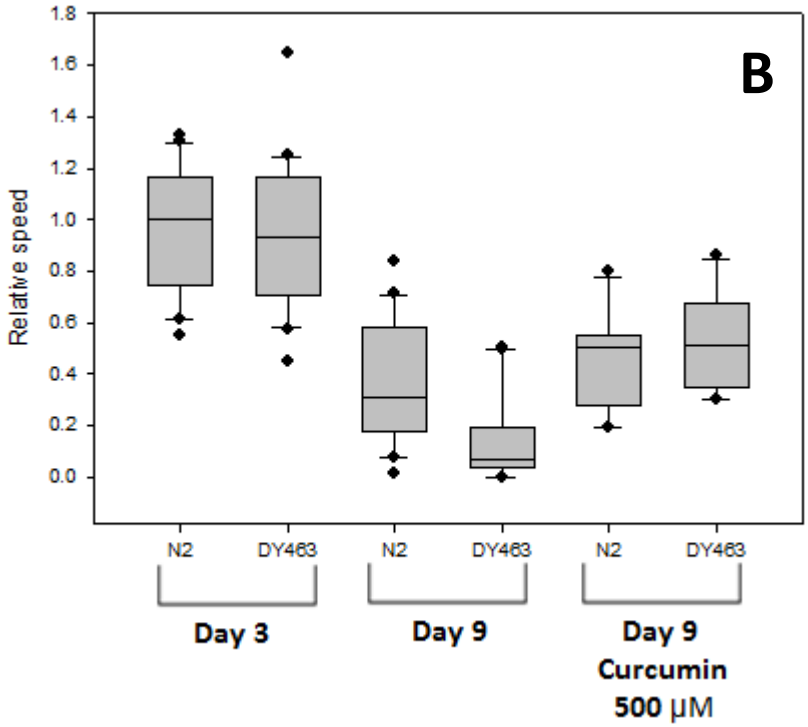
B
Relative speed
1.8
1.6
1.4
1.2
1.0
0.8
0.6
0.4
0.2
0.0
N2
DY463
N2
DY463
N2
DY463
Day 3
Day 9
Day 9
Curcumin
500 µM

Figure 7. Chronic curcumin exposure ameliorates the aging-related decline in electrotactic speed of transgenic animals expressing αSyn in DA neurons. Refer to Figure 1 for description of box plot. (A) 500 μM curcumin treatment does not affect the electrotaxis of young adult (Day 3) wild-type ($p = 0.831$) or DY463 *dat-1::*αSyn ($p = 0.987$) animals, but rescues the age-dependent speed deficits of 5-day-old DY463 worms ($p < 0.01$). The speeds of 5-day-old curcumin-treated DY463 worms are indistinguishable from those of their 3-day-old counterparts ($p = 0.498$). Curcumin treatment may also benefit 5-day-old wild-type animals, but the effect is not statistically significant ($p = 0.172$). (B) 500 μM curcumin treatment significantly improves electrotactic motility of 9-day-old DY463 ($p < 0.01$). Curcumin treatment may also benefit 9-day-old wild-type animals, but the effect is not statistically significant ($p = 0.194$).

Supplementary Information

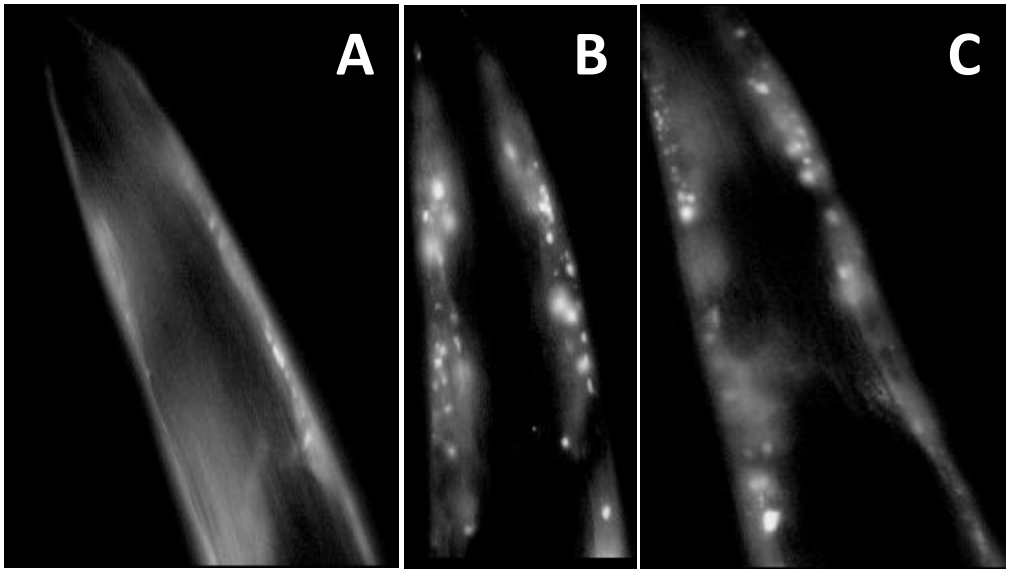

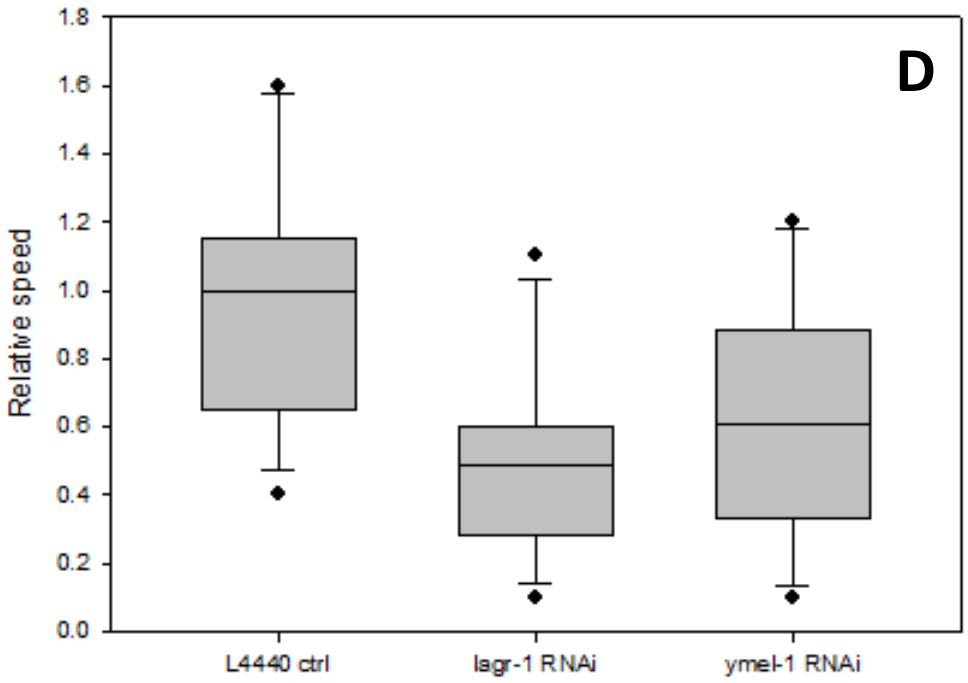

Supplementary Figure 1. RNAi knockdown of genes affecting αSyn inclusion formation exacerbates electrotactic defects of transgenic animals expressing αSyn in muscles. (A) 5-day-old NL5901 *unc-54::*αSyn::YFP transgenic animals show a

small number of αSyn clusters along the periphery of the head. (B) RNAi knockdown of the sphingolipid synthase *lagr-1*, an ortholog of human LASS1, causes an increase in the number and size of αSyn clusters developed by NL5901 animals by Day 5 of life. *lagr-1* was first identified as a modifier of αSyn inclusion formation in a screen performed by van Ham and colleagues **(***21***)**. (C) RNAi knockdown of the mitochondrial protease *ymel-1*, an ortholog of human presenilin-associated metalloprotease (PAMP), causes a similar increase in NL5901 αSyn aggregation. *ymel-1* was also identified as a modifier of αSyn inclusion formation in the screen performed by van Ham and colleagues **(***21***)**. (D) RNAi knockdown of either *lagr-1* ($p < 0.01$) or *ymel-1* ($p = 0.027$) causes significant further electrotactic slowness in young adult NL5901 transgenic worms.

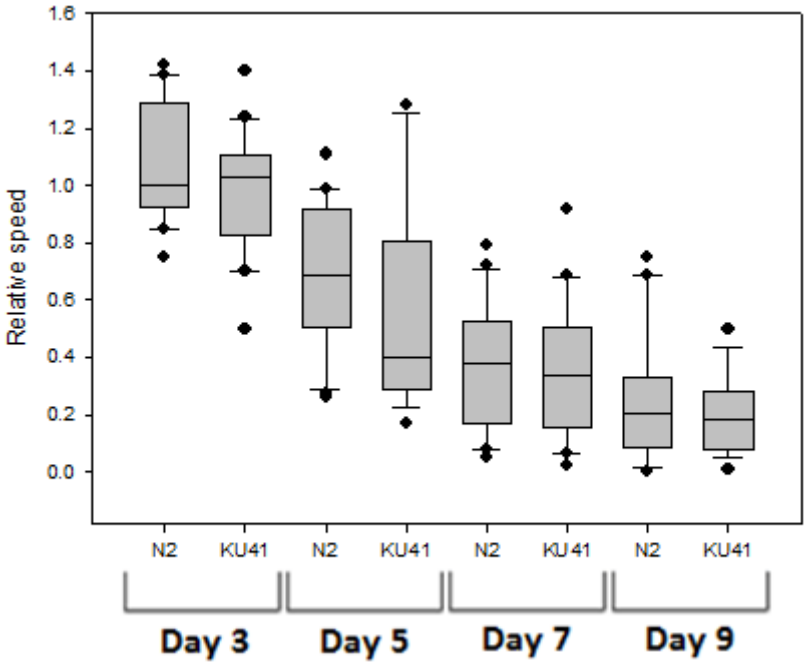

Supplementary Figure 2. Aging-related declines in electrotactic speed are not affected by *lrk-1* knockout. Regardless of age, KU41 *lrk-1(km41)* animals do not show electrotactic defects relative to age-matched N2 controls ($P > 0.05$ in all cases).

Significance

This study identifies and quantifies electrotactic locomotory abnormalities in transgenic αSyn-expressing PD model worms for the purpose of establishing the microfluidic electrotaxis platform as a means of evaluating candidate compounds for PD therapy. We construct transgenic worm lines that express αSyn in DA neurons and observe an exacerbation of age-dependent declines in motility that correlate with DA neurodegeneration. We further show that treatment with curcumin, a putative neuroprotective agent, ameliorates both the neuronal and electrotactic phenotypes that develop in αSyn-expressing worms. These findings support the utility of *C. elegans* microfluidic electrotaxis for the evaluation of potential PD therapeutics and encourage further investigation into the use of curcumin as a preventative measure against PD.

Chapter 5-Effects of environmental and genetic stresses on electrotaxis of *C. elegans*

Citation & Author Contributions

This work was led by JT under the senior supervision of PRS, RKM, and BPG. JT was directly involved in all steps including project formulation, data collection, analysis, and reporting for dissemination. The second co-author BS assisted with data collection as a junior lab member in completion of undergraduate thesis requirements.

Tong, J.; Sung, B.; Selvaganapathy, P.R.; Mishra, R.K.; & Gupta, B.P. ER stress modulates electrotactic swimming behaviour in *Caenorhabditis elegans*. (in prep, June 2014).

ER stress modulates electrotactic swimming behaviour in *Caenorhabditis elegans*

Justin Tong[1], Baekjun Sung[1], P. Ravi Selvaganapathy[2], Ram K. Mishra[3], Bhagwati P. Gupta[1*]

[1]Department of Biology, McMaster University, Hamilton, ON

[2]Department of Mechanical Engineering, McMaster University, Hamilton, ON

[3]Department of Psychiatry and Behavioural Neurosciences, McMaster University, Hamilton, ON

Key words:

C. elegans, microfluidics, electrotaxis, paraquat, tunicamycin, stress

*Contact:

guptab@mcmaster.ca; Phone: 1-905-525-9140 x26451; Fax: 1-905-522-6066

ABSTRACT

C. elegans exhibits directional locomotion known as electrotaxis in the presence of mild electric fields. When microfluidic systems are employed to maximize field uniformity, this response allows on-demand control over worms' movement, which promises to facilitate screens for agents affecting nervous and muscular systems. However, extensive inquiry into the types of stresses that perturb electrotactic swimming is still lacking. We show here that while the response is robust and able to withstand many different insults, chronic exposure to the herbicide paraquat causes significant speed deficits. As paraquat is a known inducer of both mitochondrial and ER stress, we further explored which of these two stresses is more closely associated with electrotactic swimming defects. We observed that only a few mitochondrial mutations affect electrotaxis, suggesting that mitochondrial stress and ROS production are not strong predictors of electrotactic deficit. Moreover, both gain-of-function and loss-of-function mutations in *atfs-1*, a key mediator of the mitochondrial unfolded protein response (UPR^{mt}), produce swimming speed deficits. On the other hand, worms treated with tunicamycin, an ER stressor hindering protein folding, or carrying a loss-of-function mutation in ER unfolded protein response (UPR^{ER}) mediator *ire-1* consistently exhibit slowness in the electrotactic assay, suggesting that electrotaxis may be more sensitive to ER stress than to mitochondrial stress. We provide evidence that neuronal damage may account in part for the electrotactic phenotypes of paraquat- and tunicamycin-treated animals. Furthermore, both paraquat and tunicamycin increase *hsp*-driven marker expression, implicating the heat shock transcriptional response in animals' means of coping with these chemically induced stresses. The importance of the heat shock response in preserving normal electrotaxis is underlined by the fact that *hsf-1* mutants display slow electrotaxis that is worsened by exposure to paraquat at concentrations that do not affect wild-type animals. These results suggest that electrotactic swimming behaviour is particularly susceptible to ER stress, and that multiple stress pathways contribute to its preservation in the face of stressful conditions.

1. INTRODUCTION

Behavioural responses in all organisms involve the convergence of many different pathways and are therefore influenced by a variety of factors, both genetic and environmental. Largely reliant on neuronal circuitry for control, behaviours are often negatively impacted by cellular stresses that hinder the function of neurons and other cells necessary for their exhibition. For instance, mutations inhibiting mitochondrial respiration have been reported to manifest as slowed rates of locomotion in nematodes (**1**). Movement deficits can also appear in a variety of taxa following exposure to neurotoxicants such as 1-methyl-4-

phenyl-1,2,3,6-tetrahydropyridine (MPTP) and rotenone (**2**,**3**). These compounds interfere with complex I of the mitochondrial electron transport chain, resulting in oxidative damage and death of dopaminergic neurons, which play important roles in locomotion that are conserved from nematodes to humans (**4**). In addition to mitochondrial stress, endoplasmic reticulum (ER) stress is closely associated with neurodegenerative disease and resultant behavioural abnormality (**5**,**6**,**7**). Also, the transcriptional response mediated by heat shock factor 1 (HSF-1) has been implicated in protecting dopaminergic neurons and other tissues against heat stress-induced degeneration (**8**). HSF-1 is a transcription factor activated by heat, oxidative, and other cellular stresses, its targets including the genes encoding molecular chaperones and other protective factors collectively called heat shock proteins (HSPs) (**9**).

Our knowledge of how stress affects behaviour has emerged from studies using many different models, including the nematode *Caenorhabditis elegans*. *C. elegans* is a particularly attractive model organism due to its genetic tractability, ease of culture, and short three-day life cycle, which all serve to greatly expedite the rate of discovery. Despite its relative simplicity, *C. elegans* shares roughly half of its genes with humans and utilizes many of the same processes. Its body is also appropriately sized for use in microfluidic systems, which have been used to study biological processes in live nematodes with great precision (**10**,**11**).

In earlier work, we found that a mild DC electric field in a microfluidic environment stimulates *C. elegans* to swim towards the cathode in a directed manner (**12**). Both robust and sensitive, this electrotactic behaviour provides a powerful non-invasive method to evaluate the functional output of nematode locomotory circuits under variable conditions such as exposure to neurotoxicants (**3**). However, a comprehensive investigation into the types of stress that can perturb electrotactic swimming has not yet been attempted.

In the current study, we address this gap in knowledge by exploring the impact of stress-inducing environmental manipulations and stress-related genes on the electrotaxis of *C. elegans*. We observed that the electrotactic response is generally robust and able to withstand many different insults. Interestingly, chronic exposure to paraquat, a structural relative of MPTP, was found to produce significant electrotactic speed deficits. Paraquat is a herbicide routinely used in research to induce oxidative stress and works at least partly by inhibiting the function of mitochondrial complex I, which results in increased levels of ROS (**13**) and dopamine neurodegeneration in animal models (**2**). At the same time, paraquat is also associated with endoplasmic reticulum (ER) stress (**14**), leading us to ask whether paraquat's effect on electrotaxis is mediated by mitochondria, ER, or both.

To test the impact of mitochondrial dysfunction on electrotactic behaviour, we conducted a survey of genes involved in mitochondrial function and/or stability, reasoning that the cells that mediate electrotactic behaviour, neurons and muscles, rely heavily on mitochondrial energy production to function. The following genes were included in this survey: *isp-1*, encoding a Rieske iron sulfur protein subunit of mitochondrial complex III; *gas-1*, encoding a subunit of mitochondrial complex I; *mev-1*, encoding cytochrome b, a subunit of mitochondrial complex II; *pink-1*, encoding an ortholog of PTEN-induced kinase 1 (PINK1); *ucp-4*, encoding the sole *C. elegans* ortholog of mammalian mitochondrial uncoupling protein (UCP); *sod-2* and *sod-3*, encoding mitochondrial superoxide dismutases; *clk-1*, encoding demethoxyubiquinone (DMQ) hydroxylase; and *atfs-1*, encoding a bZip transcription factor required for the mitochondrial unfolded protein response (UPR^{mt}). Furthermore, as mitochondrial function is intimately related to the production of reactive oxygen species (ROS) and oxidative stress, we also tested whether treatment with the anti-oxidant compound curcumin could be used to rescue any electrotactic defects of these mitochondrial mutants. Curcumin is a polyphenolic compound present in the South Asian spice turmeric (*Curcuma longa*) with a broad range of protective properties, including inhibition of oxidative stress-induced neuronal damage in Alzheimer's and Parkinson's disease models (**15**,**16**).

To investigate the impact of ER stress on electrotactic swimming, we tested whether treatment with tunicamycin, an established ER stressor, or mutations in key mediators of the ER stress response have any impact on the behaviour. Tunicamycin is a bacterially produced mixture of homologous antibiotics that inhibits N-linked glycosylation to promote protein misfolding, induction of the ER unfolded protein response (UPR^{ER}), and apoptosis in neurons and other cell types (**17**,**18**). The UPR^{ER} is a signal cascade responsible for sensing and protecting cells against ER stress, mediated by protein kinase RNA (PKR)-like ER kinase (PERK), inositol-requiring enzyme 1 (IRE1), and activating transcription factor 6 (ATF6) (**19**); mutants for two of these proteins, PERK/*pek-1* and IRE1/*ire-1*, were tested in this study. We also characterized the electrotaxis of worms carrying a mutation in *pqe-1*, a poorly characterized gene whose loss of function is associated with enhancement of polyglutamine toxicity (**20**), transgene expression, and possibly proteotoxic stress due to upregulation of global protein synthesis (**21**).

Lastly, we analyzed mutants for *hsf-1*, which encodes an ortholog of heat shock transcription factor 1 (HSF1) and serves as a master regulator of the heat shock transcriptional response. Given that paraquat, tunicamycin, and other stresses are known to upregulate HSPs in *C. elegans* (**22**), we hypothesized that the heat shock response might play a protective role in preserving electrotactic behaviour against environmental insults.

Together, these experiments shed light on the types of stress conditions that affect nematode electrotaxis. Our findings will inform future investigations utilizing microfluidic electrotaxis as a functional output of nematode locomotory circuits.

2. MATERIALS AND METHODS

2.1 Strains and culturing

This study used the following *C. elegans* strains: N2: wild-type Bristol isolate; CB1370: *daf-2(e1370)*; CF1038: *daf-16(mu86)*; MQ887: *isp-1(qm150)*; CW152: *gas-1(fc21)*; TK22: *mev-1(kn1)*; CY121: *ucp-4(ok195)*; DY356: *pink-1(ok3538)*; GA184: *sod-2(gk257)*; GA186: *sod-3(tm760)*; GA480: *sod-2(gk257); sod-3(tm760)*; QC115: *atfs-1(et15)*; VC3201: *atfs-1(gk3094)*; RB545: *pek-1(ok275)*; RE666: *ire-1(v33)*; SJ4100: *zcIs13(hsp-6::GFP)*; SJ4058: *zcIs9(hsp-60::GFP)*; PS3551: *hsf-1(sy441*); RB1611: *pqe-1(ok1983)*; SJ4005: *zcIs4(hsp-4::GFP)*; CL2070: *dvIs70(hsp-16.2::GFP + rol-6[su1006])*; and CF1824: *muEx265(hsf-1::HSF-1 + myo-3::GFP)*. DY356 was outcrossed in-house from RB2547: *pink-1(ok3538)*. RB2547 and all other strains were originally obtained from the Caenorhabditis Genetics Center (University of Minnesota, St. Paul, MN). Except where indicated otherwise, animals were grown and maintained at 20°C on nematode growth medium (NGM) agar plates containing *E. coli* OP50 culture using previously described methods (**23**). All experiments used age-synchronous populations obtained by bleach treatment (**24**). Wild-type, untreated control animals were allowed 69 hrs of growth before experiments; growth times for all animals bearing mutations or undergoing treatments that affect developmental rate were appropriately adjusted.

2.2 Chemicals and treatments

Curcumin, paraquat dichloride, tunicamycin, and 5-fluoro-2'-deoxyuridine (FUdR) were obtained from Sigma-Aldrich (St. Louis, MO, USA). Curcumin treatments were first prepared as 100 mM stock solutions in 100% dimethylsulfoxide (DMSO), which were then mixed into liquid NGM agar at the time of pouring plates. Paraquat treatments were first prepared as 20x solutions in M9 buffer; subsequently, 1x treatment plates were produced by spreading 500 μL of the 20x solutions across the surface of plates containing 10 mL of NGM agar. Tunicamycin treatments were first prepared as 5 mg/mL stock solutions in 100% DMSO, then diluted with water to make 20x solutions; subsequently, 1x treatment plates were produced by spreading 500 μL of the 20x solutions across the surface

of plates containing 10 mL of NGM agar. FUdR treatments were first prepared as a 400 μM stock solution in M9 buffer; subsequently, 1x treatment plates were produced by spreading 500 μL of the 400 μM solution across the surface of plates containing 10 mL of NGM agar. In the cases of all chemical treatments except for FUdR, worms were grown on chemical-containing plates from L1 until young adulthood. In the case of FUdR, worms were grown on chemical-containing plates from L4 until either young adulthood or Day 5 of life (Day 3 of adulthood).

For heat stress assays, animals were first grown at 20°C until young adulthood. Plates were then sealed with parafilm and kept in a water bath at 25°C for 5 h or at 33°C for 1 h. Control plates were also sealed but kept at 20°C. Animals were allowed to recover at 20°C with parafilm removed for 6-8 h before electrotaxis assays.

2.3 Microchannel fabrication and electrotaxis assay

Microfluidic channels were fabricated as previously described (**12**,**25**). The channel design was printed on a transparency sheet using high-resolution photoplotting to create a photomask, which was then used in conjunction with SU-8 100 negative photoresist (MicroChem Corp., MA, USA) to lithographically pattern the design onto a silicon wafer. Microchannels were then casted by pouring polydimethylsiloxane (PDMS) pre-polymer (Sylgard 184 Kit, Dow Corning Corp., MI, USA; 10:1 ratio of base and cross-linker) onto the resultant master mold and allowing 24 h for curing. The channel was then excised from the PDMS replica and fluid access ports were punched into each end. Next, the channel, a blank PDMS strip and a glass slide were oxidized via exposure to oxygen plasma for 40 s at 40 W power and stuck together to seal the microchannel. Lastly, plastic tubing and insulated copper wire were affixed to the punched reservoirs and secured with PDMS pre-polymer.

The electrotaxis assay proper has also been described (**12**,**25**). A syringe was attached to one of the inlet/outlet tubes of the PDMS microchannel to facilitate worm loading at the other tube. A power supply was connected via insulated copper wiring to the electrodes of the microchannel device to provide worms with electrical stimulus. A microscope, camera and monitor allowed visualization and recording of the electrotaxis experiment.

In preparation for the assay, worms were washed off of their culture plates, cleaned, and suspended in M9 buffer. Animals were then aspirated into the channel using the syringe pump. Individual worms were isolated by adjusting the tubes' relative height to hydrostatically manipulate the flow of M9 through the channel. Both tubes were then laid flat at the same elevation to eliminate pressure-

induced flow. Next, a 3 V/cm DC electric field was applied and the worm's resultant behaviour recorded by camera. Locomotory data was later extracted from recorded videos using custom MATLAB-based worm tracking software.

2.4 Fluorescence microscopy

Animals were anesthetized through placement in a 15-µL drop of 30 mM NaN_3 in M9, which lay on a solidified pad of 4% agar on a glass slide. Epifluorescence was visualized with a Hamamatsu ORCA-AG camera, a Nikon Eclipse 80i Nomarski fluorescence microscope, a GFP or YFP filter (31044V2 CY GFP C61331), and NIS-Elements BR software version 3.0 (*www.nis-elements.com*). Fluorescence intensity was quantified using NIH ImageJ (*http://rsbweb.nih.gov/ij/*).

2.5 Data analysis

Electrotaxis assays were carried out for up to 5 min. Animals were allowed to travel a minimum distance of 5 mm in one direction, towards the cathode, after which the field polarity was reversed to induce a turning response. Electrotaxis speed data was plotted in box plots and compared with the non-parametric Mann-Whitney test.

All other data was analyzed with Student's *t*-test. All tests were performed using the Systat SigmaPlot statistical software package version 11.0 (*www.sigmaplot.com)* with significance set at $P < 0.05$. For all assays, data from all repeats were pooled and analyzed together.

3. RESULTS

3.1 Paraquat exposure induces deficits in electrotactic speed

To determine which general stress conditions have an impact on *C. elegans*' electrotactic behaviour, we subjected worms to various insults and then loaded them into our microchannel, where we measured their speed upon activation of the electric field. We found that animals can tolerate many different conditions with no effect on electrotaxis, including extension of starvation-induced L1 arrest (**Supplementary Figure 1**), mild heat stress in young adulthood (**Supplementary Figure 2**), FUdR treatment (**Supplementary Figure 3**), diets other than *E. coli* OP50 (**Supplementary Figure 4**), and mutations in the

insulin/IGF-1 signaling pathway (**Supplementary Figure 5**). Interestingly, despite this general robustness, chronic paraquat treatment was observed to affect electrotaxis in both wild-type and mitochondrial mutant backgrounds. As shown in **Figure 1**, chronic exposure to concentrations of paraquat up to 125 μM did not significantly impact electrotactic speed; however, significant slowness was observed at 250 μM. Moreover, genetic backgrounds known to be paraquat-hypersensitive displayed electrotactic defects at exposure concentrations lower than 250 μM. *mev-1(kn1)* mutants exhibited speed deficits when cultured under chronic exposure to either 50 μM or 75 μM paraquat (**Figure 2**). Similarly, *pink-1(ok3538)* animals also showed increased sensitivity to paraquat in the electrotaxis assay, displaying significant sluggishness at 125 μM (**Figure 3**). We also examined *ucp-4(ok195)* mutants, which have not been previously reported to be paraquat-hypersensitive; however, because genetic ablation of UCP function in mammalian cells has been associated with increased ROS and oxidative stress (**26**,**27**,**28**), we included *ucp-4* as a candidate gene modulating paraquat-induced changes in electrotactic behaviour. Interestingly, *ucp-4(ok195)* animals did indeed display increased sensitivity to paraquat under our chronic exposure paradigm, exhibiting slow electrotaxis at 75 μM despite no difference from untreated wild-type at 50 μM or below (**Figure 4**). Together, these observations support the idea that paraquat-induced stress can perturb *C. elegans*' electrotactic behaviour.

Paraquat's biological effects, such as its ability to damage dopaminergic neurons, have traditionally been ascribed to oxidative stress via inhibition of mitochondrial complex I (**29**,**30**). Indeed, chronic paraquat treatment was found to upregulate expression of mitochondrial stress markers *hsp-6::GFP* and *hsp-60::GFP* (**Figure 5**), which is consistent with the findings of a past study conducted by Runkel and colleagues (**22**). However, findings by Choi and colleagues (**31**) suggest that complex I inhibition is not required for paraquat-induced dopaminergic neurodegeneration. Furthermore, in addition to mitochondrial stress, ER stress has been implicated in paraquat's mechanism of toxicity (**14**,**32**,**33**). We therefore next sought to explore whether electrotaxis is more sensitive to mitochondrial dysfunction or ER stress.

3.2 Impairment of mitochondrial respiration depresses electrotactic speed in a ROS-independent manner

To determine whether the electrotactic response is perturbed by mutations affecting mitochondrial function, we conducted a survey of mitochondrial mutants. Most of these animals, including *mev-1(kn1)*, *pink-1(ok3538)*, *ucp-4(ok195)*, *clk-1(e2519)*, *sod-2(gk257)*, *sod-3(tm760)*, and *sod-2(gk257); sod-3(tm760)* double mutants, did not display electrotactic behaviour that differed significantly from the wild-type; however, two particular mutants, *isp-1(qm150)*

and *gas-1(fc21)*, displayed very prominent defects in the electrotaxis assay (**Figure 6**). Although both genes encode components of the electron transport chain, *isp-1(qm150)* is long-lived with resistance to oxidative damage (**34**) while *gas-1(fc21)* is short-lived with increased ROS and sensitivity to oxidative damage (**35**), suggesting that neither lifespan effects nor ROS toxicity can predict electrotaxis effects. This notion is supported by the other mutant data as well, given that *mev-1(kn1)* has increased ROS and oxidative damage with short lifespan (**36**), *clk-1(e2519)* shows decreased oxidative damage and long lifespan (**36**), and *sod* mutants show increased oxidative damage with normal or extended lifespans (**37**), yet all exhibit similar electrotactic behaviour.

Despite their opposite phenotypes in terms of lifespan and sensitivity to oxidative damage, both *isp-1* and *gas-1* mutants have been reported to generate increased levels of endogenous ROS (**38**). We therefore sought to further explore the relationship, or lack thereof, between electrotaxis and ROS by investigating whether the electrotactic defects of *isp-1(qm150)* and *gas-1(fc21)* mutants could be rescued by treatment with an anti-oxidant compound. To address this question, we cultured wild-type, *isp-1(qm150)*, and *gas-1(fc21)* on plates containing 1 mM curcumin from L1 until the electrotaxis assay in adulthood. **Figure 7** shows that curcumin treatment did not affect electrotaxis in a wild-type or *gas-1(fc21)* background but modestly rescued slowness of *isp-1(qm150)*. Given that *isp-1(qm150)* has been reported to be the most resistant to oxidative stress among these three backgrounds (**36**), it is likely that curcumin treatment affected its speed through some property other than its anti-oxidant activity. Moreover, our observation that the electrotactic deficits of *isp-1(qm150)* but not *gas-1(fc21)* could be improved with curcumin indicates that different mechanisms may be responsible for the locomotory depression of these two mutants.

isp-1(qm150) and *gas-1(fc21)* mutants share another property in that both mutations activate the UPR^{mt} (**39**,**40**). We therefore asked whether manipulation of the UPR^{mt} itself would have any impact on electrotactic swimming. The UPR^{mt} is controlled primarily by ATFS-1, a bZip transcription factor that normally translocates to the nucleus only when activated by stress (**41**). We examined two *atfs-1* mutants: *atfs-1(et15)*, in which ATFS-1 is constitutively active, and *atfs-1(gk3094)*, a null mutant. As shown in **Figure 8**, both mutants displayed significantly reduced electrotactic speeds relative to wild-type controls, though the null mutant phenotype was the more severe between the two. These data suggest a complex relationship between the UPR^{mt} and electrotaxis: while the UPR^{mt} may play a role in preserving electrotactic swimming behaviour, its overactivation also produces speed deficits.

3.3 ER stress and impairment of the UPR^{ER} cause electrotactic speed deficits

Having established only a weak relationship connecting mitochondrial dysfunction and oxidative stress to electrotactic defects, we asked whether paraquat's effect on electrotactic swimming might be mediated more by ER stress. We observed a remarkable paraquat-induced increase in expression of *hsp-4::GFP*, an ER stress marker, indicating that paraquat does indeed activate the ER stress response in *C. elegans* (**Figure 9**). A statistically significant increase in expression of *hsp-16.2::GFP*, a marker of cytosolic protein misfolding, was also found following paraquat treatment; however, this increase was small in comparison to that of *hsp-4::GFP*. We then proceeded to investigate the impact of non-paraquat ER stress conditions on electrotaxis. As shown in **Figure 10**, significant electrotactic slowness was displayed by wild-type worms chronically exposed to tunicamycin at concentrations of 5 μg/mL or greater. Moreover, *ire-1(v33)* UPR^{ER}-defective mutants also exhibit motility defects in the electrotaxis assay, although *pek-1(ok275)* mutants do not (**Figure 11**). Together, these results indicate that electrotactic swimming behaviour is particularly susceptible to ER stress-inducing conditions.

We also included *pqe-1(ok1983)* mutants in our analysis as a follow-up to Yamada and colleagues' proposition that PQE-1 may regulate components of translation machinery (**21**). Reasoning that *pqe-1* mutants might suffer from proteotoxic ER stress as a result of globally increased protein synthesis, we quantified the electrotactic speed of *pqe-1(ok1983)* mutants under both standard and chemical exposure conditions. As shown in **Figure 12**, relative to wild-type animals, untreated *pqe-1(ok1983)* mutants show swimming deficits that are exacerbated by treatment with 125 μM paraquat. Furthermore, we observed that these mutants are hypersensitive to tunicamycin. Although *pqe-1(ok1983)* animals' electrotaxis is not affected by very low concentrations of tunicamycin (**Figure 12**), their survival at slightly higher concentrations is significantly compromised: while wild-type animals enjoy nearly 100% survivorship during three days of exposure to 2 μg/mL tunicamycin from L1, this treatment kills over 90% of *pqe-1(ok1983)* mutant animals before adulthood, and the few survivors display severe growth delays (data not shown). These observations support the idea that PQE-1 protects cells against ER stress, likely via regulation of protein synthesis.

3.4 Chronic exposure to paraquat or tunicamycin causes damage to dopaminergic neurons

To investigate whether neuronal damage might account in part for the electrotactic defects displayed by worms treated with paraquat and tunicamycin, we examined changes in dopaminergic neuronal phenotypes following chronic exposure to these chemicals, using *dat-1::*YFP transgenic animals. Our group has

previously demonstrated an association between chemical-induced dopaminergic neurodegeneration and electrotactic swimming deficits (**3**). In the present study, we found that both paraquat and tunicamycin could induce visible defects in neuronal morphology, with the former associated with dendritic abnormalities and the latter associated with loss of cell bodies (**Figure 13**). Quantification of these defects revealed a pronounced increase in dendritic abnormalities in worms treated with 250 μM paraquat and a statistically significant decrease in fluorescing head neurons of worms treated with 5 μg/mL tunicamycin (**Figure 14**). Given the well-established role of dopaminergic neurons in metazoan movement, these data indicate that paraquat and tunicamycin may affect electrotactic swimming at least partly through neuronal damage.

3.5 The heat shock transcriptional response contributes to preservation of electrotactic speed

The cellular response to oxidative and other stresses is a complex phenomenon involving a variety of pathways. Prominent among these is the heat shock response, mediated by transcription factor HSF-1 and itself activated by a variety of stressful stimuli (**9**). As mentioned previously, we observed increased fluorescence in *hsp-6*::*GFP*, *hsp-60*::*GFP*, *hsp-4::GFP*, and *hsp-16.2::GFP* transgenic animals following paraquat treatment (**Figures 5** and **9**); since HSPs are all regulated in part by HSF-1, these observations indicate that paraquat may induce the heat shock transcriptional response in *C. elegans*. Moreover, *hsf-1(sy441)* mutants displayed significant electrotactic deficits (**Figure 15**) that were exacerbated by paraquat treatment at 125 μM (**Figure 16**), though overexpression of HSF-1 did not rescue the slowness of animals treated with 250 μM paraquat (**Supplementary Figure 6**). We also observed that both extension of L1 diapause and mild heat stress in young adulthood leads to abnormal electrotaxis in *hsf-1* mutants (**Supplementary Figure 7** and **8**) while wild-type animals are not affected by either condition (**Supplementary Figure 1** and **2**). These results suggest that the heat shock transcriptional response plays an important role in preserving electrotactic swimming behaviour under stressful conditions. This protective role does not appear to be dependent on the insulin/IGF-1 signaling pathway, as neither *daf-2(e1370)* nor *daf-16(mu86)* mutants exhibit abnormal electrotaxis (**Supplementary Figure 5**).

4. DISCUSSION

The aforementioned experiments comprise, to our knowledge, the first attempt to characterize changes in *C. elegans*' electrotactic swimming behaviour under a variety of cellular stress conditions. Our findings show that the

electrotactic response is generally robust but can become abnormal following treatment with paraquat. Because paraquat is associated with induction of both mitochondrial and ER stress, we further pursued both lines of inquiry. We observed that only some mitochondrial mutations can cause abnormalities in electrotactic swimming, and these defects do not correlate with changes in ROS levels or lifespan. The slow electrotaxis of *atfs-1* null mutants indicates that the UPR^{mt} may contribute to maintenance of the wild-type behaviour, but the speed deficits of mutants expressing constitutively active ATFS-1 as well rule out a simple association between UPR^{mt} induction and electrotactic motility. Hence, there is likely a complex relationship between mitochondrial and oxidative stress and the electrotactic swimming of *C. elegans*. On the other hand, tunicamycin-induced ER stress and UPR^{ER}-inhibiting mutations in *ire-1* consistently result in electrotactic swimming defects, as does proteotoxic stress resulting from upregulation of global protein synthesis in *pqe-1* mutants. These results implicate ER stress as a major source of electrotactic disturbance. Like paraquat, tunicamycin is a known neurotoxicant and has been used to model Parkinson's-related neurodegeneration in other model systems (**42**); here, we show that chronic paraquat and tunicamycin exposure both damage dopaminergic neurons, albeit with different manifestations. Neuronal damage may therefore account for at least some of the electrotactic defects induced by these chemicals. We further report that the heat shock response, which is activated by both paraquat and tunicamycin treatment, is necessary for preserving the wild-type electrotactic phenotype under both standard and paraquat-induced oxidative stress conditions. Together, our results show that multiple stress responses are involved in protecting electrotactic behaviour against stress-induced defects.

Our observations regarding the partial rescue of the slow phenotype of *isp-1(qm150)* but not *gas-1(fc21)* suggests that different mechanisms are responsible for these two mutants' locomotory depression. While both genetic backgrounds are associated with electron transport hindrance and increased ROS generation, *isp-1(qm150)* actually exhibits oxidative stress resistance due to low oxygen consumption and increased expression of mitochondrial superoxide dismutase SOD-3 (**34**). On the other hand, *gas-1(fc21)* is hypersensitive to oxidative stresses such as paraquat (**35**,**43**). *isp-1(qm150)* animals also enjoy a long lifespan whereas that of *gas-1(fc21)* mutants is truncated, possibly due to these mutants' different levels of ROS production and ROS-associated enzymatic activity (**34**). These studies support the idea that the slow phenotypes of *isp-1(qm150)* and *gas-1(fc21)* are the behavioural manifestations of abnormalities in distinct pathways. Moreover, it is entirely possible that curcumin rescues the speed of *isp-1(qm150)* not through its anti-oxidant activity, but rather through one of its other pharmacological properties. Meanwhile, the concentration of curcumin used in this study may have been insufficient to rescue the oxidative stress-induced defects in *gas-1(fc21)*, as its bioavailability is poor (**15**).

It is similarly possible that the paraquat-induced electrotactic defects observed in this study were caused not by paraquat's property as an inhibitor of mitochondrial complex I, but by one of its other properties. Although paraquat's capabilities as a ROS generator are well characterized (**44**,**45**), Choi and colleagues (**31**) found that complex I inhibition is not required for the dopaminergic neurodegeneration induced by rotenone, MPTP, or paraquat. Alternatively, or perhaps in conjunction, we propose that paraquat may perturb electrotactic swimming behaviour by means of ER stress, with which it is already well associated in the literature (**14**,**32**,**33**). This possibility is reinforced by our observations that ER-specific stresses such as tunicamycin and UPR^{ER}-hampering mutations in *ire-1* can induce electrotactic defects as well. We also tested *pek-1* deletion mutants, which are known to be tunicamycin-hypersensitive; however, the electrotaxis of untreated *pek-1(ok275)* mutants does not differ from that of wild-type animals, indicating that not all branches of the UPR^{ER} are necessary for preserving electrotactic behaviour under standard conditions (**46**).

We note that while the ability of paraquat to increase expression of mitochondrial *hsp* markers in *C. elegans* has been reported previously by Runkel and colleagues (**22**), this same group did not observe any increase in expression of ER or cytosolic *hsp* markers following paraquat treatment. This discrepancy may be due to differences in exposure paradigm: whereas Runkel and colleagues exposed worms for two days beginning at L3, we exposed worms continuously from L1 to young adulthood. Nonetheless, as already stated, the relationship between paraquat and ER stress is well established in other models.

We also report an interesting result from culturing *ucp-4(ok195)* mutants under chronic paraquat exposure conditions. In mammalian cells, mutations in UCP are associated with increased ROS and oxidative stress (**26**,**27**,**28**). Iser and colleagues (**47**) have reported that *ucp-4(ok195)* worms exhibit wild-type lifespan and survival in a traditional paraquat sensitivity assay, though they do display elevation of ATP levels. As mentioned in the Discussion of the same paper, one explanation is that any elevation of ROS in *ucp-4(ok195)* is minor compared to the levels necessary to shorten lifespan or raise sensitivity to their paradigm of paraquat exposure, which uses high concentrations but begins at adulthood (**47**). In the present study, it is possible that our exposure protocol beginning at the L1 larval stage is sufficient, in spite of lower paraquat concentrations, to induce *ucp-4*-dependent defects. Future studies directly measuring the extent of oxidative damage following paraquat exposure in different genetic backgrounds will be helpful in further illuminating the relationship between ROS and locomotion.

5. CONCLUSION

In summary, we have shown for the first time that ER stress and perturbation of the associated response pathways, including the heat shock transcriptional response, appear to have a strong impact on electrotactic speed. Our findings promote the use of behavioural assays for the dissection of stress response pathways and will inform future studies that utilize microfluidic electrotaxis as a functional output of nematode locomotory circuits.

Acknowledgements

Many thanks to fellow members of the Gupta laboratory for discussion and feedback. We are particularly grateful to Anum Rahman for her technical support. Many strains were acquired from the Caenorhabditis Genetics Center, which is supported by the National Institutes of Health's National Center for Research Resources. This work was funded by the Ontario Ministry of Research and Innovation and the Collaborative Health Research Projects award, co-funded by the Natural Sciences and Engineering Research Council of Canada and the Canadian Institutes of Health Research.

References

1. Cristina, D.; Cary, M.; Lunceford, A.; Clarke, C.; Kenyon, C. A regulated response to impaired respiration slows behavioral rates and increases lifespan in Caenorhabditis elegans. *PLoS Genet* **2009,** *5* (4), e1000450.

2. Blesa, J.; Phani, S.; Jackson-Lewis, V.; Przedborski, S. Classic and new animal models of Parkinson's disease. *J Biomed Biotechnol* **2012,** *2012,* 845618.

3. Salam, S.; Ansari, A.; Amon, S.; Rezai, P.; Selvaganapathy, P. R.; Mishra, R. K.; Gupta, B. P. A microfluidics set up to study neuronal degeneration and identification of neuroprotective compounds in C. elegans. *Worm* **2013,** *2* (3), e24558.

4. Nass, R.; Hall, D. H.; Miller, D. M.; Blakely, R. D. Neurotoxin-induced degeneration of dopamine neurons in Caenorhabditis elegans. *Proc Natl Acad Sci U S A* **2002,** *99,* 3264-3269.

5. Stefani, I. C.; Wright, D.; Polizzi, K. M.; Kontoravdi, C. The role of ER stress-induced apoptosis in neurodegeneration. *Curr Alzheimer Res* **2012,** *9* (3), 373-387.

6. Liu, D.; Zhang, M.; Yin, H. Signaling pathways involved in endoplasmic reticulum stress-induced neuronal apoptosis. *Int J Neurosci* **2013,** *123* (3), 155-162.

7. Roussel, B. D.; Kruppa, A. J.; Miranda, E.; Crowther, D. C.; Lomas, D. A.; Marciniak, S. J. Endoplasmic reticulum dysfunction in neurological disease. *Lancet Neurol* **2013,** *12* (1), 105-118.

8. Kourtis, N.; Nikoletopoulou, V.; Tavernarakis, N. Small heat-shock proteins protect from heat-stroke-associated neurodegeneration. *Nature* **2012,** *490* (7419), 213-218.

9. Shamovsky, I.; Nudler, E. New insights into the mechanism of heat shock response. *Cell Mol Life Sci* **2008,** *65* (6), 855-861.

10. Chronis, N.; Zimmer, M.; Bargmann, C. I. Microfluidics for in vivo imaging of neuronal and behavioral activity in Caenorhabditis elegans. *Nat Meth* **2007,** *4*, 727-731.

11. Chung, K.; Crane, M. M.; Lu, H. Automated on-chip rapid microscopy, phenotyping and sorting of C. elegans. *Nat Methods* **2008,** *5* (7), 637-643.

12. Rezai, P.; Siddiqui, A.; Selvaganapathy, P. R.; Gupta, B. P. Electrotaxis of Caenorhabditis elegans in a microfluidic environment. *Lab Chip* **2010,** *10*, 220-226.

13. Cochemé, H. M.; Murphy, M. P. Complex I is the major site of mitochondrial superoxide production by paraquat. *J Biol Chem* **2008,** *283* (4), 1786-1798.

14. Chinta, S. J.; Rane, A.; Poksay, K. S.; Bredesen, D. E.; Andersen, J. K.; Rao, R. V. Coupling endoplasmic reticulum stress to the cell death program in dopaminergic cells: effect of paraquat. *Neuromolecular Med* **2008,** *10* (4), 333-342.

15. Hamaguchi, T.; Ono, K.; Yamada, M. REVIEW: Curcumin and Alzheimer's disease. *CNS Neurosci Ther* **2010,** *16* (5), 285-297.

16. Lee, W. H.; Loo, C. Y.; Bebawy, M.; Luk, F.; Mason, R. S.; Rohanizadeh, R. Curcumin and its derivatives: their application in neuropharmacology and neuroscience in the 21st century. *Curr Neuropharmacol* **2013,** *11* (4), 338-378.

17. Sun, L.; Zhao, Y.; Zhou, K.; Freeze, H. H.; Zhang, Y. W.; Xu, H. Insufficient ER-stress response causes selective mouse cerebellar granule cell degeneration resembling that seen in congenital disorders of glycosylation. *Mol Brain* **2013,** *6*, 52.

18. Hwang, H. J.; Jung, T. W.; Ryu, J. Y.; Hong, H. C.; Choi, H. Y.; Seo, J. A.; Kim, S. G.; Kim, N. H.; Choi, K. M.; Choi, D. S.; Baik, S. H.; Yoo, H. J. Dipeptidyl Petidase-IV Inhibitor (Gemigliptin) Inhibits Tunicamycin-induced Endoplasmic Reticulum Stress, Apoptosis and Inflammation in H9c2 Cardiomyocytes. *Mol Cell Endocrinol* **2014,** [Epub ahead of print].

19. Cookson, M. R. α-Synuclein and neuronal cell death. *Mol Neurodegener* **2009,** *4*, 9.

20. Faber, P. W.; Voisine, C.; King, D. C.; Bates, E. A.; Hart, A. C. Glutamine/proline-rich PQE-1 proteins protect Caenorhabditis elegans neurons from huntingtin polyglutamine neurotoxicity. *Proc Natl Acad Sci USA* **2002,** *99* (26), 17131-17136.

21. Yamada, K.; Tsuchiya, J.; Iino, Y. Mutations in the pqe-1 gene enhance transgene expression in Caenorhabditis elegans. *G3 (Bethesda)* **2012,** *2* (7), 741-751.

22. Runkel, E. D.; Liu, S.; Baumeister, R.; Schulze, E. Surveillance-activated defenses block the ROS-induced mitochondrial unfolded protein response. *PLoS Genet* **2013,** *9* (3), e1003346.

23. Brenner, S. The genetics of Caenorhabditis elegans. *Genetics* **1974,** *77* (1), 71-94.

24. Stiernagle, T. Maintenance of C. elegans, 2006. WormBook. http://wormbook.org/chapters/www_strainmaintain/strainmaintain.html.

25. Tong, J.; Rezai, P.; Salam, S.; Selvaganapathy, P. R.; Gupta, B. P. Microfluidic-based electrotaxis for on-demand quantitative analysis of Caenorhabditis elegans' locomotion. *J Vis Exp* **2013,** *75*, e50226.

26. Kim-Han, J. S.; Reichert, S. A.; Quick, K. L.; Dugan, L. L. BMCP1: a mitochondrial uncoupling protein in neurons which regulates mitochondrial function and oxidant production. *J Neurochem* **2001,** *79* (3), 658-668.

27. Krauss, S.; Zhang, C. Y.; Scorrano, L.; Dalgaard, L. T.; St-Pierre, J.; Grey, S. T.; Lowell, B. B. Superoxide-mediated activation of uncoupling protein 2 causes pancreatic beta cell dysfunction. *J Clin Invest* **2003,** *112* (12), 1831-1842.

28. Vidal-Puig, A. J.; Grujic, D.; Zhang, C. Y.; Hagen, T.; Boss, O.; Ido, Y.; Szczepanik, A.; Wade, J.; Mootha, V.; Cortright, R.; Muoio, D. M.; Lowell, B. B. Energy metabolism in uncoupling protein 3 gene knockout mice. *J Biol Chem* **2000,** *275* (21), 16258-16266.

29. Gregus, Z.; Klaassen, C. D. Mechanisms of toxicity. In *Casarett and Doull's Toxicology: The Basic Science of Poisons*, 6th ed.; Klaassen, C. D., Ed.; McGraw-Hill: New York, 2001; pp 35-81.

30. Moore, D. J.; West, A. B.; Dawson, V. L.; Dawson, T. M. Molecular pathophysiology of Parkinson's disease. *Annu Rev Neurosci* **2005,** *28,* 57-87.

31. Choi, W. S.; Kruse, S. E.; Palmiter, R. D.; Xia, Z. Mitochondrial complex I inhibition is not required for dopaminergic neuron death induced by rotenone, MPP+, or paraquat. *Proc Natl Acad Sci USA* **2008,** *105* (39), 15136-15141.

32. Chen, Y. W.; Yang, Y. T.; Hung, D. Z.; Su, C. C.; Chen, K. L. Paraquat induces lung alveolar epithelial cell apoptosis via Nrf-2-regulated mitochondrial dysfunction and ER stress. *Arch Toxicol* **2012,** *86* (10), 1547-1558.

33. Huang, C. L.; Lee, Y. C.; Yang, Y. C.; Kuo, T. Y.; Huang, N. K. Minocycline prevents paraquat-induced cell death through attenuating endoplasmic reticulum stress and mitochondrial dysfunction. *Toxicol Lett* **2012,** *209* (3), 203-210.

34. Feng, J.; Bussière, F.; Hekimi, S. Mitochondrial electron transport is a key determinant of life span in Caenorhabditis elegans. *Dev Cell* **2001,** *1* (5), 633-644.

35. Hartman, P. S.; Ishii, N.; Kayser, E. B.; Morgan, P. G.; Sedensky, M. M. Mitochondrial mutations differentially affect aging, mutability and anesthetic sensitivity in Caenorhabditis elegans. *Mech Ageing Dev* **2001,** *122* (11), 1187-1201.

36. Sedensky, M. M.; Morgan, P. G. Mitochondrial respiration and reactive oxygen species in C. elegans. *Exp Gerontol* **2006,** *41* (10), 957-967.

37. Van Raamsdonk, J. M.; Hekimi, S. Deletion of the mitochondrial superoxide dismutase sod-2 extends lifespan in Caenorhabditis elegans. *PLoS Genet* **2009,** *5* (2), e1000361.

38. Lee, S.-J.; Hwang, A. B.; Kenyon, C. Inhibition of respiration extends C. elegans' lifespan via reactive oxygen species that increase HIF-1 activity. *Curr Biol* **2010,** *20* (23), 2131-2136.

39. Nargund, A. M.; Pellegrino, M. W.; Fiorese, C. J.; Baker, B. M.; Haynes, C. M. Mitochondrial import efficiency of ATFS-1 regulates mitochondrial UPR activation. *Science* **2012,** *337* (6094), 587-590.

40. Pujol, C.; Bratic-Hench, I.; Sumakovic, M.; Hench, J.; Mourier, A.; Baumann, L.; Pavlenko, V.; Trifunovic, A. Succinate dehydrogenase upregulation destabilize complex I and limits the lifespan of gas-1 mutant. *PLoS One* **2013,** *8* (3), e59493.

41. Runkel, E. D.; Baumeister, R.; Schulze, E. Mitochondrial stress: Balancing friend and foe. *Exp Gerontol* **2014,** [Epub ahead of print].

42. Matsui, H.; Ito, H.; Taniguchi, Y.; Takeda, S.; Takahashi, R. Ammonium chloride and tunicamycin are novel toxins for dopaminergic neurons and induce Parkinson's disease-like phenotypes in medaka fish. *J Neurochem* **2010,** *115* (5), 1150-1160.

43. Kayser, E. B.; Morgan, P. G.; Hoppel, C. L.; Sedensky, M. M. Mitochondrial expression and function of GAS-1 in Caenorhabditis elegans. *J Biol Chem* **2001,** *276* (23), 20551-20558.

44. McCormack, A. L.; Atienza, J. G.; Johnston, L. C.; Andersen, J. K.; Vu, S.; Di Monte, D. A. Role of oxidative stress in paraquat-induced dopaminergic cell degeneration. *J Neurochem* **2005,** *93* (4), 1030-1037.

45. McCormack, A. L.; Atienza, J. G.; Langston, J. W.; Di Monte, D. A. Decreased susceptibility to oxidative stress underlies the resistance of specific dopaminergic cell populations to paraquat-induced degeneration. *Neuroscience* **2006,** *141* (2), 929-937.

46. Shen, X.; Ellis, R. E.; Lee, K.; Liu, C. Y.; Yang, K.; Solomon, A.; Yoshida, H.; Morimoto, R.; Kurnit, D. M.; Mori, K.; Kaufman, R. J. Complementary signaling pathways regulate the unfolded protein response and are required for C. elegans development. *Cell* **2001,** *107* (7), 893-903.

47. Iser, W. B.; Kim, D.; Bachman, E.; Wolkow, C. Examination of the requirement for ucp-4, a putative homolog of mammalian uncoupling proteins, for stress tolerance and longevity in C. elegans. *Mech Ageing Dev* **2005,** *126* (10), 1090-1096.

Figures

Figure 1. Electrotaxis of wild-type animals following paraquat treatment. Boxes represent measurements from 25th to 75th percentiles, central horizontal lines represent medians, vertical lines extend to 10th and 90th percentiles, and dots represent outliers. Treatment with paraquat does not induce speed abnormalities at 50 µM ($p = 0.128$), 75 µM ($p = 0.102$), or 125 µM ($p = 0.102$), but results in speed deficits at 250 µM ($p < 0.001$). N2 untreated: $n = 80$, N2 + 50 µM PQ: $n = 20$, N2 + 75 µM PQ: $n = 20$, N2 + 125 µM PQ: $n = 50$, N2 + 250 µM PQ: $n = 45$.

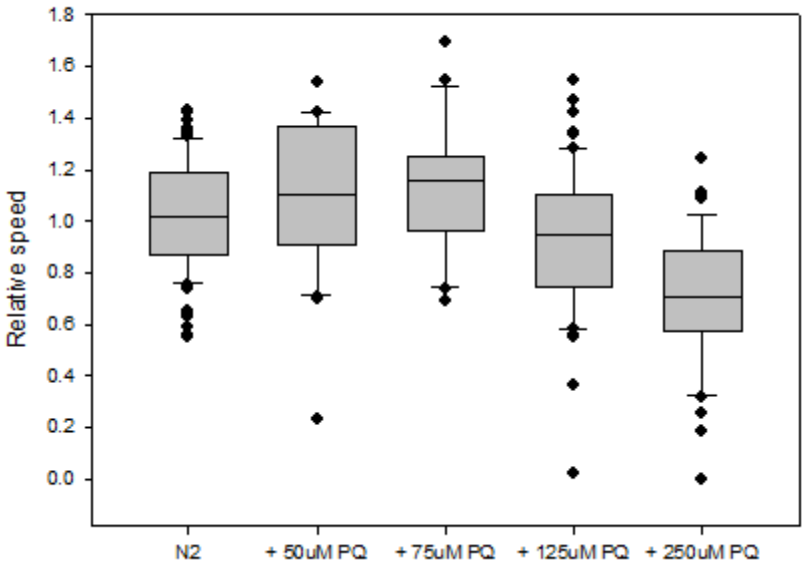

Figure 2. Electrotaxis of paraquat-treated *mev-1* mutants. Refer to Figure 1 for description of box plot. *mev-1(kn1)* animals exhibit significant slowness following treatment with 50 µM ($p = 0.003$) or 75 µM ($p < 0.001$) paraquat. TK22 *mev-1*(*kn1*) untreated: n = 20, TK22 + 50 µM PQ: n = 18, TK22 + 75 µM PQ: n = 20.

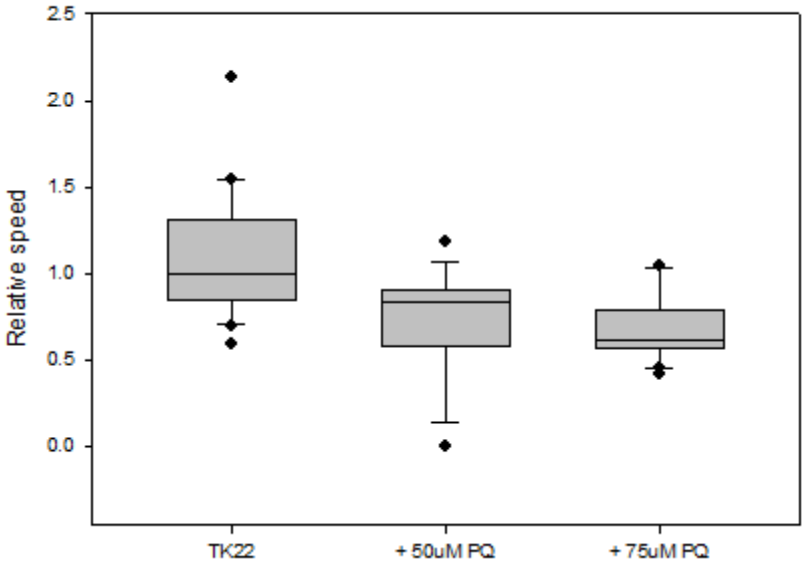

Figure 3. Electrotaxis of paraquat-treated *pink-1* mutants. Refer to Figure 1 for description of box plot. *pink-1(ok3538)* animals do not show abnormal electrotaxis following treatment with 50 µM ($p = 0.394$) or 75 µM ($p = 0.694$) paraquat, but show significant slowness following treatment with 125 µM paraquat ($p < 0.001$). DY356 *pink-1*(*ok3538*) untreated: n = 33, DY356 + 50 µM PQ: n = 20, DY356 + 75 µM PQ: n = 40, DY356 + 125 µM PQ: n = 27.

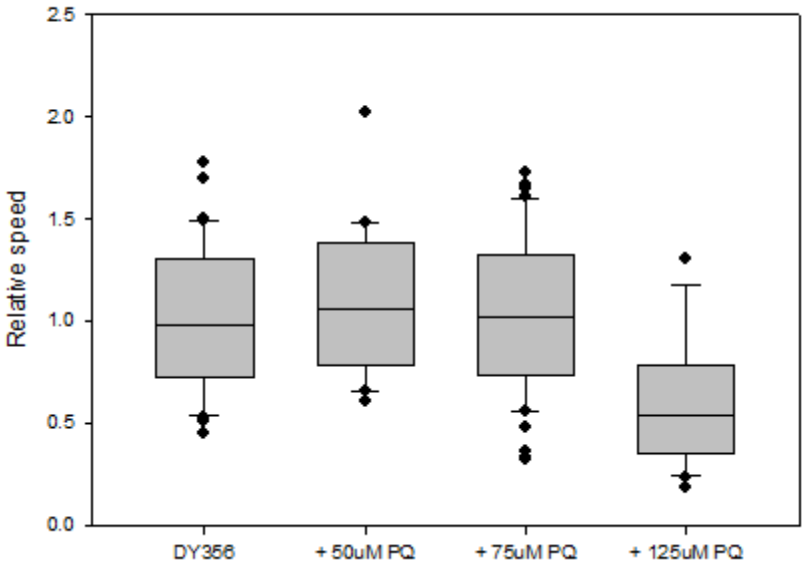

Figure 4. Electrotaxis of paraquat-treated *ucp-4* mutants. Refer to Figure 1 for description of box plot. *ucp-4(ok195)* animals do not show abnormal electrotaxis following treatment with 50 µM ($p = 0.946$), but show significant slowness following treatment with 75 µM paraquat ($p = 0.002$). CY121 *ucp-4*(*ok195*) untreated: n = 20, CY121 + 50 µM PQ: n = 20, CY121 + 75 µM PQ: n = 20.

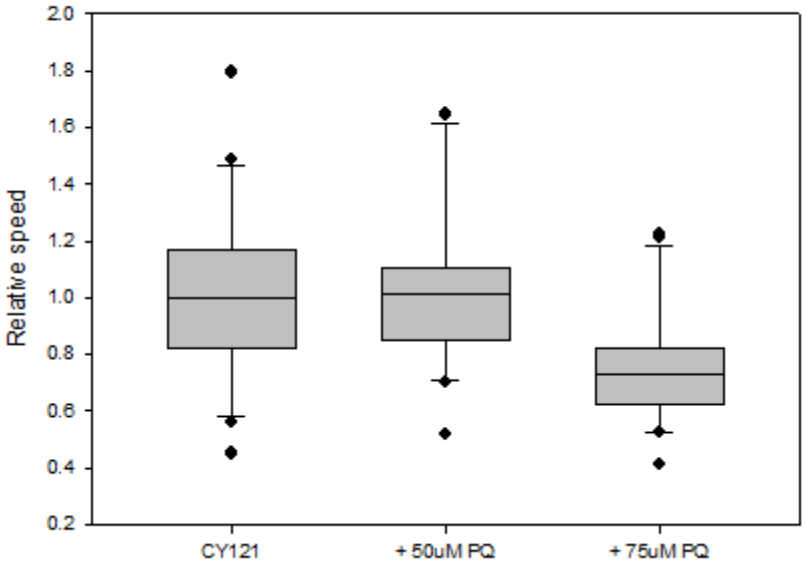

Figure 5. Fluorescence intensity of paraquat-treated animals expressing GFP under mitochondrial *hsp* promoters. Both *zcIs13*(*hsp-6::GFP*) and *zcIs9*(*hsp-60::GFP*) show increased fluorescence following treatment with 125 µM paraquat ($p < 0.001$ in both cases). Both strains show further increases in fluorescence if treated with 250 µM paraquat instead ($p < 0.001$ and $p = 0.003$ respectively). SJ4100 *zcIs13*(*hsp-6::GFP*) untreated: n = 40, SJ4100 + 125 µM PQ: n = 32, SJ4100 + 250 µM PQ: n = 31, SJ4058 *zcIs9*(*hsp-60::GFP*) untreated: n = 33, SJ4058 + 125 µM PQ: n = 34, SJ4058 + 250 µM PQ: n = 35.

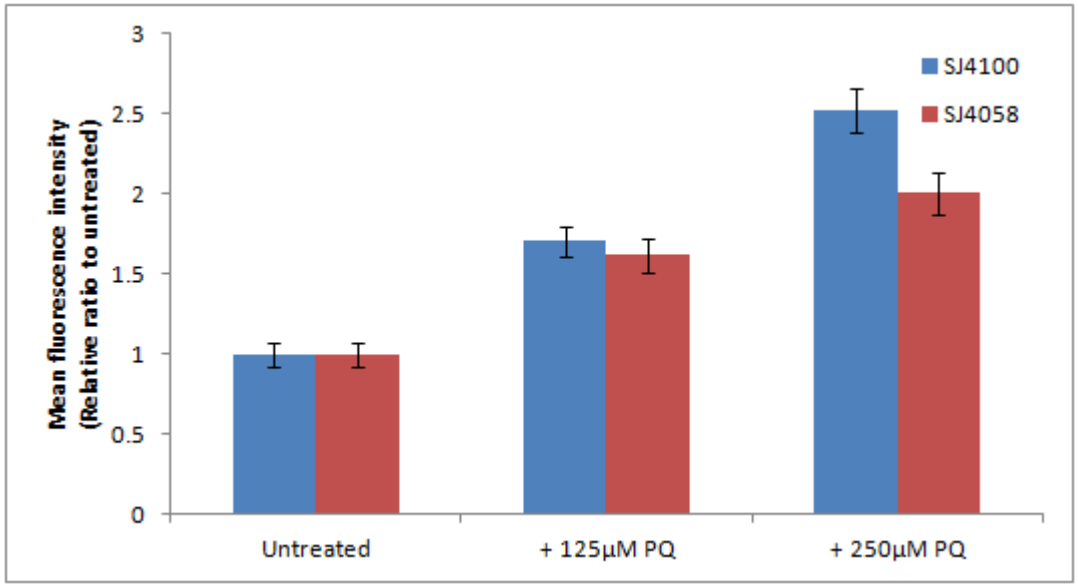

Figure 6. Electrotaxis of various mitochondrial mutants. Refer to Figure 1 for description of box plot. Both *isp-1(qm150)* ($p < 0.001$) and *gas-1(fc21)* ($p < 0.001$) animals exhibit pronounced speed defects during electrotaxis. In contrast, *mev-1(kn1)* ($p = 0.567$), *pink-1(ok3538)* ($p = 0.239$), *ucp-4(ok195)* ($p = 0.942$), *clk-1(e2519)* ($p = 0.065$), *sod-2(gk257)* ($p = 0.509$), *sod-3(tm760)* ($p = 0.578$), and *sod-2(gk257); sod-3(tm760)* double ($p = 0.485$) mutants did not differ significantly from wild-type controls. N2: n = 40, MQ887 *isp-1(qm150)*: n = 39, CW152 *gas-1(fc21)*: n = 29, TK22 *mev-1(kn1)*: n = 40, DY356 *pink-1(ok3538)*: n = 61, CY121 *ucp-4(ok195)*: n = 40, CB4876 *clk-1(e2519)*: n = 30, GA184 *sod-2(gk257)*: n = 21, GA186 *sod-3(tm760)*: n = 20, GA480 *sod-2(gk257); sod-3(tm760)*: n = 20.

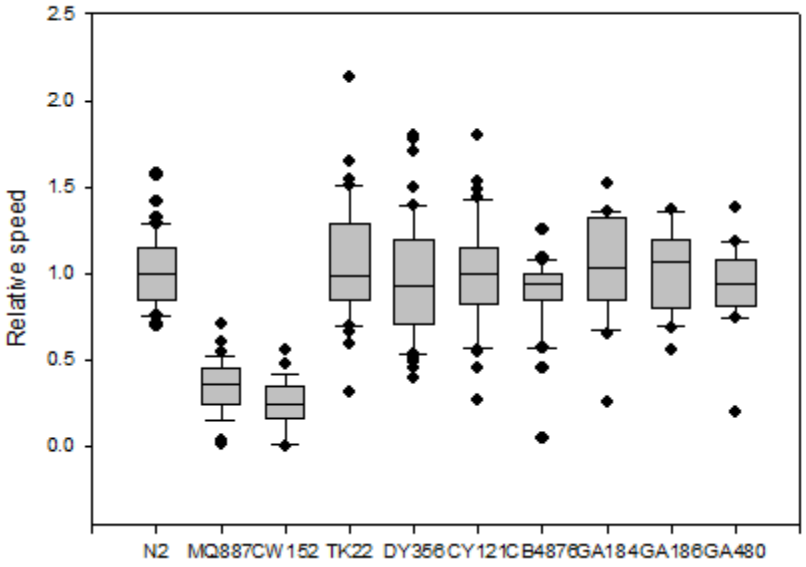

Figure 7. Electrotaxis of curcumin-treated mitochondrial mutants. Refer to Figure 1 for description of box plot. Treatment with 1mM curcumin does not affect the electrotactic speed of wild-type ($p = 0.616$) or *gas-1(fc21)* ($p = 0.134$) animals, but does ameliorate the speed defects of *isp-1(qm150)* mutants ($p < 0.001$). N2 untreated: n = 31, N2 + 1mM curcumin: n = 20, MQ887 *isp-1(qm150)* untreated: n = 30, MQ887 + 1mM curcumin: n = 30, CW152 *gas-1(fc21)* untreated: n = 17, CW152 + 1mM curcumin: n = 21.

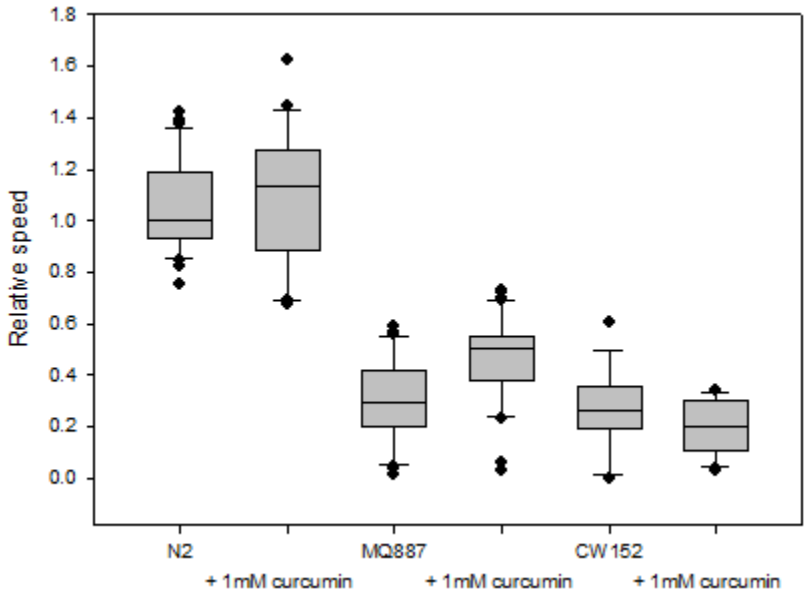

Figure 8. Electrotaxis of UPR^{mt} gain-of-function and loss-of-function mutants. Refer to Figure 1 for description of box plot. *atfs-1(et15)* gain-of-function mutants exhibit pronounced speed defects during electrotaxis ($p < 0.001$). *atfs-1(gk3094)* null mutants exhibit even more severe speed defects than *atfs-1(et15)* ($p = 0.008$). N2: n = 29, QC115 *atfs-1(et15)*: n = 26, VC3201 *atfs-1(gk3094)*: n = 26.

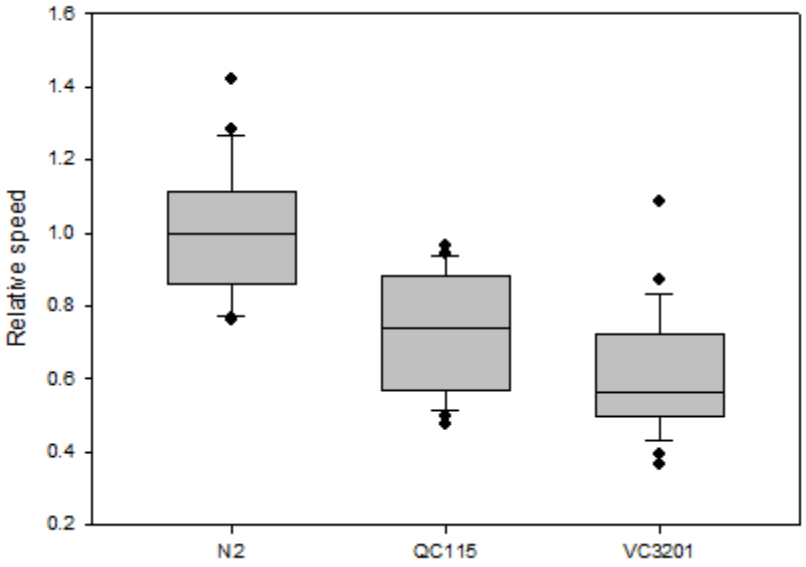

Figure 9. Fluorescence intensity of paraquat-treated animals expressing GFP under ER and cytosolic *hsp* promoters. Both *zcIs4*(*hsp-4::GFP*), an ER stress marker, and *dvIs70*(*hsp-16.2::GFP*), a marker of cytosolic protein misfolding, show increased fluorescence following treatment with 250 µM paraquat ($p < 0.001$ in both cases), but the change in *hsp-4::GFP* expression is much more pronounced. SJ4005 *zcIs4*(*hsp-4::GFP*) untreated: n = 27, SJ4005 + 250 µM PQ: n = 29, CL2070 *dvIs70*(*hsp-16.2::GFP*) untreated: n = 31, CL2070 + 250 µM PQ: n = 20.

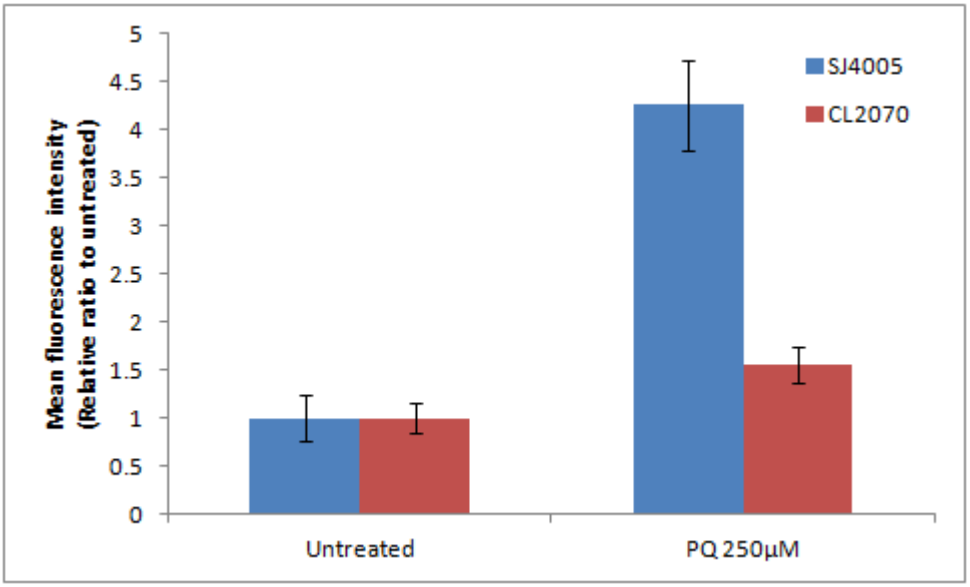

Figure 10. Electrotaxis of wild-type animals following tunicamycin treatment. Refer to Figure 1 for description of box plot. Treatment with tunicamycin does not induce speed abnormalities at 2 µg/mL ($p = 0.590$), but results in speed deficits at 5 µg/mL ($p = 0.002$) and at 10 µg/mL ($p = 0.008$). N2 untreated: $n = 30$, N2 + 2 µg/mL TUN: $n = 15$, N2 + 5 µg/mL TUN: $n = 32$, N2 + 10 µg/mL TUN: $n = 10$.

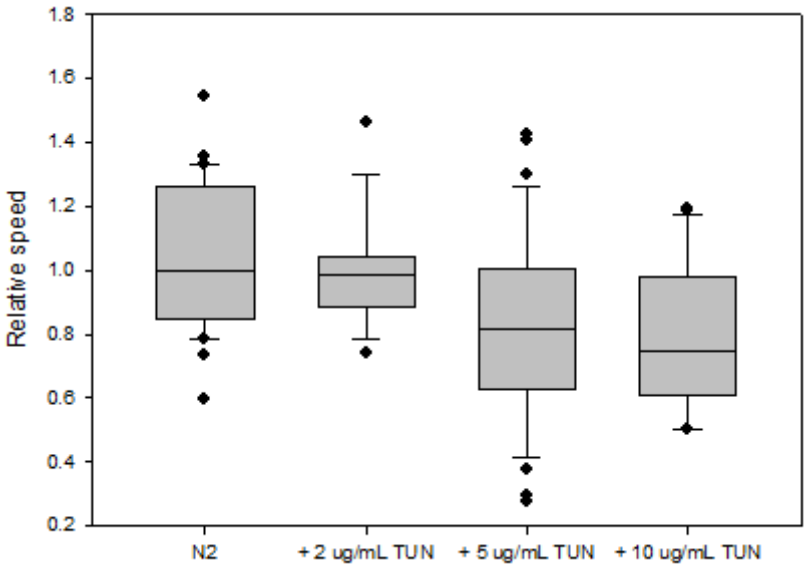

Figure 11. Electrotaxis of UPR^{ER} mutants. Refer to Figure 1 for description of box plot. *pek-1(ok275)* animals do not exhibit speed defects relative to wild-type controls ($p = 0.934$), but *ire-1(v33)* mutants are significantly slower ($p < 0.001$). N2: n = 24, RB545 *pek-1(ok275)*: n = 28, RE666 *ire-1(v33)*: n = 22.

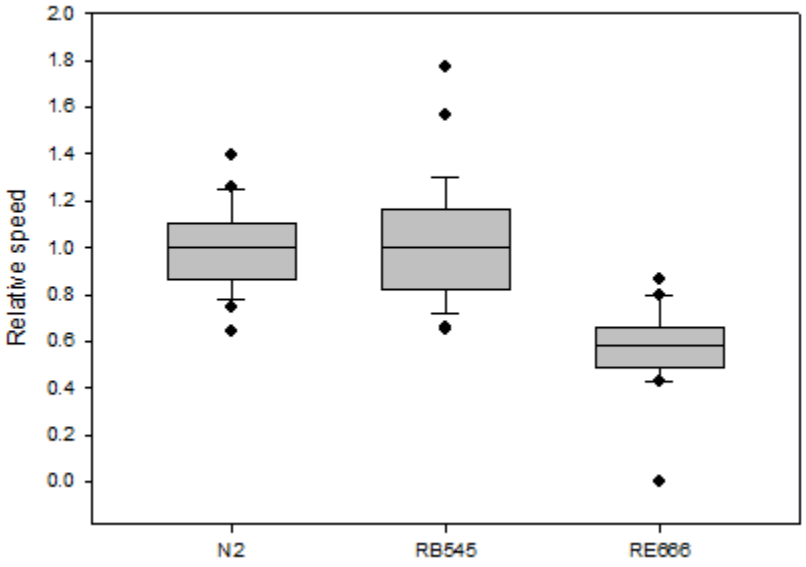

Figure 12. Electrotaxis of *pqe-1* mutants. Refer to Figure 1 for description of box plot. *pqe-1(ok1983)* animals exhibit pronounced electrotactic speed defects ($p < 0.001$) that are exacerbated by treatment with 125 µM paraquat ($p = 0.009$). The electrotaxis of *pqe-1(ok1983)* animals is not affected by 0.5 µg/mL tunicamycin ($p = 0.680$) or 1 µg/mL tunicamycin ($p = 0.858$). N2: n = 38, RB1611 *pqe-1(ok1983)* untreated: n = 44, RB1611 + PQ 125 µM: n = 30, RB1611 + TUN 0.5 µg/mL: n = 30, RB1611 + TUN 1 µg/mL: n = 32.

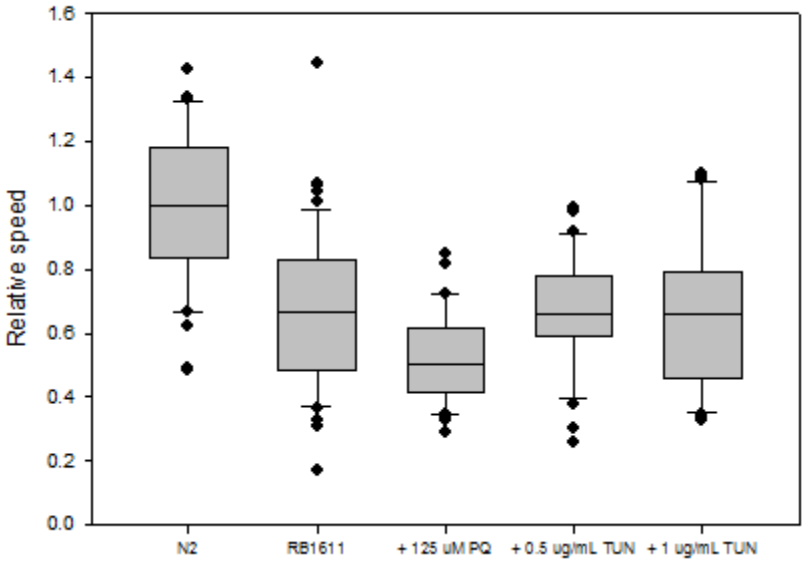

Figure 13. Degenerative phenotypes of head dopaminergic neurons in young adult *dat-1::*YFP transgenic animals resulting from chronic paraquat or tunicamycin exposure. (A-B) Dopaminergic neurons and processes are healthy in untreated control animals. (C-D) Dopaminergic neurons and processes in animals cultured with 125 μM paraquat are indistinguishable from those in untreated controls. (E-F) Animals cultured with 250 μM paraquat develop wrinkles and punctate patterns in dopaminergic neuronal processes. (G-H) Animals cultured with 5 μg/mL tunicamycin sometimes develop wrinkles and punctate patterns in dopaminergic neuronal processes, and present in adulthood with a lower number of fluorescing cells.

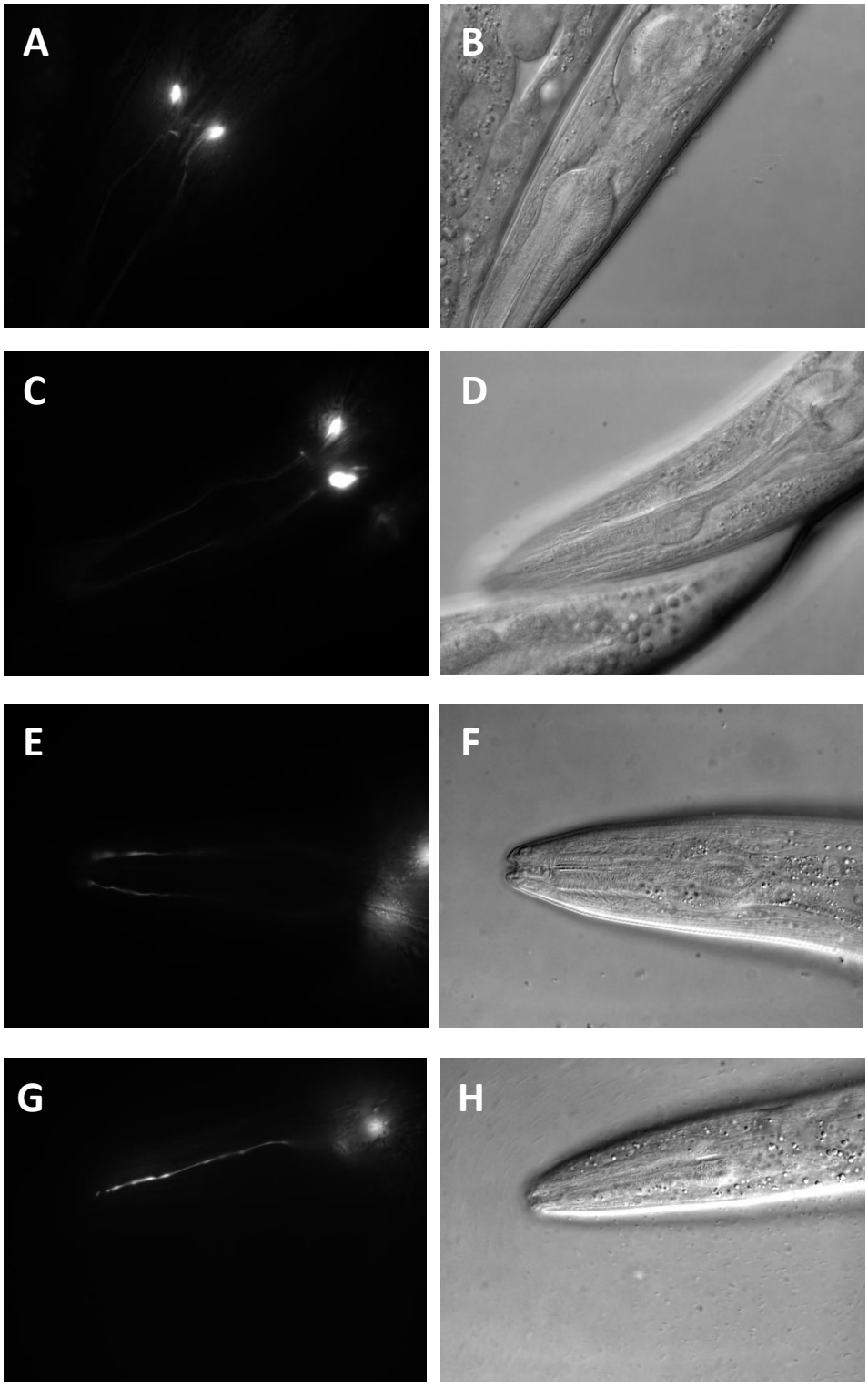
A
B
C
D
E
F
G
H

Figure 14. Transgenic *dat-1::*YFP animals develop different neuronal damage phenotypes from chronic paraquat and chronic tunicamycin exposure. DY353 *bhex138*(*dat-1::*YFP) untreated: n = 60, DY353 + PQ 125 µM: n = 61, DY353 + PQ 250 µM: n = 65, DY353 + TUN 5 µg/mL: n = 50. (A) Dendritic damage appears more frequently in worms cultured with 250 µM paraquat (p = 0.005) but not 125 µM paraquat (p = 0.191) or 5 µg/mL tunicamycin (p = 0.294). (B) On average, fewer dopaminergic head neurons survive to adulthood when worms are cultured with 5 µg/mL tunicamycin (p = 0.039) but not 125 µM paraquat (p = 0.277) or 250 µM paraquat (p = 0.218).

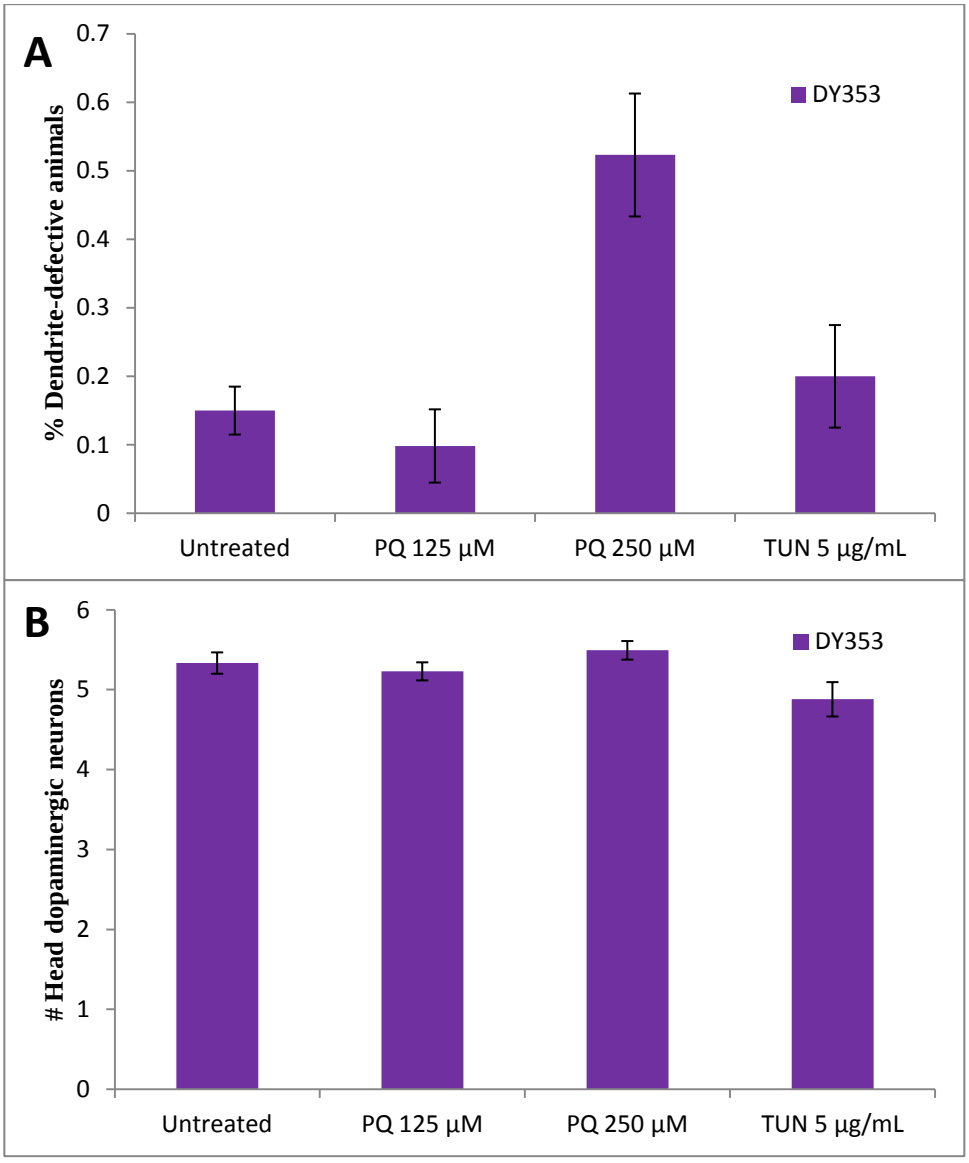

Figure 15. Electrotaxis of *hsf-1* mutants. Refer to Figure 1 for description of box plot. *hsf-1(sy441)* animals exhibit significant slowness relative to wild-type animals ($p < 0.001$). N2: n = 70, PS3551 *hsf-1*(*sy441*): n = 90.

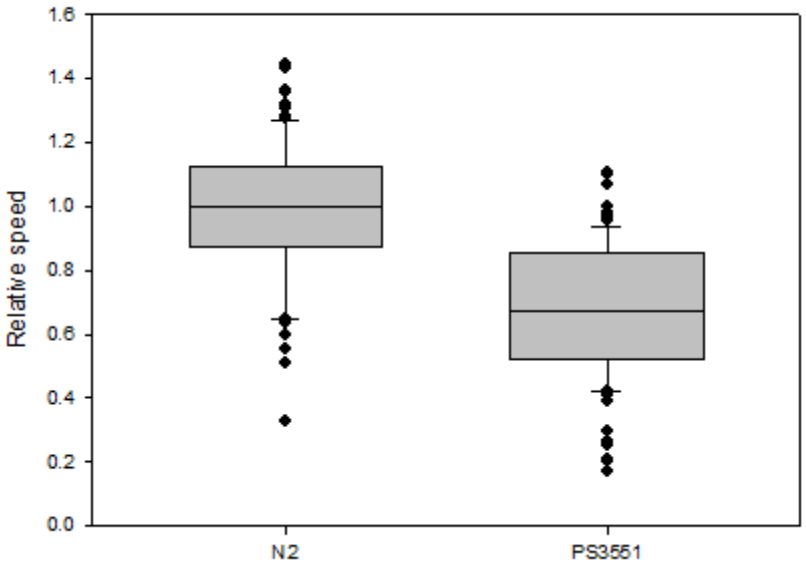

Figure 16. Electrotaxis of paraquat-treated *hsf-1* mutants. Refer to Figure 1 for description of box plot. Speed of *hsf-1(sy441)* animals is not affected by treatment with 75 µM paraquat ($p = 0.344$) but is further depressed by treatment with 125 µM paraquat ($p < 0.001$). PS3551 *hsf-1(sy441)* untreated: n = 70, PS3551 + 75 µM PQ: n = 20, PS3551 + 125 µM PQ: n = 46.

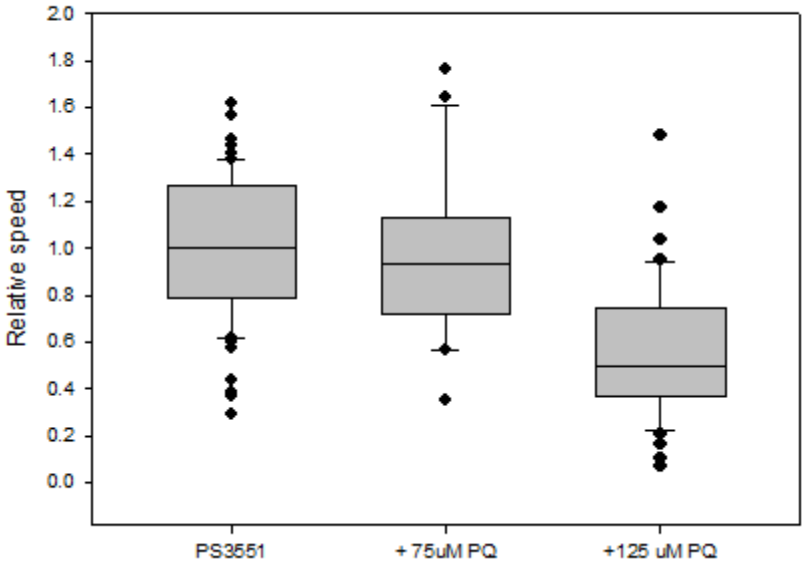

Supplementary Information

Supplementary Figure 1. Electrotaxis of adult wild-type animals that have been starved in M9 for variable lengths of time at L1. Refer to Figure 1 for description of box plot. No significant difference was observed between the electrotactic speeds of animals arrested at L1 for 24 h and animals arrested at L1 for 168 h ($p = 0.660$). N2 starved 24h: $n = 21$, N2 starved 168h: $n = 21$.

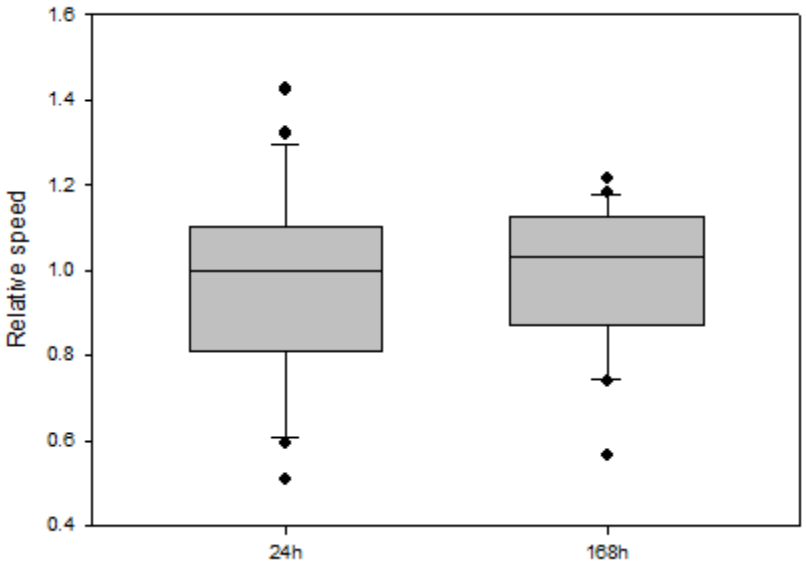

Supplementary Figure 2. Electrotaxis of wild-type animals following mild heat stress in young adulthood. Refer to Figure 1 for description of box plot. No significant difference was observed between the electrotactic speeds of controls and animals subjected to a 25°C water bath for 5 h ($p = 0.970$) or animals subjected to a 33°C water bath for 1 h ($p = 0.101$). N2 untreated: n = 57, N2 heat-shocked at 25°C for 5h: n = 49, N2 heat-shocked at 33°C for 1h: n = 31.

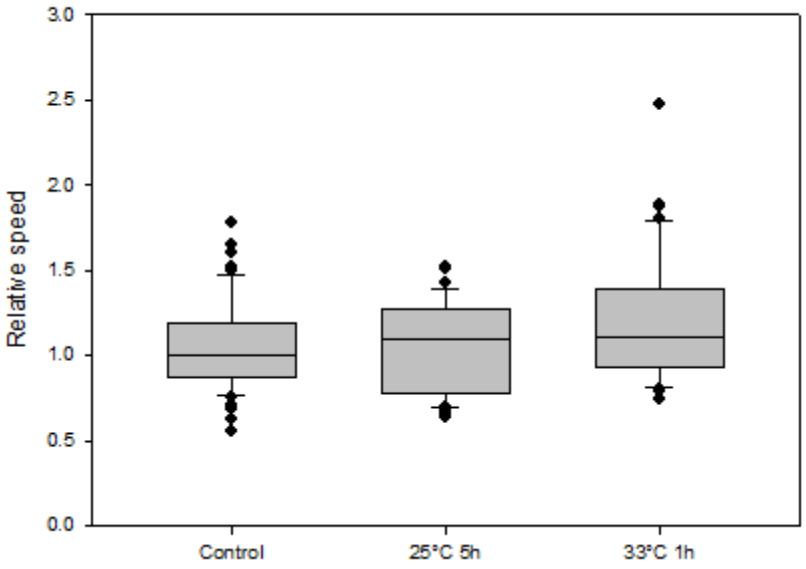

Supplementary Figure 3. Electrotaxis of wild-type animals following 5-fluoro-2'-deoxyuridine (FUdR) treatment. Refer to Figure 1 for description of box plot. Treatment with 20 µM FUdR, beginning at the L4 larval stage, does not induce speed abnormalities either at young adulthood ($p = 0.456$) or on Day 5 ($p = 0.208$). Day 5 animals are slower than young adults whether untreated ($p = 0.014$) or treated ($p = 0.048$). N2 untreated young adult: $n = 14$, N2 + 20 µM FUdR young adult: $n = 12$, N2 untreated 5-day-old: $n = 12$, N2 + 20 µM FUdR 5-day-old: $n = 14$.

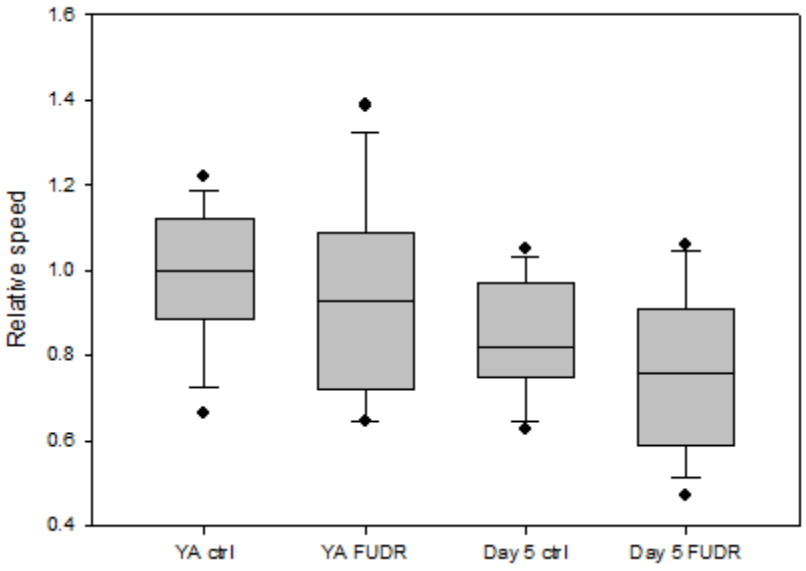

Supplementary Figure 4. Electrotaxis of wild-type animals cultured on different bacterial strains. Refer to Figure 1 for description of box plot. No significant difference was observed between the electrotactic speeds of animals fed *E. coli* OP50 and animals fed *E. coli* HB101 (p = 0.964), *E. coli* HT115 (p = 0.348), *E. coli* DH5a (p = 0.673), *C. aquaticus* DA1877 (p = 0.866), *A. tumefaciens* GV3101 (p = 0.147), or *E. carotovora* SCC3193 (p = 0.725). OP50-fed: n = 20, HB101-fed: n = 25, HT115-fed: n = 16, DH5a-fed: n = 25, DA1877-fed: n = 30, GV3101-fed: n = 25, SCC3193-fed: n = 19.

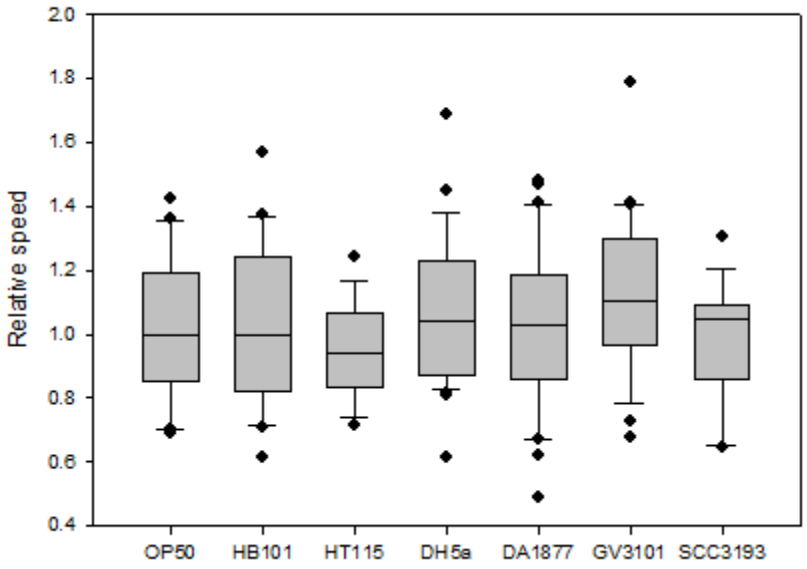

Supplementary Figure 5. Electrotaxis of insulin/IGF-1 pathway mutants. Refer to Figure 1 for description of box plot. Neither *daf-2(e1370)* (p = 0.946) nor *daf-16(mu86)* (p = 0.870) mutants exhibit electrotactic speed abnormalities relative to wild-type. N2: n = 50, CB1370 *daf-2*(*e1370*): n = 25, CF1038 *daf-16*(*mu86*): n = 30.

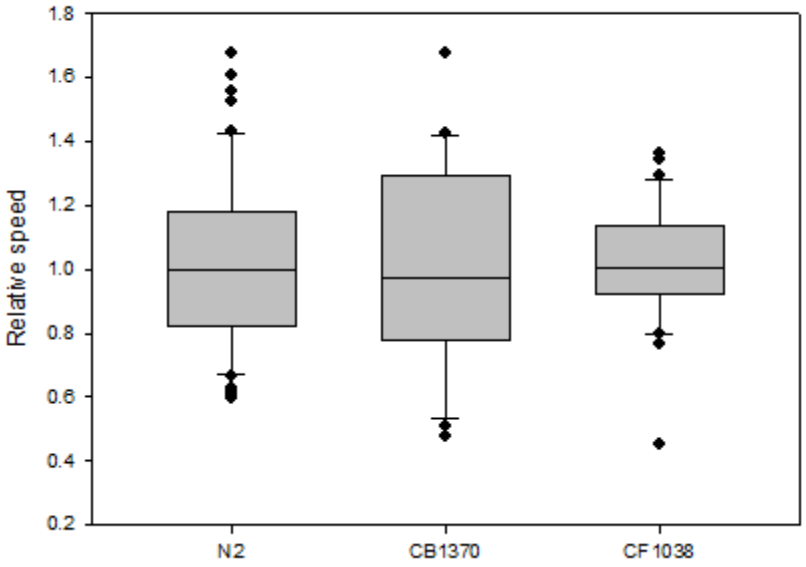

Supplementary Figure 6. Electrotaxis of HSF-1-overexpressing animals treated with paraquat. Refer to Figure 1 for description of box plot. Speed of *muEx265*(*hsf-1*::*HSF-1* + *myo-3::GFP*) transgenic animals is not significantly different from that of wild-type animals either in the absence of treatment ($p = 0.157$) or following treatment with 250 μM paraquat ($p = 0.374$). Treatment with 250 μM paraquat depresses electrotactic speed of both wild-type animals ($p < 0.001$) and HSF-1-overexpressing animals ($p < 0.001$). N2 untreated: n = 41, N2 + 250uM PQ: n = 45, CF1824 *muEx265*(*hsf-1*::*HSF-1* + *myo-3::GFP*) untreated: n = 20, CF1824 + 250uM PQ: n = 20.

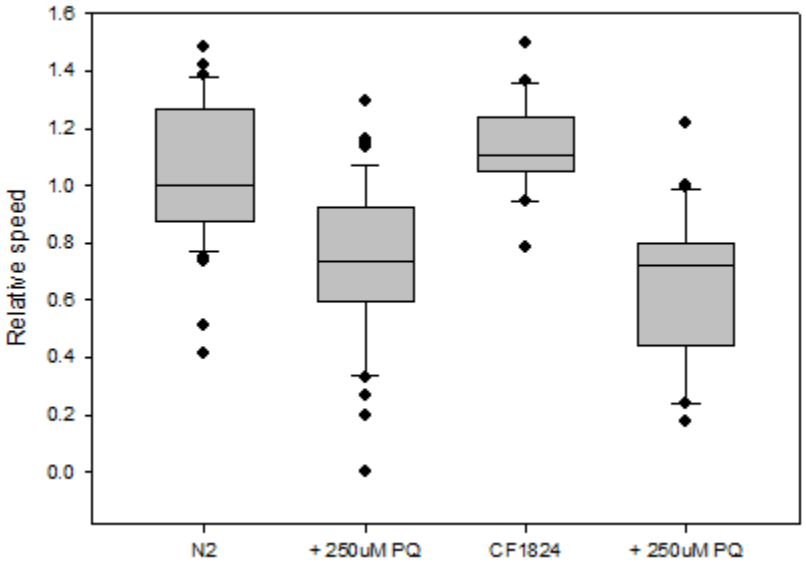

Supplementary Figure 7. Electrotaxis of adult *hsf-1* animals that have been starved in M9 for variable lengths of time at L1. Refer to Figure 1 for description of box plot. *hsf-1(sy441)* animals arrested at L1 for 48 h or 72 h show significant slowness relative to control animals that were starved at L1 for 24 h ($p < 0.001$ in both cases). PS3551 *hsf-1(sy441)* starved 24h: n = 37, PS3551 starved 48h: n = 24, PS3551 starved 72h: n = 27.

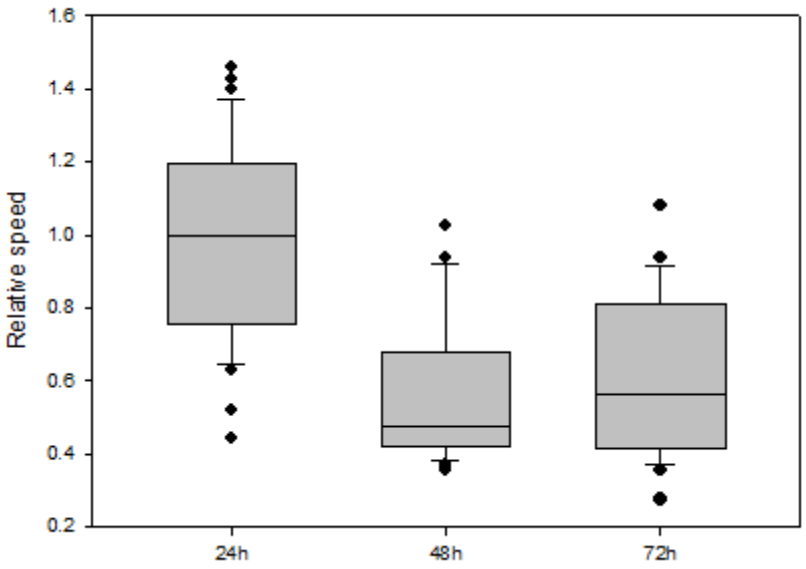

Supplementary Figure 8. Electrotaxis of *hsf-1* animals following mild heat stress in young adulthood. Refer to Figure 1 for description of box plot. Relative to untreated *hsf-1(sy441)* worms, animals subjected to a 25°C water bath for 5 h exhibit significant slowness ($p = 0.012$) while animals subjected to a 33°C water bath for 1 h exhibit speed enhancement ($p < 0.001$). PS3551 *hsf-1(sy441)* untreated: n = 63, PS3551 heat-shocked at 25°C for 5h: n = 51, PS3551 heat-shocked at 33°C for 1h: n = 31.

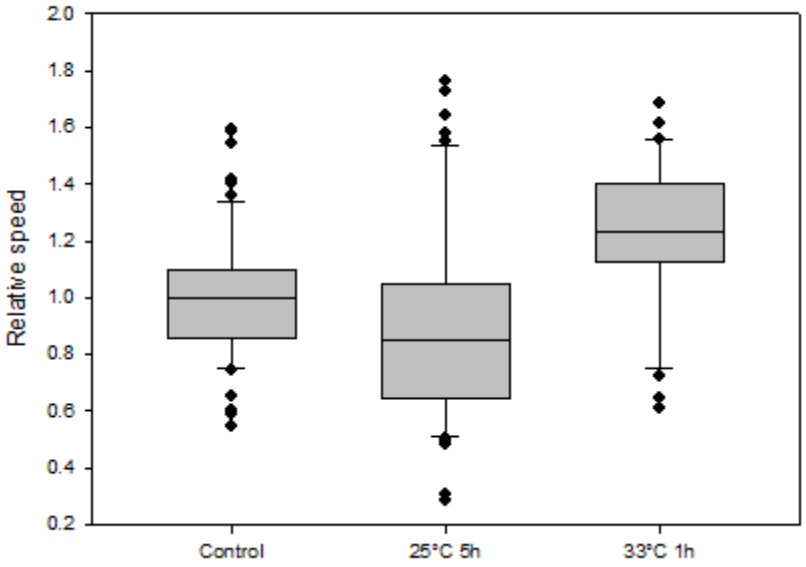

Significance

This study explores the effects of various stressful environmental and genetic manipulations on worms' electrotactic swimming. We report that stresses associated with the ER and the UPR^{ER} are particularly capable of inducing electrotactic swimming deficits, with additional roles for the UPR^{mt} and the heat shock response. We further show that at least some of these stresses, namely paraquat and tunicamycin, have detrimental effects on neuronal morphology, which may account in part for their impact on electrotaxis behaviour. These results provide evidence for relationships between stress responses and electrotactic swimming, and support the value of the microfluidic electrotaxis assay for further investigation of stress response pathways.

Chapter 6-Discussion, Conclusions, and Future Directions

6.1 Exposure to metal salts causes neurodegeneration-associated electrotactic swimming defects

This dissertation reports the development of a micro-electro-fluidic assay for the quantitative measurement of changes in the electrotactic swimming response of *C. elegans*, and the use of this assay for the dissection of genetic and environmental factors that affect this behaviour. In one study (***1***), we found that electrotactic swimming behaviour is sensitive to metal toxicity, with a decrease in locomotion being associated with metal bioaccumulation and neuronal damage. Results indicate that electrotactic motility is a better indicator than brood size, growth, or lifespan of toxicity from metal salts, but not other environmental pollutants. This study is the first to report an effect of metal exposure on electrotactic swimming, as well as the first to demonstrate the bioaccumulation of Ag, Cu, and inorganic Hg in *C. elegans*. Furthermore, these findings open up the question of why metal salts, among other chemicals, should have an especially strong impact on electrotaxis. This work will lead to further exploration of how metals affect electrotactic swimming, which may shed light on the underlying regulatory mechanisms. Additionally, this study supports microfluidic electrotaxis as a sensitive endpoint for metal toxicology studies in *C. elegans*.

6.2 Familial Parkinson mutant αSyn causes electrotactic swimming defects that are ameliorated with curcumin

In a second study (***2***), we found that ectopic expression of A53T αSyn is associated with electrotactic swimming defects. The effect is subtle when αSyn expression is restricted to head neurons, but we found that age-related declines in electrotactic motility are quantifiably exacerbated in *dat-1*::αSyn transgenic animals, which also display dopamine neuronal damage. This phenomenon appears to be specific to dopamine neurons, as *lin-11-int3*::αSyn animals exhibit wild-type electrotactic swimming regardless of age. Interestingly, both the neuronal and electrotactic phenotypes of *dat-1*::αSyn worms can be ameliorated

with chronic curcumin treatment. Together, these results show that "genetic stress"-induced dopaminergic neuronal damage manifests as electrotactic swimming defects, which supports our group's earlier finding that neurotoxicant-induced dopaminergic neuronal damage causes electrotactic defects (***3***). Moreover, this study provides the first evidence showing that curcumin can protect against dopamine neurodegeneration and the associated locomotory phenotypes in *C. elegans*, which supports further exploration of curcumin as a therapy for PD and possibly other neurodegenerative disorders. Additionally, this work suggests that the microfluidic electrotaxis platform may serve as a useful tool for drug discovery.

6.3 ER and other stresses modulate electrotactic swimming behaviour

In a third study (***4***), we found that the activation and action of multiple stress response pathways, including the UPR^{mt}, UPR^{ER}, and heat shock response, are associated with changes in electrotactic motility. Perhaps the most interesting aspect of this work was our observation that mutation in the poorly characterized *pqe-1* gene, which lacks obvious mammalian orthologs, causes tunicamycin hypersensitivity and electrotaxis defects that are exacerbated by low concentrations of paraquat. *pqe-1* was originally identified in independent genetic screens for proteins protecting transgenic huntingtin-expressing *C. elegans* neurons against polyglutamine toxicity (***5***) and for mutations that enhance the expression of transgenes (***6***), leading to speculation that PQE-1 functions as a negative regulator of protein synthesis; however, no further experiments had been done to verify this conjecture, and *pqe-1* mutations have never before been reported to confer ER stress sensitivity. By shedding light on the function of *pqe-1* in *C. elegans*, our work extends our understanding of ER homeostasis regulation in multicellular eukaryotes. More broadly, this study makes a new association of ER and other stresses with electrotactic behaviour, suggesting that the UPR^{mt}, UPR^{ER}, and heat shock response may have unexplored roles in the regulation of worms' response to electric fields.

6.4 Future directions

To further explore the phenomenon of metal-induced electrotactic swimming depression, we intend to test a greater variety of metal salts and investigate whether the ability to affect electrotaxis is common to all metals. For this purpose, we have acquired five additional metal salts: $NiSO_4$, $Pb(NO_3)$, $Cd(NO)_2$, $FeSO_4$, and $MnCl_2$. We will shortly be conducting experiments to see whether these salts induce electrotactic motility defects at concentrations that do not generate obvious plate-level phenotypes. Additionally, we plan to better characterize the metals' effects on neurons. Firstly, we will use *dat-1*::YFP and *lin-11-int3*::GFP neuronal marker animals to investigate the effects of metal exposure on dopaminergic neurons and head sensory neurons. Secondly, we will establish whether there is a quantitative relationship between the neuronal and electrotactic defects by examining both phenotypes across a time course of metal exposure. Together, these experiments stand to strengthen the association between metal toxicity and electrotaxis abnormality, and further support the potency of electrotaxis for use in environmental toxicology.

As a follow-up to our findings regarding the beneficial effects of curcumin on the neuronal and electrotactic phenotypes of *dat-1*::αSyn worms, we would like to test curcumin's ability to rescue other abnormalities associated with αSyn expression and dopaminergic neurodegeneration. Among other questions, we are interested in whether curcumin rescues dopamine-dependent behaviours that are defective in *dat-1*::αSyn animals, such as the food-sensing basal slowing response. We would also like to investigate whether curcumin can ameliorate the movement defects and inclusion formation phenotypes of *unc-51*::αSyn and *unc-54*::αSyn worms, in which case we could demonstrate the compound's efficacy beyond dopaminergic neurons. Additionally, we could test whether curcumin rescues the phenotypes of neurotoxicant PD worm models, which have previously been shown to exhibit severe electrotaxis deficits (***3***). These experiments stand to lend further support to the growing body of evidence that curcumin may be a promising candidate neuroprotective agent with potency for prevention of PD and other neurodegenerative diseases.

To build on our findings regarding the relationships between cellular stress pathways and electrotactic swimming, we intend to identify the specific cells responsible for mediating the locomotory deficits. We have found that

dopaminergic neurons are damaged by paraquat and tunicamycin treatment; however, it remains to be seen whether these neurons are damaged by the "genetic stresses" that we have shown to affect electrotaxis. To address this question, we intend to express the *dat-1*::YFP marker in the relevant mutants to facilitate evaluation of their dopaminergic neuronal phenotypes. We have already constructed a *pqe-1(ok1983)*; *dat-1*::YFP line via genetic crossing, and although more careful scrutiny is required, preliminary work shows that some damage may be present; therefore, the behavioural abnormalities of *pqe-1* mutants may be at least partly attributable to neurodegeneration. We would also be interested in the phenotypes of other subsets of neurons, such as the head sensory neurons marked by *lin-11-int3*::GFP and the GABAergic neurons marked by *unc-47*::GFP, as well as the body wall muscles. These experiments will allow us to provide a cellular basis for the effects of stress conditions on electrotactic swimming. Additionally, we would like to use fluorescent stress markers such as *hsp-6*::GFP and *hsp-4*::GFP to investigate whether the metal exposures and ectopic αSyn expression of Chapters 3 and 4 are associated with the UPR^{mt} and UPR^{ER}, which is in fact a connection that has been made in other model systems (***7,8,9***). These experiments stand to strengthen the association between these stress pathways and electrotactic behaviour.

6.5 Further applications of microfluidic electrotaxis platform

The work described in this dissertation is yet a mere taste of how the microfluidic electrotaxis assay can further *C. elegans* research. Our group is in fact planning or conducting a number of other studies utilizing the electrotactic response as an indicator of the state of neuronal locomotory circuits. These projects are briefly outlined below.

6.5.1 Drug discovery

Since its inception, our vision for the microfluidic electrotaxis assay has always included applications for motility-based high-throughput screening (HTS) (***10***). Screening a large number of chemical compounds to identify candidates with potential therapeutic effects is the rate-limiting step in drug discovery. HTS is usually done using *in vitro* assays; however, these conventional approaches

ignore the complexity of the biological processes in multicellular organisms with distinct and interacting tissues, organs, and systems, resulting in positive screen hits that often fail to produce desired results in subsequent animal trials. Consequently, discovered drugs frequently present with poor efficacy, harmful side effects, delay in clinical trials, and an increase in the expense involved in the development of new drugs. From this perspective, an ideal screening approach would use human subjects right away, though of course such an option is precluded by expense, throughput, and ethical issues. A balance between these considerations is found in alternative eukaryotic systems such as *C. elegans*, which are simpler and easier to manipulate yet complex enough to yield data applicable to human diseases.

As mentioned previously, the ease and low costs of culturing *C. elegans* make it an excellent metazoan model for drug discovery. Several studies have used worms to identify novel compounds of interest ranging from anthelmintics to potential therapies for human diseases (***11,12,13***). These screens are generally conducted in 96-well plates to maximize throughput and therefore rely on readily apparent phenotypes such as paralysis, egg-laying defects, muscle loss, and fluorescent reporter expression; subtle behavioural phenotypes, on the other hand, may not be as easy to spot in screens of this format. The flexibility of microfluidic systems offers ways to circumvent this problem, especially, for our purposes, because they can incorporate simple electrical circuits.

We propose that the microfluidic electrotaxis assay can be used to identify compounds that mitigate the negative effects of genetic and environmental factors on neuronal and muscular function. For instance, having established that αSyn-expressing transgenic worms exhibit electrotactic swimming deficits that are ameliorated by curcumin treatment, we could use a multichannel microfluidic HTS platform (currently in development; see **Section 6.5.5**) to screen for chemicals with similar protective capabilities. Potential drug candidates can be subjected to more detailed investigation in mammalian models as well as *C. elegans*.

6.5.2 Characterization of novel drug targets

In addition to discovery of new drugs, *C. elegans* is also an excellent vehicle for genetic screens owing to its amenability to RNAi experiments. Genome-wide *C. elegans* RNAi screens have led to the discovery of genes that modulate αSyn aggregation and toxicity (***14,15***), axon regeneration (***16***), and all manner of other neurodegeneration-related phenomena (***17***).

We propose that an RNAi approach may be used to find the genes responsible for mediating curcumin's protective action on dopaminergic neurons and motility. In such a study, αSyn-expressing worms would be fed bacteria expressing double-stranded RNA (dsRNA) corresponding to candidate genes and simultaneously exposed to 1 mM curcumin, then examined for movement defects in the microfluidic electrotaxis assay. Failure of curcumin to rescue αSyn-induced electrotaxis deficits would indicate abolition of its protective effects by the RNAi knockdown, implicating that gene in curcumin's mechanism of action. However, as is the case with the drug screening mentioned in the previous sub-section, the feasibility of this research is incumbent on adaptation of the electrotaxis platform for HTS (see **Section 6.5.5**).

6.5.3 Probing neuronal signaling pathways

While large-scale screening projects figure prominently in our vision for the future of *C. elegans* electrotaxis, there is other interesting work that does not require engineering improvements to the assay and is therefore already underway. One of these studies, led by our group member and close associate Sangeena Salam, is focused on characterizing the role of dopamine signaling in modulation of electrotactic swimming behaviour (***18***). She discovered a novel dopamine-mediated phenomenon in which worms continuously exposed to mild electric fields gradually reduce their swimming speed over time. This phenomenon appears to be independent of muscle fatigue, as worms that have continually thrashed in M9 buffer without stimulus for an equivalent period of time do not then display electrotactic speed deficits upon placement in an electric field, and requires dopamine, as *cat-2*/TH-defective mutants do not slow appreciably within the allotted time. This work provides evidence for an as-yet uncharacterized dopamine-dependent response to electrical stimuli and promotes the exploration of neuronal signaling pathways in *C. elegans* using microfluidic electrotaxis.

6.5.4 Dissection of gene regulation in neuronal differentiation

Another field being investigated in our lab is the complex inter- and intra-cellular signaling that underlies the differentiation of cells into specific tissues, which relies on both spatial and temporal regulation of specific genes. Much of this communication is dependent on tissue-specific transcription factors like LIN-

11, a LIM-homeodomain protein studied extensively in our lab that is required for the differentiation of several head and tail neurons as well as various tissues of the reproductive system (***19***). The expression of *lin-11* in different tissues is regulated by enhancers in its introns and 5'-untranslated region; however, in the case of some of these enhancers, the specific sequences responsible for enhancer activity have yet to be identified. Our group member Siavash Amon is currently leading a project aimed at dissecting the enhancer region inside intron 3 via microinjection rescue experiments: in this approach, transgenic lines are generated from *lin-11* null mutants by microinjecting plasmids with LIN-11 expression driven by different regions of intron 3, and then each line is assessed for proper neuronal differentiation and function.

ASH, one of the principal neurons responsible for electrosensation, and interneurons that pioneer tracts of the ventral nerve cord are among the cells whose proper development requires *lin-11* expression; consequently, *lin-11* null mutants display severe defects in both electrosensory and swimming behaviours (***20***). Interestingly, when a sequence of intron 3 was identified whose driving of LIN-11 expression could rescue the differentiation of most amphid neurons in *lin-11* null mutants, the same construct was found to also rescue these animals' electrotaxis phenotypes (***21***). Electrotaxis therefore serves as an appropriate read-out for determining whether *lin-11*-expressing neurons are functioning properly, and could potentially be employed in similar dissection studies on other genes involved in neuronal differentiation and/or function.

6.5.5 Development of a high-throughput electrotaxis assay

Adaptation of the microfluidic electrotaxis assay for large-scale screening applications will require implementation of several modifications to increase throughput. Fortunately, microfluidic systems are well suited to parallelization, and even the electrical signals used to control worms' locomotion can be easily multiplexed using simple, well-established, low-cost electrical circuits. The necessary adjustments are already in development by our group and include software for automated video acquisition, tracking software for automated video analysis, parallel assay channels, integrated electrodes for individual and independent control of these channels, electrical sensors for locating worm position, sorters to create homogenous worm populations, and methods for automated arraying and parallel operations. These components and methods will be integrated into an automated multichannel platform for HTS of worms against libraries of chemicals.

While the aforementioned features vary in terms of current developmental status, the worm tracker is particularly mature and has been employed to some extent in the studies described in this thesis. This software is described in the following sub-section.

6.5.6 Automated electrotaxis video analysis

When Rezai and colleagues first developed the microfluidic electrotaxis assay, recorded videos required analysis by eye for extraction of speed and other relevant data. This manual analysis process is subject to human error and bias, time- and labour-intensive, and a serious bottleneck to assay throughput. To address these issues, automation of data extraction by means of worm tracking software is preferable. Several such software packages have been reported, including Track-A-Worm (***22***), the Multi-Worm Tracker (***23***), and the Parallel Worm Tracker (***24***); however, these packages require additional, specialized hardware such as motorized platforms and/or a live camera feed, with no option to use pre-recorded videos. Additionally, these programs require the user to determine sensible values for a variety of algorithm parameters, which is not always a straightforward procedure.

We therefore created our own tracker software, in collaboration with the Shirani lab at McMaster University, to quickly and robustly extract and analyze locomotory information without human interaction or calibration (***25***). The goal of this software was to provide a simple solution for tracking *C. elegans* during a variety of experiment types, requiring no manual parameter input. The program, which is capable of tracking larvae, locomotory mutants, and toxicant-exposed animals, can be installed on any PC with Matlab and its Computer Vision and image processing toolboxes. Extracted data includes speed, body oscillation frequency, and amplitude. The software is also capable of batch-processing large numbers of videos, allowing researchers to create long queues of videos to be analyzed overnight. Together, these features greatly improve the efficiency of electrotaxis experiments.

An early version of this tracker that measures speed only was used in the studies included in this thesis. Now that the software has been improved and optimized, future experiments utilizing the microfluidic electrotaxis platform will yield data describing additional aspects of worms' locomotion.

6.6 Significance of this work

Electrotaxis is a complex behaviour consisting of electrosensation, signal processing, and a motor response. The work described in this dissertation deepens our understanding of the latter, expanding our knowledge of how the output component of the electrotactic response is perturbed by environmental and genetic manipulations. From these studies, we have learned that the quality of electric field-induced locomotion is generally quite robust, withstanding insults such as exposure to non-metallic environmental pollutants, mutations in PD-related genes *lrk-1* and *pink-1*, and inhibition of mitochondrial SOD activity; yet, interestingly, the behaviour is sensitive to metal toxicity, αSyn-induced dopaminergic neurodegeneration, and UPR-activating stress. Our findings show that the worm's motor response to electric field is regulated by specific mechanisms, and provide clues to the nature of those mechanisms: specifically, our work establishes a relationship between electrotactic swimming and stress response pathways and neurons that have not previously been associated with worms' response to electric fields.

Additionally, in pursuit of our goal to dissect factors that affect electrotaxis behaviour, we further developed our group's microfluidic electrotaxis assay into a powerful technique offering quantitative measurement of changes in electrotactic swimming through custom worm-tracking software. Our subsequent findings demonstrate the utility of the system for myriad purposes and show that our microfluidic assay will accelerate further research into the phenomenon of nematode electrotaxis and related topics. In particular, we intend to employ the setup in drug and drug target screening efforts, research probing neuronal signaling pathways, and studies dissecting the genetic regulation of neuronal differentiation. These endeavours will become more straightforward and painless as currently planned engineering improvements are made to the platform.

Beyond *C. elegans*, the work described in this thesis is also relevant to the broader field of electric field-dependent behaviour. No investigations into the effects of metal toxicity on the electrosensory behaviour of fish have yet been made, nor have any connections with the UPR been considered; therefore, our findings may indicate a novel set of mechanisms regulating an organism's response to electric stimuli. Indeed, our findings warrant follow-up in these higher

metazoans to test for conservation of the regulatory mechanisms shown in this dissertation to be present in nematodes.

References

1. Tong, J.; Rezai, P.; Selvaganapathy, P. R.; Mishra, R. K.; Gupta, B. P. Chronic exposure to metal salts induces defects in the electrotactic swimming behaviour of the nematode Caenorhabditis elegans. *(in preparation)*.

2. Tong, J.; Salam, S.; Rezai, P.; Selvaganapathy, P. R.; Mishra, R. K.; Gupta, B. P. Familial Parkinson mutant α-synuclein causes defective electrotactic swimming behaviour in transgenic Caenorhabditis elegans. *(in preparation)*.

3. Salam, S.; Ansari, A.; Amon, S.; Rezai, P.; Selvaganapathy, P. R.; Mishra, R. K.; Gupta, B. P. A microfluidics set up to study neuronal degeneration and identification of neuroprotective compounds in C. elegans. *Worm* **2013,** *2* (3), e24558.

4. Tong, J.; Sung, B.; Selvaganapathy, P. R.; Mishra, R. K.; Gupta, B. P. ER stress modulates electrotactic swimming behaviour in Caenorhabditis elegans. *(in preparation)*.

5. Faber, P. W.; Voisine, C.; King, D. C.; Bates, E. A.; Hart, A. C. Glutamine/proline-rich PQE-1 proteins protect Caenorhabditis elegans neurons from huntingtin polyglutamine neurotoxicity. *Proc Natl Acad Sci USA* **2002,** *99* (26), 17131-17136.

6. Yamada, K.; Tsuchiya, J.; Iino, Y. Mutations in the pqe-1 gene enhance transgene expression in Caenorhabditis elegans. *G3 (Bethesda)* **2012,** *2* (7), 741-751.

7. Kitamura, M.; Hiramatsu, N. The oxidative stress: endoplasmic reticulum stress axis in cadmium toxicity. *Biometals* **2010,** *23* (5), 941-950.

8. Shinkai, Y.; Kaji, T. Cellular defense mechanisms against lead toxicity in the vascular system. *Biol Pharm Bull* **2012,** *35* (11), 1885-1891.

9. Hoozemans, J. J.; van Haastert, E. S.; Nijholt, D. A.; Rozemuller, A. J.; Scheper, W. Activation of the unfolded protein response is an early event in Alzheimer's and Parkinson's disease. *Neurodegener Dis* **2012,** *10* (1-4), 212-215.

10. Rezai, P.; Salam, S.; Selvaganapathy, P. R.; Gupta, B. P. Microfluidic Systems to Study the Biology of Human Diseases and Identify Potential Therapeutic Targets in Caenorhabditis elegans. In *Integrated Microsystems: Electronics, Photonics, and Biotechnology;* Iniewski, K., Ed.; CRC Press, Taylor & Francis Group: Boca Raton, 2012; pp 581-608.

11. Jones, A. K.; Buckingham, S. D.; Sattelle, D. B. Chemistry-to-gene screens in Caenorhabditis elegans. *Nat Rev Drug Discov* **2005,** *4* (4), 321-330.

12. Su, L. J.; Auluck, P. K.; Outeiro, T. F.; Yeger-Lotem, E.; Kritzer, J. A.; Tardiff, D. F.; Strathearn, K. E.; Liu, F.; Songsong, C.; Shusei, H.; Hill, K. J.; Caldwell, K. A.; Bell, G. W.; Fraenkel, E.; Cooper, A. A.; Caldwell, G. A.; McCaffery, J. M.; Rochet, J.-C.; Lindquist, S. Compounds from an unbiased chemical screen reverse both ER-to-Golgi trafficking defects and mitochondrial dysfunction in Parkinson's disease models. *Disease Models & Mechanisms* **2010,** *3* (3-4), 194-208.

13. Voisine, C.; Varma, H.; Walker, N.; Bates, E. A.; Stockwell, B. R.; Hart, A. C. Identification of Potential Therapeutic Drugs forHuntington's Disease using Caenorhabditis elegans. *PLoS ONE* **2007,** *2* (6), e504.

14. van Ham, T. J.; Thijssen, K. L.; Breitling, R.; Hofstra, R. M.; Plasterk, R. H.; Nollen, E. A. C. elegans model identifies genetic modifiers of alpha-synuclein inclusion formation during aging. *PLoS Genetics* **2008,** *4,* e1000027.

15. Kuwahara, T.; Koyama, A.; Koyama, S.; Yoshina, S.; Ren, C.-H.; Kato, T.; Mitani, S.; Iwatsubo, T. A systematic RNAi screen reveals involvement of endocytic pathway in neuronal dysfunction in a-synuclein transgenic C. elegans. *Hum Mol Genet* **2008,** *17* (19), 2997-3009.

16. Nix, P.; Hammarlund, M.; Hauth, L.; Lachnit, M.; Jorgensen, E. M.; Bastiani, M. Axon regeneration genes identified by RNAi screening in C. elegans. *J Neurosci* **2014,** *34* (2), 629-645.

17. Sin, O.; Michels, H.; Nollen, E. A. Genetic screens in Caenorhabditis elegans models for neurodegenerative diseases. *Biochim Biophys Acta* **2014,** [Epub ahead of print].

18. Salam, S.; Mishra, R. K.; Selvaganapathy, P. R.; Gupta, B. P. Dopamine signaling depresses the electrotactic swimming of C. elegans. *(in preparation).*

19. Marri, S.; Gupta, B. P. Dissection of lin-11 enhancer regions in Caenorhabditis elegans and other nematodes. *Dev Biol* **2009,** *325* (2), 402-411.

20. Amon, S. *GENETIC DISSECTION OF lin-11 REGULATION IN DIFFERENTIATION OF C. elegans AMPHID SENSORY NEURONS;* Masters Thesis; McMaster University: Hamilton, 2012.

21. Amon, S.; Salam, S.; Gupta, B. Genetic dissection of lin-11 regulation in

differentiation of C. elegans amphid sensory neurons. *(in preparation)*.

22. Wang, S. J.; Wang, Z. W. Track-a-worm, an open-source system for quantitative assessment of C. elegans locomotory and bending behavior. *PLoS One* **2013,** *8* (7), e69653.

23. Swierczek, N. A.; Giles, A. C.; Rankin, C. H.; Kerr, R. A. High-throughput behavioral analysis in C. elegans. *Nat Methods* **2011,** *8* (7), 592-598.

24. Ramot, D.; Johnson, B. E.; Berry, T. L.; Carnell, L.; Goodman, M. B. The Parallel Worm Tracker: a platform for measuring average speed and drug-induced paralysis in nematodes. *PLoS One* **2008,** *3* (5), e2208.

25. Scigajlo, A.; Tong, J.; Salam, S.; Lee, A.; Selvaganapathy, P. R.; Gupta, B.; Shirani, S. An adaptive tracking algorithm for C. elegans. *(in preparation)*.